Spring 2019

Time-dependent reliability methodologies with saddlepoint approximation

Zhangli Hu

Department: Mechanical and Aerospace Engineering

TIME-DEPENDENT RELIABILITY METHODOLOGIES WITH SADDLEPOINT APPROXIMATION

by

ZHANGLI HU

A DISSERTATION

Presented to the Faculty of the Graduate School of the

MISSOURI UNIVERSITY OF SCIENCE AND TECHNOLOGY

In Partial Fulfillment of the Requirements for the Degree

DOCTOR OF PHILOSOPHY

in

MECHANICAL ENGINEERING

2019

Approved by:

Dr. Daoru Han, Advisor
Dr. Xiaoping Du, Co-Advisor
Dr. Serhat Hosder
Dr. Ashok Midha
Dr. Anthony Okafor
Dr. Ruwen Qin

PUBLICATION DISSERTATION OPTION

This dissertation consists of the following four articles that have been published or submitted for publication as follows:

Paper I: pages 7-40 have been published in ASCE-ASME Journal of Risk and Uncertainty in Engineering Systems, Part B: Mechanical Engineering.

Paper II: pages 41-76 have been published in Structural Safety.

Paper III: pages 77-115 have been published in Engineering Optimization.

Paper IV: pages 116-145 have been accepted by the ASME 2019 International Design Engineering Technical Conferences and Computers and Information in Engineering Conference (IDETC/CIE 2019), August 18-21, 2019, Anaheim, CA, USA.

This dissertation has been prepared in the style utilized by the Missouri University of Science and Technology.

ABSTRACT

Engineers always encounter time-dependent uncertainties that ubiquitously exist, such as the random deterioration of material properties and time-variant loads. Therefore the reliability of engineering systems becomes time-dependent. It is crucial to predict the time-dependent reliability in the design stage, given possible catastrophic consequences of a failure. Although extensive research has been conducted on reliability analysis, estimating the reliability accurately and efficiently is still challenging. The objective of this work is to develop accurate and efficient reliability methodologies for engineering design. The basic idea is the integration of traditional reliability methods with saddlepoint approximation (SPA), which can accurately approximate the tail distribution of a random variable. Four methods are proposed in this work. The first three methods deal with time-independent reliability while the last one estimates the time-dependent reliability. The first method combines SPA with first-order approximation and achieves higher accuracy over the traditional first-order reliability method when bimodal distributions are involved. The second method further improves the accuracy of reliability estimation by integrating SPA with the second-order approximation. The third method extends the second method into the reliability-based design for higher accuracy, and the high efficiency is maintained by an efficient algorithm for searching for an equivalent reliability index. The fourth method uses sequential efficient global optimization to convert a time-dependent problem into a time-independent counterpart. Then the second method is utilized to estimate the time-independent reliability after the conversion. The accuracy and effectiveness of the above methods are demonstrated by both numerical examples and engineering applications.

ACKNOWLEDGEMENTS

First, I would like to express my sincere appreciation to my advisor, Dr. Daoru Han, and my co-advisor, Dr. Xiaoping Du, for their time, kindness, unwavering support, insightful guidance, and continuous encouragement during my Ph.D. study at Missouri University of Science and Technology. It has been my great honor and privilege to work with them. Their diligence, rigorous attitude to research, great passion for teaching, and modesty in life will continuously inspire me in my future career and life.

Meanwhile, I would like to extend my gratitude to all my dissertation committee members, Dr. Serhat Hosder, Dr. Ashok Midha, Dr. Anthony Okafor and Dr. Ruwen Qin. Without their guidance, insightful comments and time commitment, this dissertation would not have been possible.

Besides, I would like to thank my labmates and friends, Dr. Zhen Hu, Dr. Zhifu Zhu, Dr. Yao Cheng, Dr. Zhengwei Hu, Mr. Guannan Liu, Mr. Hao Wu, Mr. Xinpeng Wei, Dr. Fangping Yuan, Dr. Xin Wang, Dr. Chao Zhang, Mr. Junji Huang, Mr. Le Ma, Ms. Aslihan Vuruskan, Mr. Ganesh Ravi Shanker and Mr. Philip Honnold, for their support and help during my study in Rolla. I also would like to thank Dr. Cenk Undey, Dr. Myra Coufal and Dr. Elif Seyma Bayrak at Amgen Corporation for their guidance and help during my graduate co-op. I also greatly appreciate the financial support from the National Science Foundation through Grants CMMI 1562593 and CMMI 1727329 and the Intelligent Systems Center at Missouri University of Science and Technology.

Lastly but not the least, I would like to express my deepest appreciation and love to my wife, Qilian Song, my parents, my parents in law and relatives for their love, encouragement, patience and persistent support.

TABLE OF CONTENTS

Page

PUBLICATION DISSERTATION OPTION iii

ABSTRACT iv

ACKNOWLEDGEMENTS v

LIST OF ILLUSTRATIONS xi

LIST OF TABLES xiii

SECTION

1. INTRODUCTION 1

1.1. BACKGROUND 1

1.2. RESEARCH OBJECTIVE 3

1.3. ORGANIZATION OF DISSERTATION 5

PAPER

I. RELIABILITY METHODS FOR BIMODAL DISTRIBUTION WITH FIRST ORDER APPROXIMATION 7

ABSTRACT 7

1. INTRODUCTION 8

2. REVIEW OF METHODOLOGIES 12

2.1. FOSM 12

2.2. FORM 13

2.3. SPA 14

3. SADDLEPOINT APPROXIMATION FOR BIMODAL DISTRIBUTIONS . 16

3.1. SPA FOR A BIMODAL DISTRIBUTION 16

3.1.1. Case 1: Bimodal Distribution with A Mixture of Two Normal Distributions. 17

3.1.2. Case 2: Bimodal Distribution with A Mixture of Two Gumbel Distributions. 19

3.2. SPA METHODS FOR BIMODAL DISTRIBUTIONS WITH FIRST ORDER APPROXIMATIONS 21

3.2.1. MVSPA. 21

3.2.2. FOSPA. 22

3.2.3. Numerical Procedure. 23

4. NUMERICAL EXAMPLES 25

4.1. EXAMPLE 1: SIMPLE SUPPORT BEAM 25

4.2. EXAMPLE 2: SPEED REDUCER SHAFT 30

4.3. EXAMPLE 3: ROOF TRUSS 32

5. CONCLUSIONS 34

ACKNOWLEDGEMENTS 36

REFERENCES 37

II. SADDLEPOINT APPROXIMATION RELIABILITY METHOD FOR QUADRATIC FUNCTIONS IN NORMAL VARIABLES 41

ABSTRACT 41

1. INTRODUCTION 42

2. REVIEW OF FORM AND SORM 44

2.1. FORM 44

2.2. SORM 45

3. SADDLEPOINT APPROXIMATION FOR A QUADRATIC FUNCTION .. 48

3.1. QUADRATIC LIMIT-STATE FUNCTION 48

3.2. SADDLEPOINT APPROXIMATION 51

3.3. NUMERICAL PROCEDURE 53

4. EXAMPLES 55

4.1. QUADRATIC LIMIT-STATE FUNCTIONS 55

4.1.1. Example 1: Ellipse. 55

4.1.2. Example 2: Parabola. 60

4.1.3. Example 3: Hyperbola. 63

4.1.4. Example 4: High Dimensional Quadratic Function. 65

4.2. ENGINEERING EXAMPLES 67

4.2.1. Example 1: A Slider-Crank Mechanism. 67

4.2.2. Example 2: Cantilever Tube. 69

5. CONCLUSIONS 72

ACKNOWLEDGEMENTS 73

REFERENCES 74

III. EFFICIENT RELIABILITY-BASED DESIGN WITH SECOND ORDER APPROXIMATIONS 77

ABSTRACT 77

1. INTRODUCTION 78

2. REVIEW OF FUNDAMENTAL METHODOLOGIES 81

2.1. RBD AND FORM 81

2.2. RBD AND INVERSE FORM 83

2.3. SORA 84

2.4. SORM 86

2.4.1. Traditional SORM Methods. 86

2.4.2. Second Order Saddlepoint Approximation. 87

3. SORA WITH INVERSE SORM 89

3.1. OVERVIEW OF SORA/SORM 89

3.2. ALGORITHM FOR INVERSE SORM 90

3.3. ALGORITHMS FOR UPDATING γ 93

3.3.1. Additive Relationship. 94

3.3.2. Multiplicative Relationship. 95

4. SORA/SORM 99

5. EXAMPLES 102

5.1. EXAMPLE 1: MATHEMATICAL PROBLEM 102

5.2. EXAMPLE 2: CANTILEVER BEAM DESIGN 104

5.3. EXAMPLE 3: DESIGN OF A WELDED BEAM 107

6. CONCLUSIONS 110

ACKNOWLEDGEMENTS 111

REFERENCES 112

IV. SECOND ORDER RELIABILITY METHOD FOR TIME-DEPENDENT RELIABILITY ANALYSIS USING SEQUENTIAL EFFICIENT GLOBAL OPTIMIZATION 116

ABSTRACT 116

1. INTRODUCTION 117

2. REVIEW OF FUNDAMENTAL METHODOLOGIES 120

2.1. TIME-DEPENDENT RELIABILITY 120

2.2. FIRST ORDER RELIABILITY METHOD (FORM) 120

3. SEGO/SOSPA 122

3.1. OVERVIEW 122

3.2. SEGO 123

3.2.1. Sequential Optimization.....123

3.2.2. Efficient Global Optimization (EGO).....125

3.3. HESSIAN APPROXIMATION AND ENVELOP THEOREM 127

3.4. SOSPA 129

3.5. SEGO/SOSPA PROCEDURE..... 131

4. EXAMPLES 133

4.1. EXAMPLE 1: MATHEMATICAL PROBLEM 133

4.2. EXAMPLE 2: AUTOMOBILE FRONT AXLE 136

4.3. EXAMPLE 3: A VIBRATION PROBLEM..... 138

5. CONCLUSIONS..... 140

ACKNOWLEDGEMENTS..... 141

REFERENCES 142

SECTION

2. CONCLUSIONS..... 146

BIBLIOGRAPHY..... 148

VITA..... 152

LIST OF ILLUSTRATIONS

SECTION Page

Figure 1.1. Reliability analysis with saddlepoint approximation 6

PAPER I

Figure 1. A bimodal distribution with a mixture of two normal distributions..... 16

Figure 2. Flowchart of the SPA methods..... 24

Figure 3. A simple support beam..... 26

Figure 4. PDF approximation using FOSM..... 28

Figure 5. Contours of the limit-state function in the X-space 29

Figure 6. Contours of the limit-state function in the U-space..... 29

Figure 7. A speed reducer shaft 30

Figure 8. A roof truss structure..... 32

PAPER II

Figure 1. The flowchart of SOSPA..... 54

Figure 2. Elliptical contour of the quadratic function in Case 1..... 57

Figure 3. Elliptical contour of the quadratic function in Case 2..... 57

Figure 4. Elliptical contour of the quadratic function in Case 3..... 58

Figure 5. Approximated contours in Case 1 58

Figure 6. Parabolic contour of the limit-state function in Case 1 61

Figure 7. Parabolic contour of the limit-state function in Case 2 61

Figure 8. Hyperbolic contour of the limit-state function in Case 1 63

Figure 9. Hyperbolic contour of the limit-state function in Case 2 64

Figure 10. A slider crank system 67

Figure 11. The contour of the slider crank system..... 68

Figure 12. A cantilever tube..... 70

PAPER III

Figure 1. Flowchart of SORA..... 85

Figure 2. Flowchart of SORA/SORM 90

Figure 3. Flowchart of the inverse SORM..... 92

Figure 4. Convergence history..... 98

Figure 5. Flowchart of SORA/SORM method 101

Figure 6. A cantilever beam..... 104

Figure 7. The welded beam problem 107

PAPER IV

Figure 1. Flowchart of sequential optimization..... 124

Figure 2. Flowchart of SEGO/SOSPA 132

Figure 3. Extreme limit-state surface formed by instantaneous limit-state surfaces 134

Figure 4. Extreme limit-state surface..... 134

Figure 5. Convergence history of Example 1 135

LIST OF TABLES

PAPER I Page

Table 1. CGFs of some common distributions 17

Table 2. CDFs of a bimodal distribution with two normal distributions 19

Table 3. Distribution parameters of load X 20

Table 4. CDFs of a bimodal distribution with two Gumbel distributions 20

Table 5. Distributions of the variables in simple support beam 27

Table 6. Probability of failure of simple support beam 28

Table 7. Distributions of the variables in speed reducer shaft 31

Table 8. Probability of failure of speed reducer shaft 31

Table 9. Distributions of the variables in roof truss structure 33

Table 10. Probability of failure of roof truss 33

PAPER II

Table 1. p_f of the elliptical quadratic function in Case 1 59

Table 2. p_f of the elliptical quadratic function in Case 2 59

Table 3. p_f of the elliptical quadratic function in Case 3 59

Table 4. p_f of the parabolic quadratic function in Case 1 62

Table 5. p_f of the parabolic quadratic function in Case 2 62

Table 6. p_f of the hyperbola quadratic function in Case 1 65

Table 7. p_f of the hyperbola quadratic function in Case 2 65

Table 8. p_f of quadratic function with n=10 and 20 66

Table 9. p_f of quadratic function with n=30 and 40 66

Table 10. Distributions of the random variables in slider crank mechanism..... 68

Table 11. The probability of failure of nonlinear oscillator system 69

Table 12. Distributions of the random variables in cantilever tube..... 70

Table 13. p_f of cantilever tube 71

PAPER III

Table 1. Algorithms to update the reliability index 96

Table 2. Results of inverse SORM 98

Table 3. Convergence history of SORA/SORM..... 103

Table 4. Results of example 1..... 103

Table 5. Distributions of variables in example 2 106

Table 6. Results of example 2..... 106

Table 7. Distributions of variables in example 3 108

Table 8. The optimization results of welded beam design problem 109

Table 9. Reliability constraints of welded beam design problem..... 109

PAPER IV

Table 1. Algorithms of EGO..... 126

Table 2. Iteration history of MPP search for Example 1 135

Table 3. Results of Example 1 136

Table 4. Distribution of parameters for axle beam example..... 137

Table 5. Results of Example 2 138

Table 6. Distribution of parameters for vibration example..... 138

Table 7. Results of Example 3 139

SECTION

1. INTRODUCTION

1.1. BACKGROUND

Engineers are always surrounded by uncertainty that ubiquitously exists during any systems design. Examples of uncertainty include random material properties, dimensions of components, and loads. Uncertainties can be classified into time-independent uncertainties and time-dependent uncertainties. Time-independent uncertainties are usually represented by random variables, which do not vary with respect to time, such as manufacturing variations in dimensions. Time-dependent uncertainties change randomly over time and are typically described by random processes. Examples include the motion error of a mechanism and the wave loads on offshore structures. Therefore, the system performance such as reliability becomes time-dependent. Herein, reliability is defined as the probability that a product or system performs its intended function over a period of time and under specified service conditions [1]. It is very important to predict this probability in a design stage, given the possible catastrophic consequences of a failure. Reliability analysis is imperative in many engineering systems design when accounting for uncertainties.

In the past decades, extensive research has been conducted on time-independent reliability analysis where uncertainties are time-invariant. Among them, Monte Carlo simulation (MCS) [2-4] is the most widely used method. It is very easy to use and can produce high accuracy with a large sample size. So it is usually used as a benchmark method to validate the accuracy of new reliability methods. However, its computational

cost is very high since a large sample size is required. Alternatively, many methods focus on obtaining an approximation solution with high efficiency, such as the First Order Second Moment Method (FOSM) [5, 6], the First Order Reliability Method (FORM) [7-10], the Second Order Reliability Method (SORM) [11-16], and saddlepoint approximation (SPA) based methods [17-21]. FOSM is easy to use and is highly efficient. Its accuracy may not be good when a performance function or a limit-state function is highly nonlinear and the distributions of input random variables are far away from normal distributions. FORM is in general more accurate than FOSM, but is less efficient. It is commonly used among the approximation methods because of the good balance between accuracy and efficiency. SORM is generally more accurate than FORM because of the second order approximation. However, it is more computationally expensive since it requires second derivatives of the limit-state function. SPA methods have the same order of magnitude for computational demand as that of FORM but it improves the accuracy for the problems where FORM worsen the linearity of limit-state functions due to the nonnormal to normal transformation. SPA methods have been successfully applied to component reliability analysis [21-23], reliability-based design [24], and system reliability analysis [25]. However, they may not be accurate enough when the limit-state function is highly nonlinear.

Recently, many efforts have been devoted to estimating time-dependent reliability. For example, Rice's formula based methods [26-30] have been proposed to solve the time-dependent problems where the upcrossings are not strongly dependent. Surrogate modeling methods have been developed to replace the original limit-state functions that are complex and computationally expensive. Then MCS is implemented on

the surrogate model to predict the time-dependent reliability. Typical surrogate models include polynomial chaos expansions (PCE) [31, 32], artificial neural networks (ANN) [33-35], support vector machines (SVMs) [36, 37], and Kriging model [38-41], also known as Gaussian process model. Surrogate modeling methods can achieve very high accuracy for reliability estimation if the surrogate model is well trained. However, accurate training may require a high computational effort. Besides the above methods, extreme value methods [42-46] are also widely used since they can convert the time-dependent problem into a time-independent counterpart and then time-independent methods can be applied. However, obtaining the extreme value distribution accurately is still challenging and difficult.

From the state-of-the-art, we can see that many methodologies have been developed for time-independent reliability and some of them have been extended to time-dependent problems. The methodologies, however, still have their limitations and more research is needed. Motivated by the aforementioned challenges, this dissertation develops new methodologies to accurately and efficiently estimate the reliability and applies them into engineering design.

1.2. RESEARCH OBJECTIVE

The objective of this dissertation is to develop reliability methodologies under time-independent uncertainty and then extend them into time-dependent reliability analysis. The major approach is the integration of saddlepoint approximation (SPA) with traditional reliability methods. To achieve this objective, four research tasks are

performed. The first three tasks deal with time-independent reliability while the last one estimates the time-dependent reliability.

Research task 1 (RT1) focuses on time-independent reliability analysis for bimodal distributions. The bimodal distribution, which has two peaks in their probability density, is widely encountered in engineering applications, such as the distribution of the gross vehicle weight of trucks [47], axle load distribution [48], and force from human hands. When binomial distributions are involved, traditional reliability methods, such as FOSM and FORM, may not be accurate. This research task intends to improve the accuracy of reliability estimation by using the SPA with first order approximation. And it results in Paper I [49].

Research task 2 (RT2) concentrates on improving the accuracy of time-independent reliability analysis when second order approximation is used. In general, SORM is more accurate than FORM because of the second-order Taylor expansion rather than the first order approximation in FORM. In the traditional SORM methods [11-16], a rotation transformation is performed after the second-order Taylor expansion. Then the general quadratic function is approximated by a paraboloid. Finally the reliability can be evaluated by closed form formulas. However, the further approximation may introduce an extra error. So a new reliability method, integrating the SPA with second order approximation, is proposed to avoid the further approximation in traditional SORM methods. This research task produces Paper II [50].

Research task 3 (RT3) applies the developed method in RT2 to reliability-based design (RBD). The objective of RBD is to obtain an optimal design with high reliability by satisfying design constraints at desired levels. During RBD, reliability is estimated

repeatedly by reliability analysis. For reliability analysis, the first order approximation is commonly used owing to its good balance between accuracy and efficiency. However, it may result in a large error when the constraint function is highly nonlinear. So the goal of this task is to improve the accuracy of RBD by introducing second order approximation. And this research task produces Paper III [51].

Research task 4 (RT4) extends the developed time-independent methodologies into time-dependent reliability analysis. In this task, the limit-state function is explicit with respect to time. So the reliability becomes time-dependent. The time-dependent reliability problem can be converted into a time-independent problem by using the extreme value of the limit-state function. Then the developed time-independent methods are introduced to improve the accuracy of predicting time-dependent reliability. This research task produces Paper IV [52].

The outcomes of above research tasks are expected to enable engineers to understand how uncertainties affect the system performance and how they can predict the reliability accurately and efficiently. In addition, this research will also help engineers design more reliable products with reduced lifecycle cost and risk. If successful, the outputs of this research will not only impact the area of engineering design, but also reliability engineering, risk management, decision making, and operations research.

1.3. ORGANIZATION OF DISSERTATION

As discussed in Section 1.2, the four research tasks in this study have produced four papers, which constitute this dissertation. The relationship between these papers is shown in Figure 1.1. Paper I focuses on the saddlepoint approximation with first order

approximation when bimodal distributions are involved. Paper II studies the saddlepoint approximation with second order approximation. Paper III is an application of the proposed method in Paper II to the reliability-based design optimization. Paper IV is an extension of the proposed method in Paper II to the time-dependent reliability analysis.

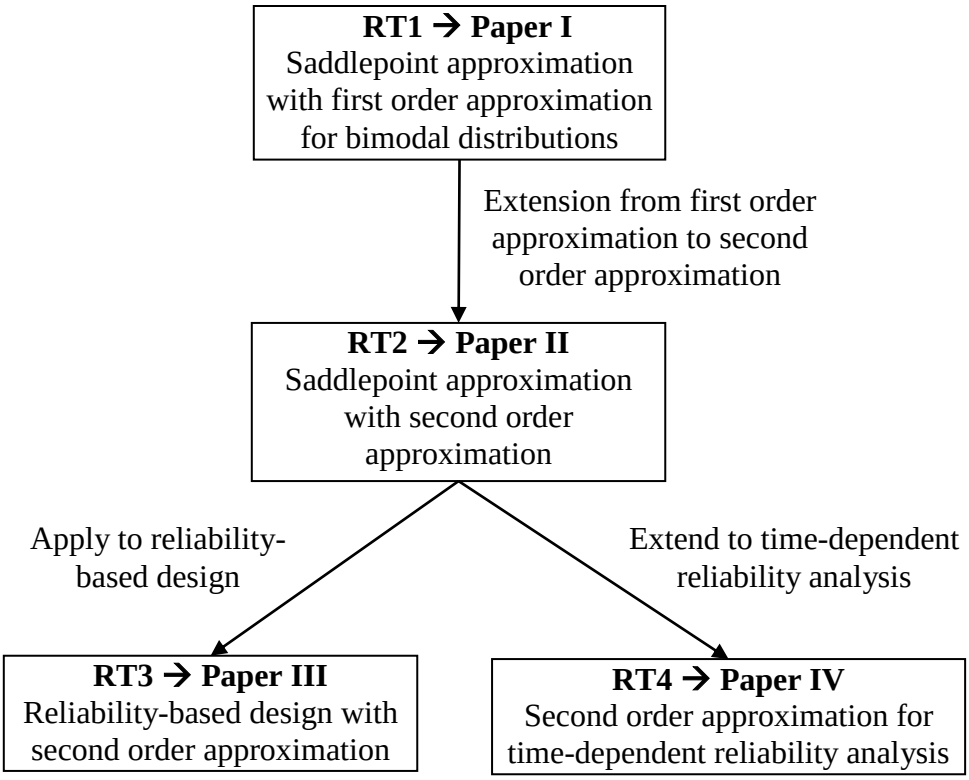

Figure 1.1. Reliability analysis with saddlepoint approximation

PAPER

I. RELIABILITY METHODS FOR BIMODAL DISTRIBUTION WITH FIRST ORDER APPROXIMATION

Zhangli Hu and Xiaoping Du

Department of Mechanical and Aerospace Engineering
Missouri University of Science and Technology

ABSTRACT

In traditional reliability problems, the distribution of a basic random variable is usually unimodal; in other words, the probability density of the basic random variable has only one peak. In real applications, some basic random variables may follow bimodal distributions with two peaks in their probability density. When binomial variables are involved, traditional reliability methods, such as the First Order Second Moment (FOSM) method and the First Order Reliability Method (FORM), will not be accurate. This study investigates the accuracy of using the saddlepoint approximation for bimodal variables and then employs saddlepoint approximation based reliability methods with first order approximation to predict the reliability. A limit-state function is at first approximated with the first-order Taylor expansion so that it becomes a linear combination of the basic random variables, some of which are bimodally distributed. The saddlepoint approximation is then applied to estimate the reliability. Examples show that the saddlepoint approximation based reliability methods are more accurate than FOSM and FORM.

1. INTRODUCTION

Reliability is the probability that a product performs its intended function without failures. The fundamental task of reliability analysis is to compute the multifold probability integral for the reliability defined by [1].

$$R = \Pr\{g(\mathbf{X}) \geq 0\} = \int_{g(\mathbf{X})\geq 0} f_{\mathbf{X}}(\mathbf{x})d\mathbf{x} \tag{1}$$

and the associated probability of failure is

$$p_f = 1 - R = \Pr\{g(\mathbf{X}) < 0\} = \int_{g(\mathbf{X})<0} f_{\mathbf{X}}(\mathbf{x})d\mathbf{x} \tag{2}$$

where $\mathbf{X} = [X_1, X_2, ..., X_n]^T$ is a vector of basic random variables, $f_{\mathbf{X}}(\mathbf{x})$ is the joint probability density function (PDF) of $\mathbf{X}$, and $g(\mathbf{X})$ is a limit-state function defined such a way that $g(\mathbf{X}) < 0$ indicates a failure event.

Accurately calculating the probability integral is difficult and computationally expensive, leading to the development of various approximation methods. Among them, the first order second moment method (FOSM) [2, 3], the first order reliability method (FORM) [4, 5], and the second order reliability method (SORM) [6-9] are the most widely used methods.

FOSM approximates the limit-state function with the first-order Taylor series expansion at the mean values of $\mathbf{X}$. It assumes $\mathbf{X}$ to be normally distributed and estimates p_f with the first two moments of the limit-state function. FOSM is easy to use and is very efficient. Its accuracy may not be good when the limit-state function is highly nonlinear and the distributions of $\mathbf{X}$ are far away from normal distributions.

FORM is in general more accurate than FOSM, but is less efficient. FORM transforms basic random variables $\mathbf{X}$ into independent standard normal variables $\mathbf{U}$. Thereafter, it linearizes the limit-state function at a point with the highest probability density at the limit state. The point is called the most probable point (MPP). Then, p_f is estimated by using the reliability index, which is the magnitude of the MPP vector [10]. FORM is most commonly used because of the good balance between accuracy and efficiency.

SORM is generally more accurate than FORM because of the second-order Taylor expansion at the MPP, and this makes the limit-state function become a complete quadratic function in standard normal variables. In the commonly used SORM methods proposed by Breitung [6] and Tvedt [7, 8], a rotation transformation is performed after the second order Taylor expansion [11]. Then the general quadratic function is approximated into a paraboloid [1, 12]. Finally the probability of failure is analytically evaluated by asymptotic formulas [6, 7, 9]. However, this method does not work well for negative curvatures at the MPP. Furthermore, the approximation of quadratic function by a paraboloid may introduce an extra error.

The aforementioned methods are used for problems when basic random variables $\mathbf{X}$ are unimodally distributed. This is the case when the PDFs of basic random variables have only one peak. In industrial applications, some random variables may follow bimodal distributions with two probability density peaks. For example, the distribution of the gross vehicle weight of trucks are characterized by a bimodal distribution having two peaks or modes based on the weigh-in-motion data [13, 14]. The study in [15, 16] also indicates that a mixture of two normal distributions could reasonably fit the observed axle

load distribution, which is used to estimate traffic levels. A bimodal distribution is also employed to model the abrupt local change of load (voltage, traffic density, or water level), which is involved in the Burgers equation for identifying the most vulnerable nodes on complex networks (power grids, road maps, and river streams) [17]. The other typical example is human-powered equipment. The force from human hands are bimodally distributed because of gender differences.

In general, the bimodal distribution can be described as a weighted sum of two specified distributions.

$$f(x) = w_1 f_1(x) + w_2 f_2(x) \tag{3}$$

where $f_1(x)$ and $f_2(x)$ are the partial PDFs' of two modes, and w_1 and w_2 are the weights that satisfy $w_1 + w_2 = 1$.

As demonstrated later in Section 4, when the bimodal variables are involved, the existing methods such as FOSM and FORM may produce large errors because they all need to transform the bimodal variables to unimodal variables that follow normal distributions. This transformation makes the limit-state function much more nonlinear. To accurately predict the reliability with bimodal random variables, we employ the saddlepoint approximation (SPA) [18-23] in this work.

There are two major contributions of this study. First, we clearly demonstrate that SPA can accurately approximate the CDF of a bimodal distribution. The significance of this finding is that there is no need to transform a bimodal distribution as traditional reliability methods do. This will therefore avoid large errors due to the transformation. Second, based on the finding, we employ the mean value SPA method (MVSPA) [24, 25] and first order SPA method (FOSPA) [26] to accommodate bimodal distribution in

reliability analysis. Both methods approximate the limit-state function by the first-order Taylor series expansion, so that the original limit-state function becomes a linear combination of basic random variables, some of which are bimodally distributed. Then the cumulant generating function (CGF) of the limit-state function is analytically available, and the SPA is applied to estimate the probability of failure.

The rest of this paper is organized as follows: Section 2 presents the theoretical background of this work, including FOSM, FORM and SPA. Then the proposed MVSPA and FOSPA are discussed in Section 3, followed by three engineering examples in Section 4. Conclusions are given in Section 5.

2. REVIEW OF METHODOLOGIES

In this section, we briefly review FOSM, FORM, and SPA. All the basic random variables used in this work are assumed to be independent.

2.1. FOSM

As implied by its name, FOSM uses the first order approximation to the limit-state function and the first two moments of basic random variables. The limit-state function is approximated with the first-order Taylor series expansion at the mean values of basic random variables [2, 27, 28]. Thus the limit-state function becomes

$$\begin{aligned} Y = g(\mathbf{X}) &\approx g(\boldsymbol{\mu}) + \sum_{i=1}^{n} \left.\frac{\partial g(\mathbf{X})}{\partial X_i}\right|_{\boldsymbol{\mu}} (X_i - \mu_i) \\ &= g(\boldsymbol{\mu}) + \nabla g(\boldsymbol{\mu})^T (\mathbf{X} - \boldsymbol{\mu}) \end{aligned} \tag{4}$$

where $\boldsymbol{\mu} = [\mu_1, \mu_2, ..., \mu_n]^T$ is a vector of the mean values of $\mathbf{X}$, and $\nabla g(\boldsymbol{\mu})$ is the gradient of $g(\mathbf{X})$ at $\mathbf{X} = \boldsymbol{\mu}$, given by

$$\nabla g(\boldsymbol{\mu}) = \left(\left.\frac{\partial g(\mathbf{X})}{\partial X_1}\right|_{\boldsymbol{\mu}}, \left.\frac{\partial g(\mathbf{X})}{\partial X_2}\right|_{\boldsymbol{\mu}}, ..., \left.\frac{\partial g(\mathbf{X})}{\partial X_n}\right|_{\boldsymbol{\mu}} \right)^T \tag{5}$$

Then the mean and standard deviation of the limit-state function are computed by

$$\mu_Y = g(\boldsymbol{\mu}) \tag{6}$$

$$\sigma_Y = \sqrt{\sum_{i=1}^{n} \left(\left.\frac{\partial g(\mathbf{X})}{\partial X_i}\right|_{\boldsymbol{\mu}} \right)^2 \sigma_i^2} \tag{7}$$

where σ_i is the standard deviation of X_i.

If all the basic random variables are assumed to be normally distributed, then the probability of failure is easily estimated by

$$p_f = \Pr\left\{g\left(\mathbf{X}\right) < 0\right\} = \Phi\left(\frac{-\mu_Y}{\sigma_Y}\right) \tag{8}$$

where $\Phi(\cdot)$ is the cumulative distribution function (CDF) of a standard normal distribution.

FOSM only requires the first two moments of basic random variables. So FOSM is easy to use and is efficient. However, it may produce a large error when the distributions of basic random variables are far away from normal distributions and the limit-state function is highly nonlinear.

2.2. FORM

FORM [29-32] first transforms $\mathbf{X}$ in the X-space into standard normal variables $\mathbf{U}$ in the U-space. The transformation is given by [33, 34]

$$F_{X_i}(X_i) = \Phi(U_i) \tag{9}$$

in which $F_{X_i}(\cdot)$ and $\Phi(\cdot)$ represents CDFs of X_i and U_i, respectively. Eq. (9) is applicable for independent variables. The transformation for dependent variables is given by the Nataf transformation [33].

After the transformation, the limit-state function becomes

$$Y = g(\mathbf{X}) = G(\mathbf{U}) \tag{10}$$

For the minimal error from the linearization, the function is expanded at the point that has the highest probability density, and this point is called the most probable point (MPP), denoted by $\mathbf{u}^*$. MPP is obtained by solving

$$\begin{cases} \min \ \ \|\mathbf{u}\| = \sqrt{\mathbf{u}^T\mathbf{u}} \\ \text{s.t.} \quad G(\mathbf{u}) = 0 \end{cases} \tag{11}$$

The limit-state function is linearized at the MPP.

$$\begin{aligned} G(\mathbf{U}) &\approx G(\mathbf{u}^*) + \sum_{i=1}^{n} \left.\frac{\partial G}{\partial U_i}\right|_{\mathbf{U}=\mathbf{u}^*} (U_i - u_i^*) \\ &= -\nabla G(\mathbf{u}^*)^T \mathbf{u}^* + \sum_{i=1}^{n} \left.\frac{\partial G}{\partial U_i}\right|_{\mathbf{U}=\mathbf{u}^*} U_i \end{aligned} \tag{12}$$

The magnitude of $\mathbf{u}^*$ is β, called the reliability index given by

$$\beta = \sqrt{\left(u_1^*\right)^2 + \ldots + \left(u_n^*\right)^2} \tag{13}$$

Then the probability of failure is computed by

$$p_f = \Phi(-\beta) \tag{14}$$

FORM has good accuracy when the nonlinearity of transformed limit-state function $G(\mathbf{U})$ is not high.

2.3. SPA

The saddlepoint approximation (SPA) was developed in statistics. It can accurately approximate the CDF of a random variable at a distribution tail [18, 35]. Let Y denote a response random variable with PDF $f_Y(y)$ and CDF $F_Y(y)$. The moment generating function (MGF) of Y is defined by

$$M_Y(t) = E(e^{tY}) = \int_{-\infty}^{+\infty} e^{tY} f_Y(y) dy \tag{15}$$

Then the cumulant generating function is given by

$$K_Y(t) = \ln\left(M_Y(t)\right) \tag{16}$$

The SPA is used to approximate the CDF of Y with [36]

$$F_Y(y) = \Pr\{Y < y\} = \Phi(w) + \phi(w)\left\{\frac{1}{w} - \frac{1}{\upsilon}\right\} \tag{17}$$

where $\phi(\cdot)$ is the PDF of the standard normal distribution.

$$w = \text{sgn}(t_s)\left\{2\left[t_s y - K_Y(t_s)\right]\right\}^{1/2} \tag{18}$$

$$\upsilon = t_s\left[K_Y''(t_s)\right]^{1/2} \tag{19}$$

in which $\text{sgn}(t_s) = +1, -1$ or 0, depending on whether t_s is positive, negative, or zero; $K_Y''(t)$ is the second derivative of $K_Y(t)$ with respect to t, and t_s is the saddlepoint obtained from

$$K_Y'(t_s) = y \tag{20}$$

Given the good accuracy of SPA, many SPA-based reliability methods have been developed, including MVSPA [24, 25] and FOSPA [26]. However, these methods are intended for basic random variables with unimodal distributions. The purpose of this study is to investigate if SPA is also applicable for bimodal random variables with good accuracy. The details are provided in Section 3.

3. SADDLEPOINT APPROXIMATION FOR BIMODAL DISTRIBUTIONS

As discussed previously, FOSM and FORM are effective, but they may not be accurate enough when bimodal random variables are involved. It is not clear if SPA could improve the accuracy. To answer this question, we at first investigate if SPA could provide an accurate estimate for a tail CDF of a bimodal random variable. With the promising results, we then introduce SPA for reliability analysis with bimodal distributions. The major strategy is to linearize the limit-state function at the mean values in the X-space or the MPP in the X-space, and then SPA is employed.

3.1. SPA FOR A BIMODAL DISTRIBUTION

The PDF of a bimodal distribution is usually given by a weighted sum of two specified distributions as indicated in Eq. (3). An example of the bimodal PDF is shown in Figure 1.

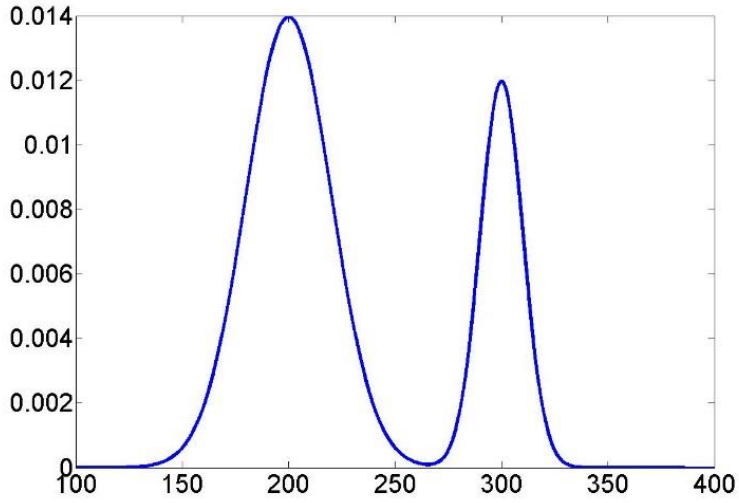

Figure 1. A bimodal distribution with a mixture of two normal distributions

For the general bimodal distribution in Eq. (3), the MGF is

$$\begin{aligned} M_X(t) &= \int_{-\infty}^{+\infty} e^{tX}\left(w_1 f_1(x) + w_2 f_2(x)\right)dx \\ &= w_1 M_1(t) + w_2 M_2(t) \end{aligned} \tag{21}$$

where $M_1(t)$ and $M_2(t)$ are the moment generating functions of $f_1(x)$ and $f_2(x)$, respectively.

Then CGF is obtained based on Eq. (16).

$$K(t) = \ln\left[w_1 M_1(t) + w_1 M_2(t)\right] \tag{22}$$

Table 1 lists the CGFs of some common distributions.

Table 1. CGFs of some common distributions

Distribution	PDF	CGF
Normal	$f(x) = \frac{1}{\sqrt{2\pi}} e^{\frac{(x-\mu)^2}{2\sigma^2}}$	$K(t) = \mu t + \frac{1}{2}\sigma^2 t^2$
Exponential	$f(x) = \lambda e^{-\lambda x}$	$K(t) = -\ln(1-\frac{t}{\lambda})$
Gumbel	$f(x) = \frac{1}{\beta} e^{\left(-\frac{x-\alpha}{\beta}\right)} e^{-e^{\left(-\frac{x-\alpha}{\beta}\right)}}$	$K(t) = \alpha t + \ln\left(\Gamma\left(1-\beta t\right)\right)$

We now investigate SPA for two cases: 1) a bimodal distribution with a mixture of two normal distributions, and 2) a bimodal distribution with a mixture of two non-normal distributions.

3.1.1. Case 1: Bimodal Distribution with A Mixture of Two Normal Distributions. For a bimodal distribution with a mixture of two normal distributions, the PDF is defined by

$$f(x) = w_1 \phi\left(\frac{x-\mu_1}{\sigma_1}\right)\frac{1}{\sigma_1} + w_2 \phi\left(\frac{x-\mu_2}{\sigma_2}\right)\frac{1}{\sigma_2} \tag{23}$$

where μ_1 and σ_1 are the mean and standard deviation of the first mode, respectively, and μ_2 and σ_2 are the mean and standard deviation of the second mode, respectively.

The CGF of X is expressed as

$$K(t) = \ln\left(w_1 e^{\mu_1 t + \frac{1}{2}\sigma_1^2 t^2} + w_2 e^{\mu_2 t + \frac{1}{2}\sigma_2^2 t^2}\right) \tag{24}$$

SPA is easily used to approximate the CDF using Eqs. (17-20). Now let us use a random load X, whose PDF is a weighted sum of two normal PDFs, as an example to investigate the accuracy of the tail CDF estimation.

The PDF of the load X is given by

$$f_X(x) = 0.6\phi\left(\frac{x-200}{20}\right)\frac{1}{20} + 0.4\phi\left(\frac{x-300}{10}\right)\frac{1}{10} \tag{25}$$

Then the CDF and CGF are obtained as

$$F_X(x) = 0.6\Phi\left(\frac{x-200}{20}\right) + 0.4\Phi\left(\frac{x-300}{10}\right) \tag{26}$$

$$K(t) = \ln\left(0.6e^{200t + \frac{1}{2}\left(20^2\right)t^2} + 0.4e^{300t + \frac{1}{2}\left(10^2\right)t^2}\right) \tag{27}$$

SPA is used to approximate the tail CDF and is compared with respect to the analytical solution given by

$$\Pr\{X \le x\} = F_X(x) \tag{28}$$

The results are presented in Table 2, which show that SPA yields high accuracy in estimating tail CDFs.

Table 2. CDFs of a bimodal distribution with two normal distributions

x	$F_X(x)$	SPA	Relative Error	Absolute Error
100	1.7199×10^{-7}	1.7234×10^{-7}	0.20%	3.5×10^{-10}
110	2.0386×10^{-6}	2.0447×10^{-6}	0.30%	6.1×10^{-9}
120	1.9003×10^{-5}	1.9090×10^{-5}	0.46%	8.7×10^{-8}
130	1.3958×10^{-4}	1.4060×10^{-4}	0.73%	1.02×10^{-6}

3.1.2. Case 2: Bimodal Distribution with A Mixture of Two Gumbel Distributions. We use a bimodal distribution with a mixture of two Gumbel distribution as an example to investigate SPA for non-normal distribution. The PDF is given by

$$f(x) = w_1 \frac{1}{\beta_1} e^{\left(-\frac{x-\alpha_1}{\beta_1}\right)} e^{-e^{\left(-\frac{x-\alpha_1}{\beta_1}\right)}} + w_2 \frac{1}{\beta_2} e^{\left(-\frac{x-\alpha_2}{\beta_2}\right)} e^{-e^{\left(-\frac{x-\alpha_2}{\beta_2}\right)}} \tag{29}$$

where α_1 and α_2 are location parameters; β_1 and β_2 are shape parameters.

Then the CDF and CGF are obtained as

$$F_X(x) = w_1 e^{-e^{\left(-\frac{x-\alpha_1}{\beta_1}\right)}} + w_2 e^{-e^{\left(-\frac{x-\alpha_2}{\beta_2}\right)}} \tag{30}$$

$$K(x) = \ln\left(w_1 e^{\alpha_1 t}\Gamma(1-\beta t) + w_2 e^{u_2 t}\Gamma(1-\beta_2 t)\right) \tag{31}$$

where $\Gamma(\cdot)$ is the gamma function.

Let us also use the load example to investigate the SPA for a bimodal distribution with a mixture of two Gumbel distributions. The distribution parameters of X are given in Table 3.

SPA is then used to estimate the tail CDFs and is compared with respect to the analytical solution. The results are given in Table 4 and show that SPA also has a high

accuracy for estimating the tail CDFs of a bimodal distribution with mixed Gumbel distributions.

Table 3. Distribution parameters of load X

Variable	Distribution	Weight	Mean μ	Standard Deviation σ
X	Bimodal Gumbel	0.6	15000	500
		0.4	30000	1000

where

$$\begin{cases} \mu = \alpha + 0.5772\beta \\ \sigma = \dfrac{\pi}{\sqrt{6}}\beta \end{cases} \tag{32}$$

Therefore

$$\begin{cases} \alpha = \mu - 0.5772\beta \\ \beta = \dfrac{\sqrt{6}}{\pi}\sigma \end{cases} \tag{33}$$

Table 4. CDFs of a bimodal distribution with two Gumbel distributions

x	$F_X(x)$	SPA	Relative Error	Absolute Error
13860	1.7297×10^{-5}	1.7460×10^{-5}	0.94%	1.63×10^{-7}
13900	4.7942×10^{-5}	4.8451×10^{-5}	1.06%	5.09×10^{-7}
14000	4.0529×10^{-4}	4.1126×10^{-4}	1.47%	5.97×10^{-6}
14060	1.1482×10^{-3}	1.1692×10^{-3}	1.82%	2.1×10^{-5}

3.2. SPA METHODS FOR BIMODAL DISTRIBUTIONS WITH FIRST ORDER APPROXIMATIONS

We have demonstrated the accuracy of SPA for a bimodal distribution. Since the output of a limit-state function could also be bimodal given the bimodal basic variables, it is expected that SPA will also work well for the prediction of the probability of failure, which is the CDF at the tail of the response distribution. As a result, bimodal distributions could be considered. In this study, we extend MVSPA and FOSPA so that bimodal basic random variables are accommodated.

3.2.1. MVSPA. The limit-state function is first approximated at the mean values of basic random variables using the first-order Taylor series expansion

$$\begin{aligned} Y = g(\mathbf{X}) &\approx L(\mathbf{X}) \\ &= g(\boldsymbol{\mu}) + \sum_{i=1}^{n} \left.\frac{\partial g(\mathbf{X})}{\partial X_i}\right|_{\boldsymbol{\mu}} (X_i - \mu_i) \\ &= \left(g(\boldsymbol{\mu}) - \sum_{i=1}^{n} \left.\frac{\partial g(\mathbf{X})}{\partial X_i}\right|_{\boldsymbol{\mu}} \mu_i \right) + \sum_{i=1}^{n} \left.\frac{\partial g(\mathbf{X})}{\partial X_i}\right|_{\boldsymbol{\mu}} X_i \end{aligned} \tag{34}$$

To obtain the CGF of $L(\mathbf{X})$, we need to use some properties of CGF [37].

1) For a constant $Y = c$, the CGF is $K_Y = ct$.

2) If $Y = aX$, then $K_Y(t) = K_X(at)$, where $K_X(t)$ and $K_Y(t)$ are the CGFs of X and Y, respectively, and a is constant.

3) If X and Y are independent, then $K_{X+Y}(t) = K_X(t) + K_Y(t)$, where $K_{X+Y}(t)$ is the CGF of $X + Y$.

Using the above properties and Eq. (34), we obtain the CGF of the limit-state function.

$$K_L(t) = \left(g(\boldsymbol{\mu}) - \sum_{i=1}^{n} \left. \frac{\partial g(\mathbf{X})}{\partial X_i} \right|_{\boldsymbol{\mu}} \mu_i \right) t + \sum_{i=1}^{n} K_{X_i} \left(\left. \frac{\partial g(\mathbf{X})}{\partial X_i} \right|_{\boldsymbol{\mu}} t \right) \tag{35}$$

If X_i follows a bimodal distribution, K_{X_i} can be obtained from Eq. (22); examples included those are given in Eqs. (24) and (31).

Thus the first and second derivatives of $K_L(t)$ are

$$K_L^{'}(t) = g(\boldsymbol{\mu}) - \sum_{i=1}^{n} \left. \frac{\partial g(\mathbf{X})}{\partial X_i} \right|_{\boldsymbol{\mu}} \mu_i + \left. \frac{\partial g(\mathbf{X})}{\partial X_i} \right|_{\boldsymbol{\mu}} \sum_{i=1}^{n} K_{X_i}^{'} \left(\left. \frac{\partial g(\mathbf{X})}{\partial X_i} \right|_{\boldsymbol{\mu}} t \right) \tag{36}$$

$$K_L^{''}(t) = \left(\left. \frac{\partial g(\mathbf{X})}{\partial X_i} \right|_{\boldsymbol{\mu}} \right)^2 \sum_{i=1}^{n} K_{X_i}^{''} \left(\left. \frac{\partial g(\mathbf{X})}{\partial X_i} \right|_{\boldsymbol{\mu}} t \right) \tag{37}$$

Once $K_L^{'}(t)$ is available, the saddlepoint is obtained by solving the equation

$$K_L^{'}(t_s) = g(\boldsymbol{\mu}) - \sum_{i=1}^{n} \left. \frac{\partial g(\mathbf{X})}{\partial X_i} \right|_{\boldsymbol{\mu}} \mu_i + \left. \frac{\partial g(\mathbf{X})}{\partial X_i} \right|_{\boldsymbol{\mu}} \sum_{i=1}^{n} K_{X_i}^{'} \left(\left. \frac{\partial g(\mathbf{X})}{\partial X_i} \right|_{\boldsymbol{\mu}} t_s \right) = 0 \tag{38}$$

Based on Eq. (17), the probability of failure is calculated by

$$p_f = \Pr\{g(\mathbf{X}) < 0\} = \Phi(w) + \phi(w) \left\{ \frac{1}{w} - \frac{1}{\upsilon} \right\} \tag{39}$$

in which

$$w = \operatorname{sgn}(t_s) \left\{ 2 \left[-K_L^{'}(t) \right] \right\}^{1/2} \tag{40}$$

$$\upsilon = t_s \left[K_L^{''}(t_s) \right]^{1/2} \tag{41}$$

3.2.2. FOSPA. The limit-state function is first linearized at point $\mathbf{x}^*$ where the integrand of the integral $p_f = \int_{g(\mathbf{X})<0} f_{\mathbf{X}}(\mathbf{x}) d\mathbf{x}$ has the maximum value in the failure

region $g(\mathbf{X}) < 0$. $\mathbf{x}^*$ is therefore the MPP in the X-space because it has the highest probability density.

The following model is used to identify the MPP $\mathbf{x}^*$:

$$\begin{cases} \max\limits_{\mathbf{x}} & \prod\limits_{i=1}^{n} f_i(x_i) \\ s.t. & g(\mathbf{x}) = 0 \end{cases} \tag{42}$$

The linear form of $g(\mathbf{X})$ at $\mathbf{x}^*$ is

$$g(\mathbf{X}) \approx L(\mathbf{X}) = \left(g(\mathbf{x}^*) - \sum_{i=1}^{n} \left. \frac{\partial g(\mathbf{X})}{\partial X_i} \right|_{\mathbf{x}^*} x_i^* \right) + \sum_{i=1}^{n} \left. \frac{\partial g(\mathbf{X})}{\partial X_i} \right|_{\mathbf{x}^*} X_i \tag{43}$$

Then the CGF of $L(\mathbf{X})$ can be easily obtained based on the procedure described in Section 3.2.1. Finally the saddlepoint is solved and is used to estimate p_f.

The procedure of FOSPA is similar to that of MVSPA. The only difference is that FOSPA linearizes the limit-state function at the MPP while MVSPA linearizes the limit-state function at the mean values.

3.2.3. Numerical Procedure. The numerical procedure of MVSPA and FOSPA is summarized as follows:

Step 1: Derive CGFs of bimodal basic random variables with Eqs. (21) and (22).

Step 2: Linearize the limit-state function at the mean values of basic random variables with Eq. (34) for MVSPA or at the MPP with Eq. (43) for FOSPA after the MPP search using Eq. (42).

Step 3: Obtain the CGF of limit-state function using Eq. (35).

Step 4: Solve Eq. (38) to obtain the saddlepoint.

Step 5: Calculate the probability of failure p_f using Eqs. (39-41)

The flowchart of MVSPA and FOSPA is given in Figure 2.

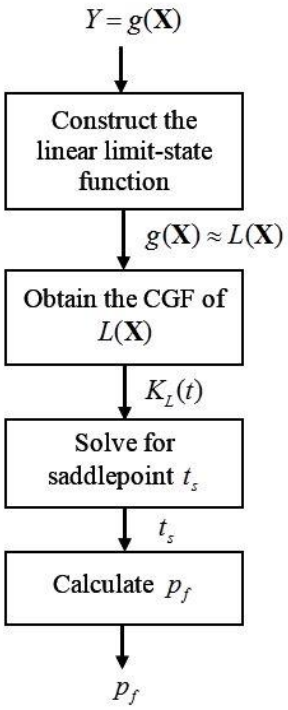

Figure 2. Flowchart of the SPA methods

The SPA methods use the first order approximation. Although they improve the accuracy of FORM, they also share the same drawbacks as FORM, especially for dependent basic random variables. The SPA methods may not be accurate when many basic random variables are strongly dependent because the dependence to independence transformation may make a limit-state function in the transformed space highly nonlinear. For large scale problems, the SPA methods can behave the same way as FORM because of the use of the MPP in the original space [38-41]. For the same reason, the SPA methods do not work well when multiple MPPs exist [42, 43].

4. NUMERICAL EXAMPLES

Three engineering problems are used to evaluate the accuracy of MVSPA and FOSPA. We at first examine a simply supported beam with a linear limit-state function. Then a speed reducer shaft is used to validate the two SPA methods for a nonlinear limit-state function. Finally a roof truss structure is modified to investigate the effectiveness of SPA methods for bimodal distributions with a mixture of non-normal distributions.

To show the benefits of MVSPA and FOSPA, we compare them with other two first-order methods, including FOSM and FORM, which have been reviewed in Section 2. The accuracy is evaluated by the error relative to the result from Monte Carlo Simulation (MCS) with a large sample size, or an analytical solution if it is available. The relative error is defined as

$$\varepsilon\% = \left| \frac{p_f - p_{f,\text{accurate}}}{p_{f,\text{accurate}}} \right| \times 100\% \tag{44}$$

where p_f is the result from FOSM, FORM, MVSPA or FOSPA, and $p_{f,\text{accurate}}$ is the MCS or analytical solution.

We also give the number of function calls, which serves as a measure of efficiency.

4.1. EXAMPLE 1: SIMPLE SUPPORT BEAM

A simply supported beam shown in Figure 3 is subjected to a random force P following a bimodal distribution. The PDF of P is a mixture of two different normal distributions and is given by

$$f_P(x) = 0.7\phi\left(\frac{x-200}{20}\right)\frac{1}{20} + 0.3\phi\left(\frac{x-300}{10}\right)\frac{1}{10} \tag{45}$$

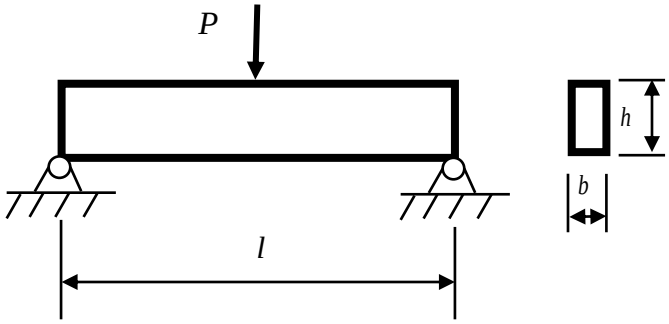

Figure 3. A simple support beam

A failure occurs if the applied stress is larger than the yield strength. Then the limit-state function of the beam is defined by

$$g(\mathbf{X}) = S_y - \frac{3l}{bh^2}P \tag{46}$$

in which $\mathbf{X} = (S_y, P)$, S_y is the yield strength, l is the length of beam, b is the length of the cross section, and h is the height of the cross section. The limit-state function is linear with respect to the two basic random variables. The distributions and parameters of these variables are given in Table 5.

The probability of failure is computed by FOSM, FORM, MVSPA and FOSPA. The results are compared with respect to an analytical solution which exists for this problem.

In FOSM, the mean and standard deviation of force P, which is bimodally distributed, are calculated by

$$\mu_P = w_1\mu_1 + w_2\mu_2 = 230 \tag{47}$$

$$\sigma_P = \sqrt{w_1[\sigma_1^2 + \mu_1^2] + w_2[\sigma_2^2 + \mu_2^2] - \mu_P^2} = 49.09 \tag{48}$$

μ_P and σ_P are used for the non-normal to normal transformation in Eq. (9) when FORM is used.

Table 5. Distributions of the variables in simple support beam

Variables	Distribution	Weight	Mean	Standard Deviation
S_y(kpsi)	Normal	-	110	12.5
P (lb)	Bimodal Normal	(0.7, 0.3)	(200, 300)	(20, 10)
l (in)	Deterministic	-	6	-
b (in)	Deterministic	-	0.2	-
h (in)	Deterministic	-	0.6	-

For this example, the probability of failure can be analytically evaluated by

$$\begin{aligned} p_f &= \Pr\{g(\mathbf{X}) < 0\} \\ &= \Pr\left\{S_y - \frac{3l}{bh^2}P < 0\right\} \\ &= \int_0^{+\infty} F_{S_y}\left(\frac{3l}{bh^2}x\right) f_P(x)\,dx \end{aligned} \tag{49}$$

The above univariate integration can be estimated by a numerical integration method, such as adaptive Simpson quadrature [44, 45].

The results are presented in Table 6, which show MVSPA and FOSPA produce the most accurate results, while MVSPA maintains the same efficiency as FOSM.

The relative error of FOSM is 43.4 %. The reason for this large error is explained in Figure 4. It shows that FOSM approximates the actual bimodal normal distribution (solid line) of the response by a unimodal normal distribution (dotted line) using the first two moments. The two distributions are quite different, including the left tail area, where a failure occurs. This causes a large error.

Table 6. Probability of failure of simple support beam

Method	p_f	Relative Error	Absolute Error	Function Calls
FOSM	1.3635×10^{-3}	43.4%	4.1289×10^{-4}	3
FORM	1.2839×10^{-3}	35.1%	3.3329×10^{-4}	44
MVSPA	9.4416×10^{-4}	0.68%	6.45×10^{-6}	3
FOSPA	9.4416×10^{-4}	0.68%	6.45×10^{-6}	12
Analytical Solution	9.5061×10^{-4}	-	-	-

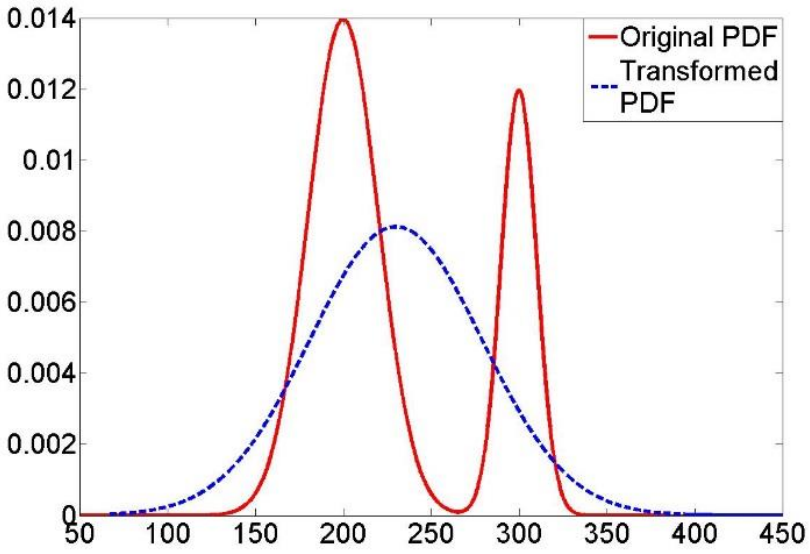

Figure 4. PDF approximation using FOSM

The error of FORM is 35.1%. Figures 5 and 6 explain the reason for this error. Figure 5 indicates that the limit-state function in the X-space is linear. However, the limit-state function in the U-space becomes highly nonlinear after the bimodal to unimodal transformation shown in Figure 6. The linearization in the U-space produces a large error.

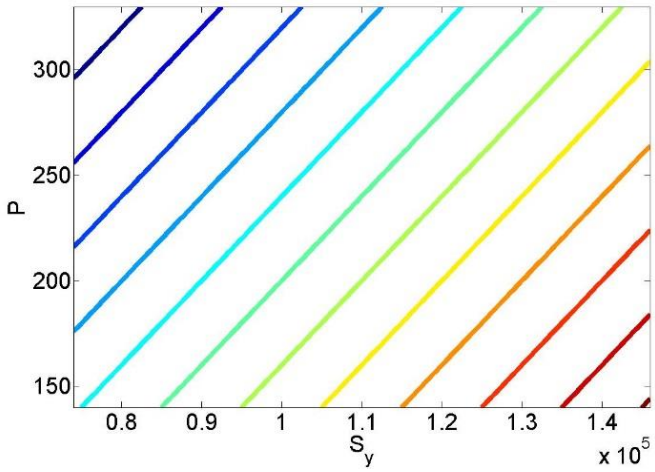

Figure 5. Contours of the limit-state function in the X-space

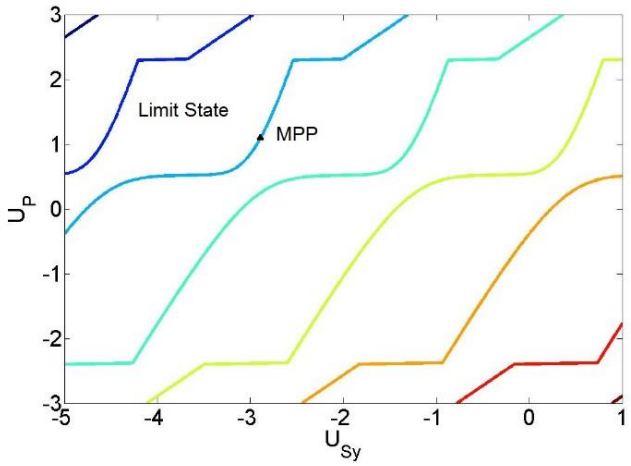

Figure 6. Contours of the limit-state function in the U-space

4.2. EXAMPLE 2: SPEED REDUCER SHAFT

A speed reducer shaft shown in Figure 7 is subjected to a random force P and a random torque T, which are bimodally normally distributed. The PDFs of the two loads are given by

$$f_P(x) = 0.6\phi\left(\frac{x-1500}{150}\right)\frac{1}{150} + 0.4\phi\left(\frac{x-2200}{50}\right)\frac{1}{50} \tag{50}$$

$$f_T(x) = 0.7\phi\left(\frac{x-400}{100}\right)\frac{1}{100} + 0.3\phi\left(\frac{x-500}{50}\right)\frac{1}{50} \tag{51}$$

The limit-state function is defined by the difference between the strength and the maximum equivalent stress and is given by

$$g(\mathbf{X}) = S_y - \frac{16}{\pi d^3}\sqrt{4P^2l^2 + 3T^2} \tag{52}$$

where $\mathbf{X} = (S_y, d, l, P, T)$. The distributions and parameters of the basic random variables are described in the Table 7.

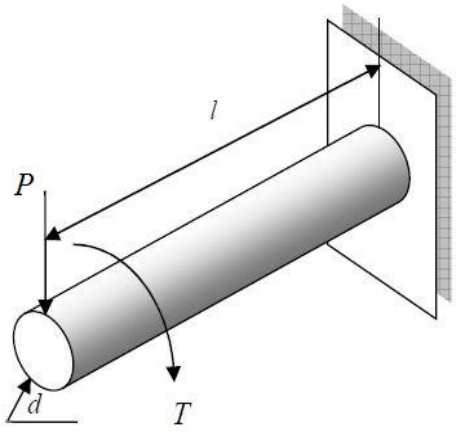

Figure 7. A speed reducer shaft

Table 7. Distributions of the variables in speed reducer shaft

Variables	Distribution	Weight	Mean	Standard Deviation
S_y (MPa)	Normal	-	250	35
d (mm)	Normal	-	40	0.1
l (mm)	Normal	-	400	0.1
P (N)	Bimodal Normal	(0.6, 0.4)	(1500, 2200)	(150, 50)
T (N·m)	Bimodal Normal	(0.7, 0.3)	(400, 500)	(100, 50)

FOSM, FORM, MVSPA and FOSPA are compared with respect to the solution from MCS with 10^6 runs. The results are shown in Table 8, and they indicate that both SPA based methods yield high accuracy. FOSPA is the most accurate method but it is not as efficient as MVSPA because of the MPP search in the X-space.

Table 8. Probability of failure of speed reducer shaft

Method	p_f	Relative Error	Absolute Error	Function Calls
FOSM	1.4716×10^{-3}	16.4%	2.076×10^{-4}	11
FORM	2.2018×10^{-3}	74.2%	9.378×10^{-4}	60
MVSPA	1.2038×10^{-3}	4.76%	6.02×10^{-5}	11
FOSPA	1.2411×10^{-3}	1.81%	2.29×10^{-5}	102
MCS	1.2640×10^{-3}	-	-	1×10^{6}

FOSM is not accurate since it only uses the first two moments, which cannot capture the full information of bimodal distribution. FORM also produces a significant error because it linearizes the limit-state function at the MPP, while the nonlinearity is high due to the bimodal distributions.

4.3. EXAMPLE 3: ROOF TRUSS

A roof truss structure problem [46, 47] shown in Figure 8 is modified and is used as the third example. In this structure, the top chords and compression bars of the truss are reinforced by concrete, and the bottom chords and tension bars are made of steel. A uniformly distributed load q is assumed to be applied on the roof truss, and then it can be transformed into the nodal load $P = ql/4$. A failure occurs if the perpendicular deflection of truss peak node is larger than 5.4 cm. Then the limit-state function of truss structure is defined by

$$g(\mathbf{X}) = 0.054 - \frac{ql^2}{2}\left(\frac{3.81}{A_C E_C} + \frac{1.13}{A_S E_S}\right) \tag{53}$$

where $\mathbf{X} = [q, l, A_s, A_c, E_S, E_C]$. Table 9 presents the parameters of basic random variables in the limit-state function.

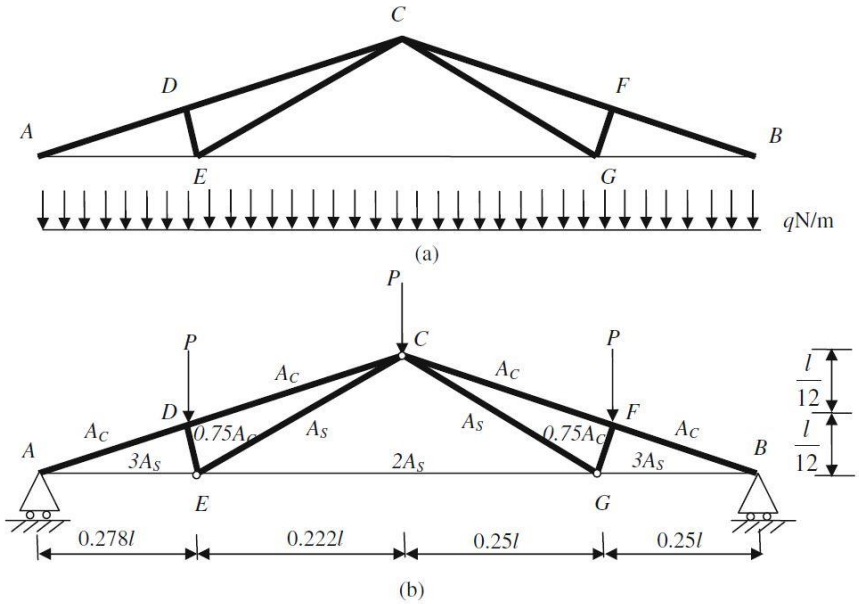

Figure 8. A roof truss structure

The results of the roof truss structure are presented in Table 10. They indicate that FOSPA is the most accurate method. FOSM and FORM are not accurate since both of them need to transform the bimodal distribution to a unimodal distribution. MVSPA produces a large error due to the linearization of limit-state function at the mean values, where the nonlinearity is high.

Table 9. Distributions of the variables in roof truss structure

Variables	Distribution	Weight	Mean	Standard Deviation
$q(\mathrm{N/m})$	Bimodal Gumbel	(0.7, 0.3)	(15000, 30000)	(1500, 3000)
$l(\mathrm{m})$	Normal	-	12.6	0.01
$A_s(\mathrm{m}^2)$	Normal	-	9.82×10^{-4}	1×10^{-5}
$A_c(\mathrm{m}^2)$	Normal	-	4×10^{-2}	1×10^{-5}
$E_s(\mathrm{Pa})$	Normal	-	1×10^{11}	1×10^{10}
$E_c(\mathrm{Pa})$	Normal	-	2×10^{10}	2×10^{9}

Table 10. Probability of failure of roof truss

Method	p_f	Relative Error	Absolute Error	Function Calls
FOSM	1.1722×10^{-3}	60.9%	1.8296×10^{-3}	13
FORM	2.5357×10^{-3}	15.5%	4.661×10^{-4}	75
MVSPA	1.4208×10^{-3}	52.7%	1.581×10^{-3}	13
FOSPA	2.8616×10^{-3}	4.67%	1.402×10^{-4}	188
MCS	3.0018×10^{-3}	-	-	5×10^{6}

5. CONCLUSIONS

Bimodal distributions are encountered in many engineering applications, but traditional reliability methods may not be able to handle them well due to large reliability prediction errors. This work at first investigates if high accuracy can be maintained when saddlepoint approximation is used for a single bimodal random variable. The experiments on a random variable with a mixture of two normal distributions and two Gumbel distributions indicate that saddlepoint approximation can accurately approximate the probability in the tail areas of the bimodal distribution. This finding suggests that the saddlepoint approximation could be potentially used for reliability analysis with bimodal basic random variables with good accuracy, and this is confirmed by two saddlepint approximation based reliability methods: mean value saddlepoint approximation method (MVSPA) and first order saddlepoint approximation method (FOSPA). MVSPA approximates a limit-state function with the first-order Taylor expansion at the mean values of basic random variables while FOSPA approximates the limit-state function at MPP. Thereafter, saddlepoint approximation is applied to estimate the probability of failure.

Both methods avoid approximating bimodal distributions with unimodal distributions and therefore avoid the chance of increasing the nonlinearity of the limit-state function. The three examples demonstrate the accuracy and efficiency of saddlepoint approximation based reliability methods.

Since MVSPA linearizes the limit-state function at mean values, its accuracy may not be good if the limit-state function is highly nonlinear at mean values. The accuracy

can be improved by integrating the saddlepoint approximation with the first and second order reliability methods.

FOSPA is generally more accurate than MVSPA, but less efficient. It linearizes the limit-state function at the MPP, the point where joint PDF of the basic random variables is at its maximum value. However, FOSPA will not work if some of the basic random variables do not have closed-form CGFs. In this case, these random variables need to be transformed into other random variables that have CGFs before linearization.

Saddlepoint approximation can accurately approximate the CDF of a random variable at a distribution tail. Although bimodal distributions are only investigated in the work, saddlepoint approximation based reliability methods are potentially applicable for multimodal basic random variables. So the possible future research task is to investigate the use of saddlepoint approximation for multimodal distributions with more than two probability density peaks. The other potential research tasks may include investigating the applicability of saddlepoint approximation for dependent basic random variables and high dimensional reliability problems.

ACKNOWLEDGEMENTS

This material is based upon work supported by the National Science Foundation under grants CMMI 1562593 and the Intelligence Systems Center at Missouri University of Science and Technology.

REFERENCES

[1] Choi, S.-K., Grandhi, R., and Canfield, R. A., 2006, Reliability-based structural design, Springer Science & Business Media.

[2] Elishakoff, I., Van Manen, S., and Arbocz, J., 1987, "First-order second-moment analysis of the buckling of shells with random imperfections," AIAA journal, 25(8), pp. 1113-1117.

[3] Mahadevan, S., and Haldar, A., 2000, "Probability, reliability and statistical method in engineering design," John Wiley & Sons, New York.

[4] Hasofer, A., Lind, N., and Division, UoWSM., 1973, "An exact and invariant first-order reliability format," University of Waterloo, Solid Mechanics Division.

[5] Hohenbichler, M., and Rackwitz, R., 1983, "First-order concepts in system reliability," Structural safety, 1(3), pp. 177-188.

[6] Breitung, K., 1984, "Asymptotic approximations for multinormal integrals," Journal of Engineering Mechanics, 110(3), pp. 357-366.

[7] Tvedt, L., 1983, "Two second-order approximations to the failure probability," Section on structural reliability.

[8] Tvedt, L., 1990, "Distribution of quadratic forms in normal space-application to structural reliability," Journal of Engineering Mechanics, 116(6), pp. 1183-1197.

[9] Zhao, Y.-G., and Ono, T., 1999, "New approximations for SORM: Part 1," Journal of Engineering Mechanics, 125(1), pp. 79-85.

[10] Madsen, H. O., Krenk, S., and Lind, N. C., 2006, Methods of structural safety, Courier Corporation.

[11] Ditlevsen, O., and Madsen, H. O., 1996, Structural reliability methods, Wiley New York.

[12] Mansour, R., and Olsson, M., 2014, "A closed-form second-order reliability method using noncentral chi-squared distributions," Journal of Mechanical Design, 136(10), p. 101402.

[13] Laman, J. A., and Nowak, A. S., 1996, "Fatigue-load models for girder bridges," Journal of Structural Engineering, 122(7), pp. 726-733.

[14] Tallin, A., and Petreshock, T., 1990, "Modeling fatigue loads for steel bridges," Transportation research record, 1275, pp. 23-26.

[15] Haider, S. W., Harichandran, R. S., and Dwaikat, M. B., 2008, "Estimating Bimodal Distribution Parameters and Traffic Levels from Axle Load Spectra," Proc. Transportation Research Board 87th Annual Meeting.

[16] Haider, S. W., Harichandran, R. S., and Dwaikat, M. B., 2009, "Closed-form solutions for bimodal axle load spectra and relative pavement damage estimation," Journal of transportation engineering, 135(12), pp. 974-983.

[17] Mones, E., Araújo, N. A., Vicsek, T., and Herrmann, H. J., 2014, "Shock waves on complex networks," Scientific reports, 4.

[18] Daniels, H. E., 1954, "Saddlepoint approximations in statistics," The Annals of Mathematical Statistics, pp. 631-650.

[19] Lugannani, R., and Rice, S., 1980, "Saddle point approximation for the distribution of the sum of independent random variables," Advances in applied probability, pp. 475-490.

[20] Daniels, H. E., 1987, "Tail probability approximations," International Statistical Review/Revue Internationale de Statistique, pp. 37-48.

[21] Goutis, C., and Casella, G., 1999, "Explaining the saddlepoint approximation," The American Statistician, 53(3), pp. 216-224.

[22] Du, X., and Sudjianto, A., 2004, "A saddlepoint approximation method for uncertainty analysis," Proc. ASME 2004 International Design Engineering Technical Conferences and Computers and Information in Engineering Conference, American Society of Mechanical Engineers, pp. 445-452.

[23] Du, X., 2008, "Saddlepoint approximation for sequential optimization and reliability analysis," Journal of Mechanical Design, 130(1), p. 011011.

[24] Huang, B., and Du, X., 2008, "Probabilistic uncertainty analysis by mean-value first order saddlepoint approximation," Reliability Engineering & System Safety, 93(2), pp. 325-336.

[25] Meng, D., Huang, H.-Z., Wang, Z., Xiao, N.-C., and Zhang, X.-L., 2014, "Mean-value first-order saddlepoint approximation based collaborative optimization for multidisciplinary problems under aleatory uncertainty," Journal of Mechanical Science and Technology, 28(10), pp. 3925-3935.

[26] Du, X., and Sudjianto, A., 2004, "First-order saddlepoint approximation for reliability analysis," AIAA journal, 42(6), pp. 1199-1207.

[27] Dolinski, K., 1982, "First-order second-moment approximation in reliability of structural systems: critical review and alternative approach," Structural Safety, 1(3), pp. 211-231.

[28] Lee, T. W., and Kwak, B. M., 1987, "A reliability-based optimal design using advanced first order second moment method," Journal of Structural Mechanics, 15(4), pp. 523-542.

[29] Du, X., and Chen, W., 2004, "Sequential optimization and reliability assessment method for efficient probabilistic design," Journal of Mechanical Design, 126(2), pp. 225-233.

[30] Du, X., Guo, J., and Beeram, H., 2008, "Sequential optimization and reliability assessment for multidisciplinary systems design," Structural and Multidisciplinary Optimization, 35(2), pp. 117-130.

[31] Lee, I., Choi, K., and Gorsich, D., 2010, "System reliability-based design optimization using the MPP-based dimension reduction method," Structural and Multidisciplinary Optimization, 41(6), pp. 823-839.

[32] McDonald, M., and Mahadevan, S., 2008, "Design optimization with system-level reliability constraints," Journal of Mechanical Design, 130(2), p. 021403.

[33] Rosenblatt, M., 1952, "Remarks on a multivariate transformation," The annals of mathematical statistics, 23(3), pp. 470-472.

[34] Hohenbichler, M., and Rackwitz, R., 1981, "Non-normal dependent vectors in structural safety," Journal of the Engineering Mechanics Division, 107(6), pp. 1227-1238.

[35] Stockholm, F. E., 1932, "On the Probability Function in the Collective Theory of Risk." Skandinavisk Aktuarietidskrift 15, 175–95.

[36] Lugannani, R., and Rice, S., 1980, "Saddle point approximation for the distribution of the sum of independent random variables," Advances in applied probability, 12(02), pp. 475-490.

[37] Zhang, J., and Du, X., 2010, "A second-order reliability method with first-order efficiency," Journal of Mechanical Design, 132(10), p. 101006.

[38] Alibrandi, U., Alani, A., and Koh, C., 2015, "Implications of high-dimensional geometry for structural reliability analysis and a novel linear response surface method based on SVM," International Journal of Computational Methods, 12(04), p. 1540016.

[39] Hurtado, J. E., 2012, "Dimensionality reduction and visualization of structural reliability problems using polar features," Probabilistic Engineering Mechanics, 29, pp. 16-31.

[40] Katafygiotis, L. S., and Zuev, K. M., 2008, "Geometric insight into the challenges of solving high-dimensional reliability problems," Probabilistic Engineering Mechanics, 23(2-3), pp. 208-218.

[41] Valdebenito, M., Pradlwarter, H., and Schuëller, G., 2010, "The role of the design point for calculating failure probabilities in view of dimensionality and structural nonlinearities," Structural Safety, 32(2), pp. 101-111.

[42] Alibrandi, U., Alani, A. M., and Ricciardi, G., 2015, "A new sampling strategy for SVM-based response surface for structural reliability analysis," Probabilistic Engineering Mechanics, 41, pp. 1-12.

[43] Hurtado, J. E., and Alvarez, D. A., 2010, "An optimization method for learning statistical classifiers in structural reliability," Probabilistic Engineering Mechanics, 25(1), pp. 26-34.

[44] Gander, W., and Gautschi, W., 2000, "Adaptive quadrature—revisited," BIT Numerical Mathematics, 40(1), pp. 84-101.

[45] Malcolm, M. A., and Simpson, R. B., 1975, "Local versus global strategies for adaptive quadrature," ACM Transactions on Mathematical Software (TOMS), 1(2), pp. 129-146.

[46] Song, S., Lu, Z., and Qiao, H., 2009, "Subset simulation for structural reliability sensitivity analysis," Reliability Engineering & System Safety, 94(2), pp. 658-665.

[47] Zhao, H., Yue, Z., Liu, Y., Gao, Z., and Zhang, Y., 2015, "An efficient reliability method combining adaptive importance sampling and Kriging metamodel," Applied Mathematical Modelling, 39(7), pp. 1853-1866.

II. SADDLEPOINT APPROXIMATION RELIABILITY METHOD FOR QUADRATIC FUNCTIONS IN NORMAL VARIABLES

Zhangli Hu and Xiaoping Du

Department of Mechanical and Aerospace Engineering
Missouri University of Science and Technology

ABSTRACT

If the state of a component can be predicted by a limit-state function, the first and second order reliability methods are commonly used to calculate the reliability of the component. The latter method is more accurate because it approximates the limit-state function with a quadratic form in standard normal variables. To further improve the accuracy, this study develops a saddlepoint approximation reliability method that does not require additional transformations and approximations on the quadratic function. Analytical equations are derived for the cumulant generating function (CGF) of the limit-state function in standard normal variables, and then the saddlepoint is found by equating the derivative of the CGF to the limit state. Thereafter a closed form solution to the reliability is available. The method can also be applied to general nonlinear limit-state functions after they are approximated by a second order Taylor expansion. Examples show the better accuracy than the traditional second order reliability methods.

1. INTRODUCTION

When a physics-based approach is used, reliability is calculated by [1]

$$R = \Pr\{g(\mathbf{X}) \geq 0\} = \int_{g(\mathbf{X})\geq 0} f_{\mathbf{X}}(\mathbf{x})d\mathbf{x} \tag{1}$$

and the associated probability of failure is given by

$$p_f = 1 - R = \Pr\{g(\mathbf{X}) < 0\} = \int_{g(\mathbf{X})<0} f_{\mathbf{X}}(\mathbf{x})d\mathbf{x} \tag{2}$$

where $g(\mathbf{X})$ is a limit-state function, $\mathbf{X} = [X_1, ..., X_n]$ is a vector of random input variables, and $f_{\mathbf{X}}(\mathbf{x})$ is the joint probability density function (PDF) of $\mathbf{X}$.

Directly calculating the integral is difficult and computationally expensive, and thus approximation methods are needed. The widely used approximation methods are the First Order Second Moment Method (FOSM) [2, 3], the First Order Reliability Method (FORM) [4-6], and the Second Order Reliability Method (SORM) [7-12].

FOSM approximates the limit-state function with the first-order Taylor series expansion at the mean values of $\mathbf{X}$. It assumes $\mathbf{X}$ to be normally distributed and estimates p_f with the mean and standard deviation of the limit-state function. FOSM is easy to use and has good efficiency. Its accuracy, however, is poor when the limit-state function is highly nonlinear, standard deviations of $\mathbf{X}$ are large, and the distributions of $\mathbf{X}$ are far away from normal.

FORM is more accurate than FOSM, but less efficient. FORM transforms random variables $\mathbf{X}$ into independent standard normal variables $\mathbf{U}$. Thereafter, it linearizes the limit-state function at a point with the highest probability density at the limit state. (The point is called the MPP, or the most probable point). Then, p_f is estimated by using the

reliability index, which is the magnitude of the MPP vector [13]. FORM is most commonly used because of the good balance between accuracy and efficiency.

SORM is more accurate than FORM because of the second-order Taylor expansion at the MPP, which makes the limit-state function a complete quadratic function in standard normal variables. In the commonly used SORM methods proposed by Breitung [7] and Tvedt [8, 9], a rotation transformation is performed after the second-order Taylor expansion [14]. Then the general quadratic function is approximated by a paraboloid, ignoring the last row and last column in the transformed Hessian matrix [1, 15]. Finally the probability of failure can be analytically evaluated by asymptotic formulas [7, 8, 10]. However, this method does not work well for negative curvatures at the MPP. Furthermore, the further approximation may introduce an extra error.

To further improve the accuracy of SORM, we extend the first-order saddlepoint approximation (FOSPA) [16] to the second-order saddlepoint approximation (SOSPA). The new method does not need any additional transformations and approximations after the MPP and Hessian matrix at the MPP are found. After the limit-state function is approximated by the second order Taylor expansion at the MPP with respect to independent standard normal variables, the cumulant generating function (CGF) of the limit-state function is analytically available. Then the saddlepoint approximation is directly applied to estimate the probability of failure. Given the high accuracy of the saddlepoint approximation itself and no further approximations, SOSPA is more accurate than the two existing SORM methods.

2. REVIEW OF FORM AND SORM

In this section, we briefly review the commonly used reliability methods FORM and SORM.

2.1. FORM

FORM [17-21] transforms the original random variables **X** in the X-space into standard normal variables **U** in the U-space. This transformation is called the Rosenblatt transformation and is given by [22, 23]

$$F_{X_i}(X_i) = \Phi(U_i) \tag{3}$$

in which $F_{X_i}(\cdot)$ and $\Phi(\cdot)$ represents the cumulative distribution functions (CDF) of X_i and U_i, respectively. Eq. (3) is applicable for independent variables in **X**. The transformation for dependent variables is given by the Nataf transformation [22].

After the transformation, the limit-state function becomes

$$Y = g(\mathbf{X}) = G(\mathbf{U}) \tag{4}$$

To minimize the error from the linearization of the limit-state function, one expands the function at the point that has the highest probability density, and this point is called the most probable point (MPP), denoted by $\mathbf{u}^*$. MPP is obtained by solving the following model:

$$\begin{cases} \min \ \|\mathbf{u}\| = \sqrt{\mathbf{U}\mathbf{U}^T} \\ \text{s.t.} \quad G(\mathbf{U}) = 0 \end{cases} \tag{5}$$

Let the magnitude of $\mathbf{u}^*$ be β, namely

$$\beta = \left\| \mathbf{u}^* \right\| = \sqrt{\left(u_1^*\right)^2 + ... + \left(u_n^*\right)^2} \tag{6}$$

The probability of failure is then computed by

$$p_f = \Phi(-\beta) \tag{7}$$

FORM uses the first-order approximation to $G(\mathbf{U})$. It is accurate when the nonlinearity of $G(\mathbf{U})$ is not high. Otherwise, SORM may be used if high accuracy is needed.

2.2. SORM

SORM approximates $G(\mathbf{U})$ with a second-order Taylor expansion at $\mathbf{u}^*$. The approximation is given by

$$G(\mathbf{U}) \approx Q(\mathbf{U}) = G(\mathbf{u}^*) + \nabla G(\mathbf{u}^*)(\mathbf{U} - \mathbf{u}^*)^T + \frac{1}{2}(\mathbf{U} - \mathbf{u}^*)\nabla^2 G(\mathbf{u}^*)(\mathbf{U} - \mathbf{u}^*)^T \tag{8}$$

where $\nabla G(\mathbf{u}^*) = \left(\left.\frac{\partial G}{\partial U_1}\right|_{\mathbf{u}^*}, \cdots, \left.\frac{\partial G}{\partial U_n}\right|_{\mathbf{u}^*} \right)$ is the gradient, and $\nabla^2 G(\mathbf{u}^*)$ is the Hessian matrix, given by

$$\nabla^2 G(\mathbf{u}^*) = \left[\begin{array}{cccc} \frac{\partial^2 G}{\partial U_1^2} & \frac{\partial^2 G}{\partial U_1 U_2} & \cdots & \frac{\partial^2 G}{\partial U_1 U_n} \\ \frac{\partial^2 G}{\partial U_2 U_1} & \frac{\partial^2 G}{\partial U_2^2} & \cdots & \frac{\partial^2 G}{\partial U_2 U_n} \\ \vdots & \vdots & \ddots & \vdots \\ \frac{\partial^2 G}{\partial U_n U_1} & \frac{\partial^2 G}{\partial U_n U_2} & \cdots & \frac{\partial^2 G}{\partial U_n^2} \end{array} \right]_{\mathbf{u}^*} \tag{9}$$

Still no analytical solution to p_f exists using Eq. (8). Breitung's and Tvedt's methods then rotate the U-space into a new standard normal space called Y-space whose

last coordinate Y_n coincides with the MPP vector. Then the limit-state function is rewritten as

$$Q(\mathbf{Y}) = -Y_n + \beta + \frac{1}{2}(\mathbf{Y} - \mathbf{y}^*)\mathbf{W}(\mathbf{Y} - \mathbf{y}^*)^T \tag{10}$$

where $\mathbf{y}^* = (0, 0, \cdots, \beta)^T$ is the MPP in the Y-space, and $\mathbf{W}$ is the transformed Hessian matrix and given by

$$\mathbf{W} = \frac{\mathbf{R}\nabla^2 g(\mathbf{u}^*)\mathbf{R}}{\left\|\nabla g(\mathbf{u}^*)\right\|} \tag{11}$$

in which $\mathbf{R}$ is an orthogonal rotational matrix and can be determined by the Gram-Schmidt orthogonalization.

After the rotation, $Q(\mathbf{Y})$ is further approximated by a paraboloid by setting the last row and last column of $\mathbf{W}$ to be zero and then diagonalizing $\mathbf{W}$. Eq. (10) becomes

$$Q(\mathbf{Y}') = -Y_n' + \beta + \frac{1}{2}\sum_{i=1}^{n-1} k_i Y_i'^2 \tag{12}$$

where k_i are the main curvatures of $G(\mathbf{U})$ at the MPP and can be computed from the eigenvalues of the $(n-1)\times(n-1)$ leading submatrix of $\mathbf{W}$.

Finally, the probability of failure is estimated, according to Breitung's formula and Tvedt's formula, by

$$p_{f,\text{Breitung}} = \Phi(-\beta)\prod_{i=1}^{n-1}(1 + k_i\beta)^{-1/2} \tag{13}$$

and

$$p_{f,\text{Tvedt}} = T_1 + T_2 + T_3 \tag{14}$$

where

$$\begin{cases} T_1 = \Phi(-\beta)\prod_{i=1}^{n-1}(1+k_i\beta)^{-1/2} \\ T_2 = \left[\beta\Phi(-\beta)-\phi(\beta)\right]\left[\prod_{i=1}^{n-1}(1+k_i\beta)^{-1/2} - \prod_{i=1}^{n-1}(1+k_i(\beta+1))^{-1/2}\right] \\ T_3 = (\beta+1)\left[\beta\Phi(-\beta)-\phi(\beta)\right]\left\{\prod_{i=1}^{n-1}(1+k_i\beta)^{-1/2} - \mathrm{Re}\left[\prod_{i=1}^{n-1}(1+k_i(\beta+1))^{-1/2}\right]\right\} \end{cases} \quad (15)$$

in which, $\mathrm{Re}(\cdot)$ denotes the real part of an imaginary number.

The second-order approximation makes SORM in general more accurate than FORM. However, neither Breitung's method nor Tvedt's method work when $k_i\beta \le -1$. Furthermore, an extra error may be introduced because some components of the transformed Hessian matrix are ignored in the approximation into a paraboloid.

3. SADDLEPOINT APPROXIMATION FOR A QUADRATIC FUNCTION

The objective of this study is to improve the accuracy of SORM by eliminating further approximations. The major strategy is to use the complete information of the MPP and the Hessian matrix, and the major approach is the saddlepoint approximation. The advantage of the proposed second order saddlepoint approximation (SOSPA) is that an analytical solution is available after the saddlepoint is found.

3.1. QUADRATIC LIMIT-STATE FUNCTION

After the MPP is found, Eq. (8) is rewritten as

$$Q(\mathbf{U}) = a + \mathbf{b}^T\mathbf{U} + \mathbf{U}^T\mathbf{C}\mathbf{U} \tag{16}$$

where

$$\begin{cases} a = \dfrac{1}{2}\left(\mathbf{u}^*\right)^T \nabla^2 G(\mathbf{u}^*)\mathbf{u}^* - \nabla G(\mathbf{u}^*)^T\mathbf{u}^* \\ \mathbf{b} = \nabla G(\mathbf{u}^*) - \nabla^2 G(\mathbf{u}^*)\mathbf{u}^* \\ \mathbf{C} = \dfrac{1}{2}\nabla^2 G(\mathbf{u}^*) \end{cases} \tag{17}$$

The saddlepoint approximation then can be used. Its use requires to know the cumulant generating function (CGF) of $Q(\mathbf{U})$. Next we discuss how to obtain the CGF.

To analytically derive the CGF, we at first eliminate the cross terms in Eq. (16) with the following transformation

$$\tilde{\mathbf{U}} = \mathbf{D}^{-1}\mathbf{U} \tag{18}$$

where $\mathbf{D}$ is an orthogonal matrix whose column vectors are the eigenvectors of $\mathbf{C}$, and $\tilde{\mathbf{U}} = \left(\tilde{U}_1, \tilde{U}_2, \cdots, \tilde{U}_n\right)$ is a n-dimensional vector with independent standard normal random variables.

Thus, the limit-state function becomes

$$Q(\tilde{\mathbf{U}}) = a + \tilde{\mathbf{b}}^T \tilde{\mathbf{U}} + \tilde{\mathbf{U}}^T \tilde{\mathbf{C}} \tilde{\mathbf{U}} \tag{19}$$

in which

$$\begin{cases} \tilde{\mathbf{b}} = \mathbf{D}^T \mathbf{b} = \left(\tilde{b}_1, \tilde{b}_2, \cdots, \tilde{b}_n\right) \\ \tilde{\mathbf{C}} = \mathbf{D}^T \mathbf{C} \mathbf{D} = diag\left(\tilde{c}_1, \tilde{c}_2, \cdots, \tilde{c}_n\right) \end{cases} \tag{20}$$

Since $\tilde{\mathbf{C}}$ is diagonal, Eq. (19) can be written as

$$Q(\tilde{\mathbf{U}}) = \sum_{i=1}^{n} Q_i(\tilde{\mathbf{U}}) = \sum_{i=1}^{n} \left(\tilde{a}_i + \tilde{b}_i \tilde{U}_i + \tilde{c}_i \tilde{U}_i^2\right) \tag{21}$$

where

$$\tilde{a}_i = \frac{a}{n} \tag{22}$$

According to the signs of $\tilde{c}_i$, $Q_i(\tilde{\mathbf{U}})$ is further rewritten as

$$\begin{aligned} Q_i(\tilde{\mathbf{U}}) &= \begin{cases} \left(\sqrt{\tilde{c}_i}\tilde{U}_i + \dfrac{\tilde{b}_i}{2\sqrt{\tilde{c}_i}}\right)^2 + \tilde{a}_i - \dfrac{\tilde{b}_i^2}{4\tilde{c}_i} & \tilde{c}_i > 0 \\ -\left(\sqrt{-\tilde{c}_i}\tilde{U}_i - \dfrac{\tilde{b}_i}{2\sqrt{-\tilde{c}_i}}\right)^2 + \tilde{a}_i - \dfrac{\tilde{b}_i^2}{4\tilde{c}_i} & \tilde{c}_i < 0 \\ \tilde{a}_i + \tilde{b}_i \tilde{U}_i & \tilde{c}_i = 0 \end{cases} \\ &= \begin{cases} Z_i^2 + d_i & \tilde{c}_i > 0 \\ -Z_i^2 + d_i & \tilde{c}_i < 0 \\ \tilde{a}_i + \tilde{b}_i \tilde{U} & \tilde{c}_i = 0 \end{cases} \end{aligned} \tag{23}$$

where

$$d_i = \tilde{a}_i - \frac{\tilde{b}_i^2}{4\tilde{c}_i} \tag{24}$$

and

$$\begin{cases} Z_i = \sqrt{\tilde{c}_i}\tilde{U}_i + \dfrac{\tilde{b}_i}{2\sqrt{\tilde{c}_i}} & \tilde{c}_i > 0 \\ Z_i = \sqrt{-\tilde{c}_i}\tilde{U}_i - \dfrac{\tilde{b}_i}{2\sqrt{-\tilde{c}_i}} & \tilde{c}_i < 0 \end{cases} \tag{25}$$

Z_i is a linear function of the standard normal random variable, and thus it is also normally distributed with the mean and standard deviation given by

$$\mu_{Z_i} = \begin{cases} \dfrac{\tilde{b}_i}{2\sqrt{\tilde{c}_i}} & \tilde{c}_i > 0 \\ -\dfrac{\tilde{b}_i}{2\sqrt{-\tilde{c}_i}} & \tilde{c}_i < 0 \end{cases} \tag{26}$$

and

$$\sigma_{Z_i} = \begin{cases} \sqrt{\tilde{c}_i} & \tilde{c}_i > 0 \\ \sqrt{-\tilde{c}_i} & \tilde{c}_i < 0 \end{cases} \tag{27}$$

Let $V_i = \left(\dfrac{Z_i}{\sigma_{Z_i}} \right)^2$. Then V_i follows a noncentral chi-square distribution with freedom of 1 [24-26]; namely, $V_i \sim \chi^2(1, \lambda)$, where λ is a noncentrality parameter and given by

$$\lambda = \left(\frac{\mu_{Z_i}}{\sigma_{Z_i}} \right)^2 \tag{28}$$

Hence we can further rewrite Eq. (23) as

$$Q_i(\tilde{\mathbf{U}}) = \begin{cases} \sigma_{Z_i}^2 V_i + d_i & \tilde{c}_i > 0 \\ -\sigma_{Z_i}^2 V_i + d_i & \tilde{c}_i < 0 \\ \tilde{a}_i + \tilde{b}_i \tilde{U}_i & \tilde{c}_i = 0 \end{cases} \tag{29}$$

Therefore, the limit-state function $Q(\tilde{\mathbf{U}}) = \sum_{i=1}^{n} Q_i(\tilde{\mathbf{U}})$ is finally expressed as a linear combination of chi-square variables and standard normal variables. Note that there are no approximations during the above process.

3.2. SADDLEPOINT APPROXIMATION

We now use the saddlepoint approximation (SPA) to calculate p_f based on Eq. (29). SPA can produce an accurate estimation of the cumulative distribution function (CDF) in a tail area [16, 27-31]. As discussed previously, we need to know the CGF of $Q(\tilde{\mathbf{U}}) = \sum_{i=1}^{n} Q_i(\tilde{\mathbf{U}})$.

The CGF of a noncentral chi-square variable V_i is [32]

$$K_{V_i}(t) = \frac{\lambda_i t}{1-2t} - \frac{1}{2}\log(1-2t) \tag{30}$$

For the standard normal variable $\tilde{U}_i$, the CGF is

$$K_{\tilde{U}_i} = \frac{1}{2}t^2 \tag{31}$$

Based on the properties of CGF [32], the CGF of $Q_i(\tilde{\mathbf{U}})$ can be easily obtained by

$$K_{Q_i}(t)=\begin{cases}\dfrac{\lambda_i\sigma_{Z_i}^2 t}{1-2\sigma_{Z_i}^2 t}-\dfrac{1}{2}\log(1-2\sigma_{Z_i}^2 t)+d_i t & \tilde{c}_i>0\\ -\dfrac{\lambda_i\sigma_{Z_i}^2 t}{1+2\sigma_{Z_i}^2 t}-\dfrac{1}{2}\log(1+2\sigma_{Z_i}^2 t)+d_i t & \tilde{c}_i<0\\ \tilde{a}_i t+\dfrac{1}{2}b_i^2 t^2 & \tilde{c}_i=0\end{cases} \tag{32}$$

Then we have CGF of $Q(\tilde{\mathbf{U}})$

$$K_Q(t)=\sum_{i=1}^{n}K_{Q_i}(t) \tag{33}$$

Once $K_Q(t)$ is available, we solve for the saddlepoint t_s by

$$K_Q^{'}(t)=0 \tag{34}$$

where $K_Q^{'}(t)$ is the first derivative of $K_Q(t)$ with respect to t. According to the Lugannani and Rice's formula [28], p_f is computed by

$$p_f=\Pr\left\{Q(\tilde{\mathbf{U}})<0\right\}=\Phi(w)+\phi(w)\left(\frac{1}{w}-\frac{1}{\upsilon}\right) \tag{35}$$

where $\Phi(\cdot)$ and $\phi(\cdot)$ are CDF and probability density function (PDF) of the standard normal distribution, respectively.

$$w=\mathrm{sgn}(t_s)\left\{2\left[-K_Q(t_s)\right]\right\}^{1/2} \tag{36}$$

$$\upsilon=t_s\left[K_Q^{''}(t_s)\right]^{1/2} \tag{37}$$

in which $\mathrm{sgn}(t_s)=+1,-1$ or 0, depending on whether t_s is positive, negative, or zero; $K_Q^{''}(t)$ is the second derivative of $K_Q(t)$ with respect to t.

As will be shown in the examples, SPA can produce an accurate estimation of p_f for the function form in Eq. (29).

3.3. NUMERICAL PROCEDURE

The numerical procedure of the proposed SOSPA is summarized below.

Step 1: Perform the MPP search and obtain the MPP $\mathbf{u}^*$, the gradient $\nabla G(\mathbf{u}^*)$, and the Hessian matrix $\nabla^2 G(\mathbf{u}^*)$. This step is the same as the one in the traditional SORM methods.

Step 2: Construct the general quadratic form of the limit-state function shown in Eq. (16) by using $\mathbf{u}^*$, $\nabla G(\mathbf{u}^*)$, and $\nabla^2 G(\mathbf{u}^*)$.

Step 3: Transform the general quadratic limit-state function into a linear combination of chi-square distribution variables shown in Eq. (29) by the diagonalizable transformation $\tilde{\mathbf{U}} = \mathbf{D}^{-1}\mathbf{U}$.

Step 4: Obtain the CGF of the limit-state function $Q(\tilde{\mathbf{U}})$ using Eq. (33).

Step 5: Compute p_f by SPA using Eq. (35).

The flowchart of SOSPA is given in Figure 1.

SOSPA is easy to implement. Since it uses all the components of the Hessian matrix without any further approximations, SOSPA is in general more accurate than the Breitung's and Tvedt's methods.

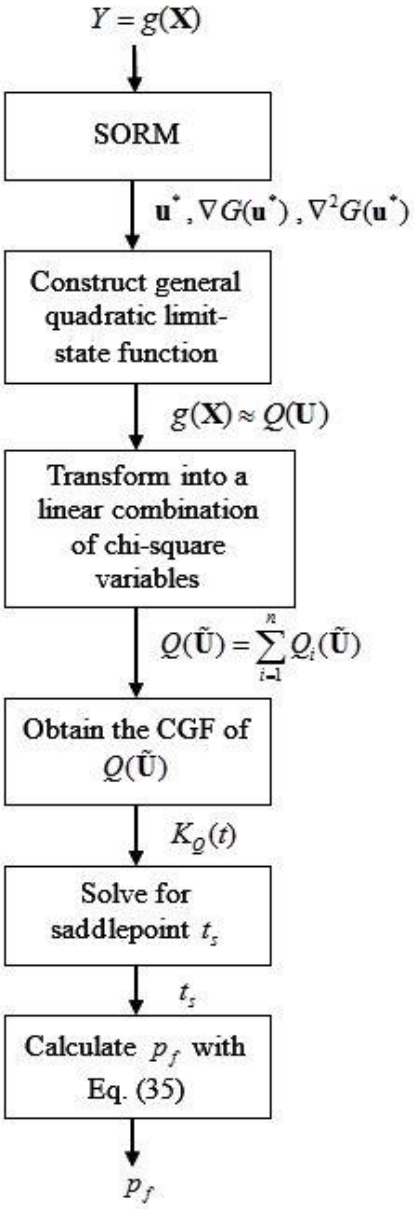

Figure 1. The flowchart of SOSPA

4. EXAMPLES

In this section, we use a number of testing problems to evaluate the accuracy of SOSPA. We at first examine general quadratic limit-state functions. Since the contour of a quadratic function may be an ellipse, a parabola, or a hyperbola, we first provide three mathematical examples that represent the three cases. We then perform SOSPA for a high dimensional quadratic limit-sate function. Thereafter, we demonstrate that SOSPA could also be applied to general engineering problems where limit-state functions are not necessarily quadratic.

To show the benefits of using SOSPA, we compare it with the other two variants of SORM, including Breitung's and Tvedt's methods, which have been reviewed in Section 2. We also provide the results from FORM. The accuracy is evaluated by the error relative to the result from Monte Carlo Simulation (MCS) with a large sample size. We also give the number of functional calls as the measure of efficiency.

4.1. QUADRATIC LIMIT-STATE FUNCTIONS

Three mathematical examples are tested for cases of an ellipse, a parabola, and a hyperbola. To easily plot the curves, the functions in the first three examples are all two dimensional. Then we test SOSPA with the fourth example that involves a large number of random variables. The random input variables in the examples are assumed to be independent standard normal variables.

4.1.1. Example 1: Ellipse. Three limit-state functions with elliptic contours are given by

$$G_1(\mathbf{U}) = \frac{(U_1 - 3)^2}{0.4^2} + \frac{(U_2 - 3)^2}{0.3^2} - 1 \tag{38}$$

$$G_2(\mathbf{U}) = \frac{(U_1 - 3)^2}{2^2} + \frac{(U_2 - 3)^2}{1^2} - 1 \tag{39}$$

$$G_3(\mathbf{U}) = \frac{(U_1 - 1.7)^2}{2^2} + \frac{(U_2 - 0.4)^2}{1^2} - 1 \tag{40}$$

where $\mathbf{U} = [U_1, U_2]$. U_1 and U_2 are independent standard normal variables.

Figure 2 shows the contour of G_1, lying far away from the origin. Figure 3 shows the contour of G_2, which lies close to the origin. Figure 4 shows the contour of G_3, which encloses the origin.

The probability of failure is computed by SOSPA and other two SORM formulas. The results are compared with respect to that of MCS with 10^8 simulations. The relative error is defined as

$$\varepsilon\% = \left| \frac{p_f - p_{f,\mathrm{MCS}}}{p_{f,\mathrm{MCS}}} \right| \times 100\% \tag{41}$$

where p_f is the result from a non-MCS method, and $p_{f,\mathrm{MCS}}$ is the result from MCS.

The approximated contours for G_1 obtained from the two SORM methods and FORM are plotted in Figure 5. It is shown that FORM approximates the elliptical contour with a straight line, the SORM methods approximate the limit-state function with a parabola, and SOSPA does not approximate but directly use the original contour of limit-state function. So the SOSPA should produce the most accurate results. This is demonstrated by the results given in Tables 1 through 3.

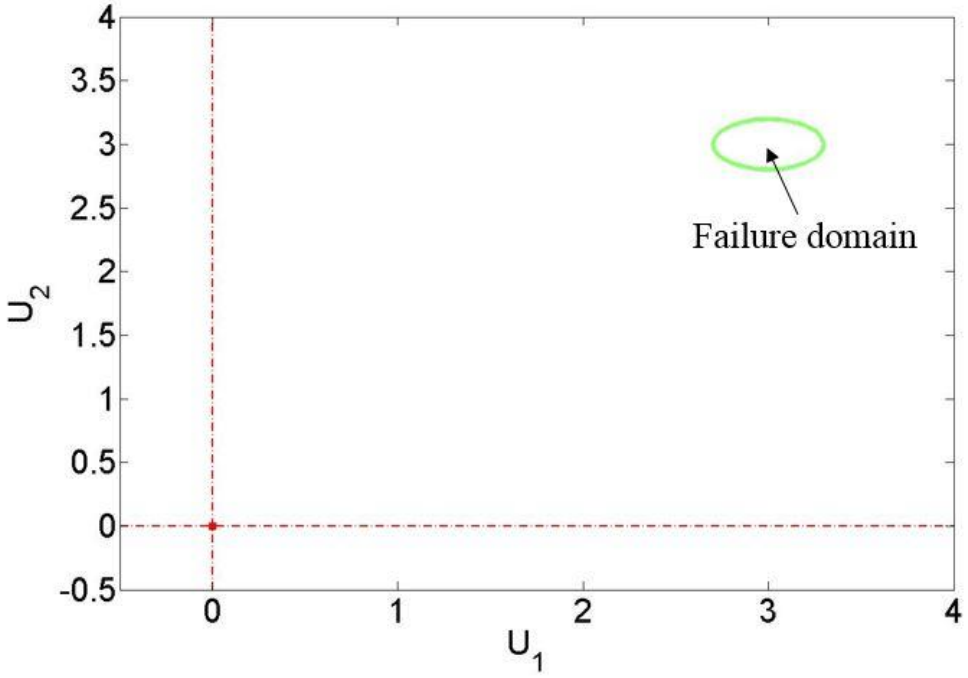

Figure 2. Elliptical contour of the quadratic function in Case 1

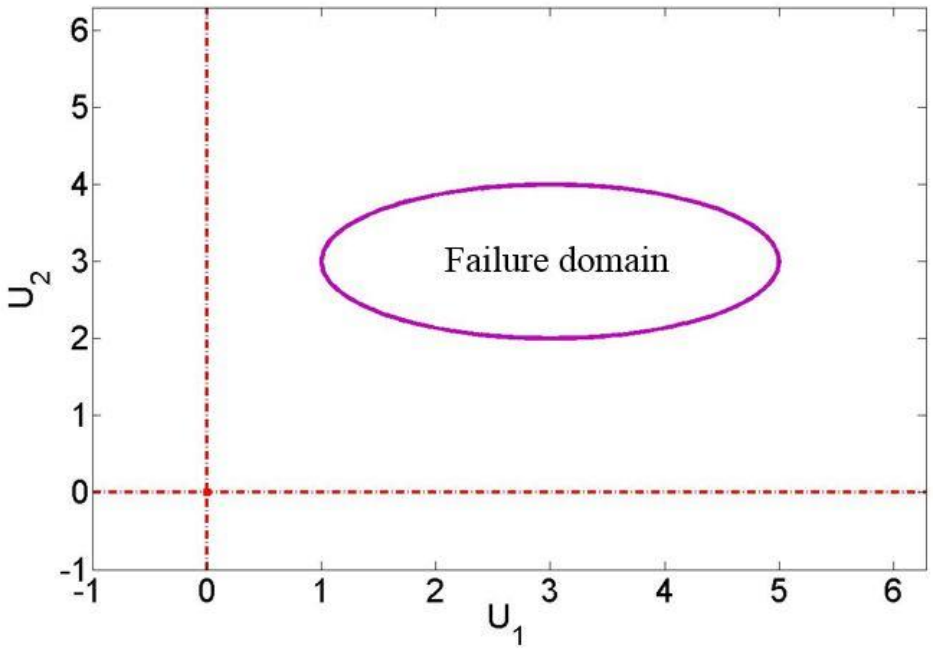

Figure 3. Elliptical contour of the quadratic function in Case 2

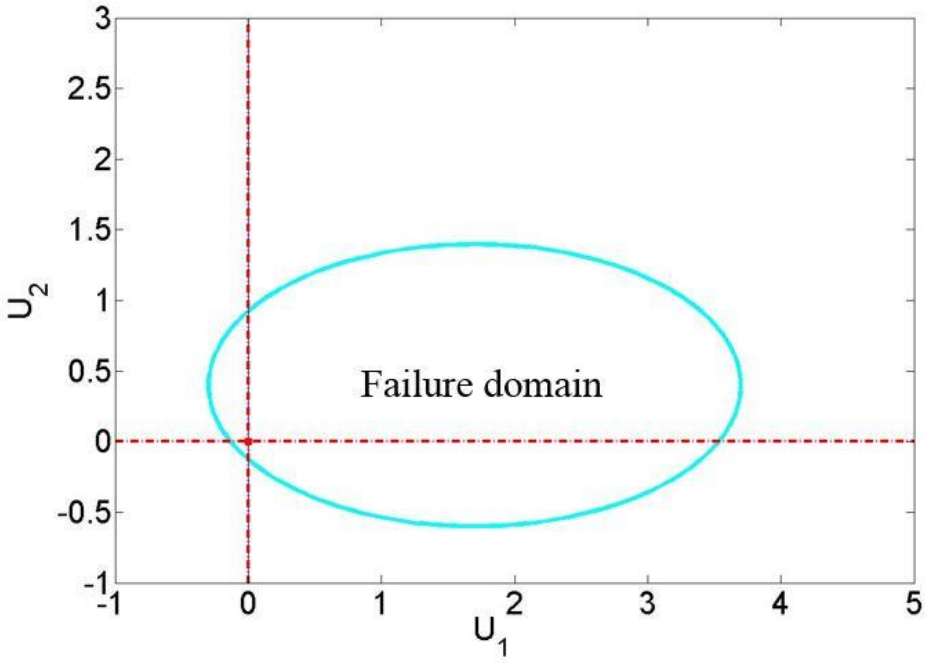

Figure 4. Elliptical contour of the quadratic function in Case 3

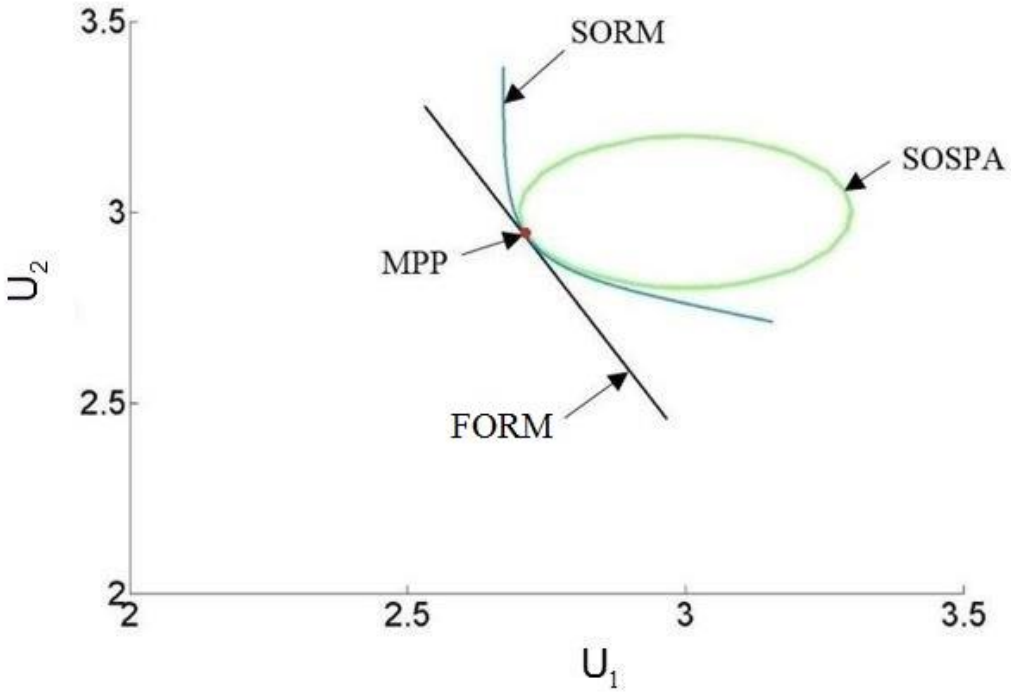

Figure 5. Approximated contours in Case 1

Table 1. p_f of the elliptical quadratic function in Case 1

Method	p_f	ε%	Absolute Error	Function Calls	β
FORM	5.0071×10^{-5}	459%	4.1121×10^{-5}	30	3.89
SORM (Breitung)	1.4031×10^{-5}	56.8%	5.081×10^{-6}	33	3.89
SORM (Tvedt)	1.3385×10^{-5}	49.5%	4.435×10^{-6}	33	3.89
SOSPA	9.2403×10^{-6}	3.24%	2.903×10^{-7}	33	3.89
MCS	8.950×10^{-6}	N/A	N/A	10^8	N/A

Table 2. p_f of the elliptical quadratic function in Case 2

Method	p_f	ε%	Absolute Error	Function Calls	β
FORM	2.7546×10^{-3}	88%	1.2938×10^{-3}	24	2.78
SORM (Breitung)	1.6697×10^{-3}	14.3%	2.089×10^{-4}	27	2.78
SORM (Tvedt)	1.5859×10^{-3}	8.56%	1.251×10^{-4}	27	2.78
SOSPA	1.4685×10^{-3}	0.527%	7.7×10^{-6}	27	2.78
MCS	1.4608×10^{-3}	N/A	N/A	10^8	N/A

Table 3. p_f of the elliptical quadratic function in Case 3

Method	p_f	ε%	Absolute Error	Function Calls	β
FORM	5.3814×10^{-1}	75.5%	2.3144×10^{-1}	28	0.096
SORM (Breitung)	5.1598×10^{-1}	68.2%	2.0928×10^{-1}	31	0.096
SORM (Tvedt)	N/A	N/A	N/A	N/A	0.096
SOSPA	3.1289×10^{-1}	2.02%	6.19×10^{-3}	31	0.096
MCS	3.0670×10^{-1}	N/A	N/A	10^8	N/A

The results show that SOSPA is more accurate than the other two SORM methods. FORM produces the largest error because of the first order approximation.

The MPP and the Hessian matrix are identified numerically, and the numerical process calls the limit-state function repeatedly. SOSPA is as efficient as the other two SORM methods since the three methods have the same number of function calls.

It is noted that, for Case 3, the origin is in the failure domain. To let FORM and SORM work properly, we need to use $-G_3(\mathbf{U})$. Namely, we perform the following transformation:

$$\begin{aligned} p_f &= \Pr\{G_3(\mathbf{U}) < 0\} = 1 - \Pr\{G_3(\mathbf{U}) \geq 0\} \\ &= 1 - \Pr\{-G_3(\mathbf{U}) < 0\} \\ &= 1 - \Pr\{G_{3,\text{new}}(\mathbf{U}) < 0\} \end{aligned} \tag{42}$$

The contour of the new limit-state function $G_{3,\text{new}}(\mathbf{U})$ is the same as the original $G_3(\mathbf{U})$, but the failure domain changes from the region inside the contour to be outside. Then the FORM and two SORM methods can be used to calculate p_f. However, the main curvature of the new limit-state function is $k = -0.93$, leading to the failure of the Tvedt's formula.

4.1.2. Example 2: Parabola. In this example, the limit-state function is a quadratic function with a parabolic contour. Two cases are considered. The two limit-state functions are given by

$$G_1(\mathbf{U}) = 0.5U_1^2 - U_2 + 4 \tag{43}$$

$$G_2(\mathbf{U}) = U_1^2 - U_2 - 0.5 \tag{44}$$

The contours of the two limit-state functions are plotted in Figures 6 and 7. The origin is outside the contour in Figure 6 but inside the contour in Figure 7.

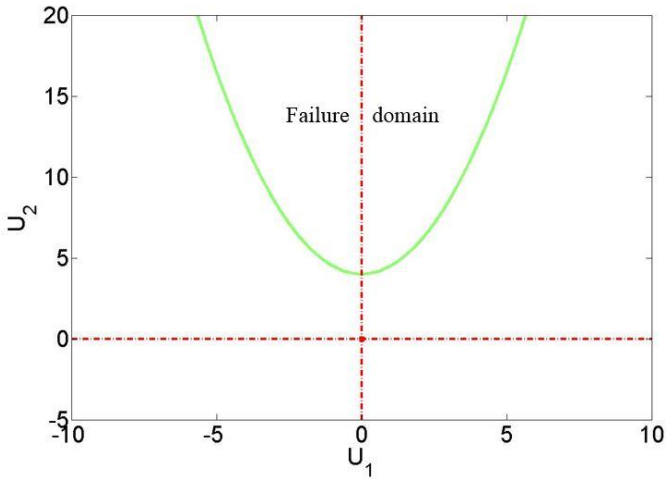

Figure 6. Parabolic contour of the limit-state function in Case 1

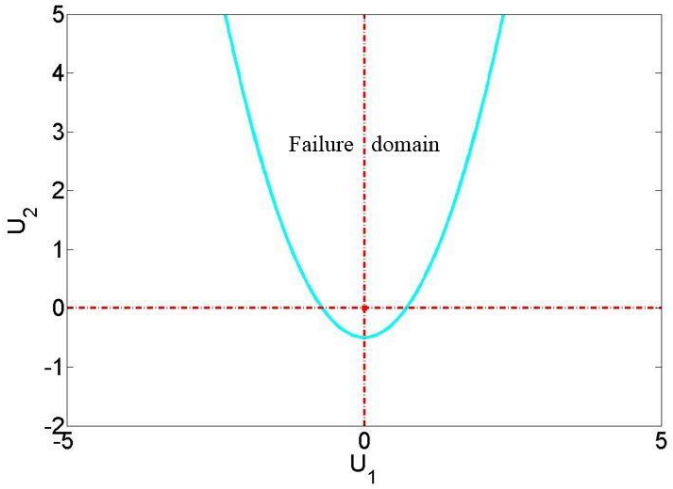

Figure 7. Parabolic contour of the limit-state function in Case 2

The results are given in Tables 4 and 5, indicating that SOSPA has the highest accuracy in both cases. FORM still produces significant errors because it linearizes the

limit-state function at the MPP. Both SORM methods have good accuracy in Case 1 but do not work in Case 2. In Case 2, the failure domain contains the origin, so a transformation is needed to obtain a new limit-state function $G_{2,\text{new}}(\mathbf{U}) = -G_2(\mathbf{U}) = -U_1^2 + U_2 + 0.5$. Then FORM and the two SORM methods are used to calculate $p_f = 1 - \Pr\left\{G_{2,\text{new}}(\mathbf{U}) < 0\right\}$. However, the main curvature of the new limit-state function is $k = -2$ and thus $k\beta = -1$. So the two SORM methods cannot work for this case.

Table 4. p_f of the parabolic quadratic function in Case 1

Method	p_f	ε%	Absolute Error	Function Calls	β
FORM	3.1671×10^{-5}	131%	1.7931×10^{-5}	31	4
SORM (Breitung)	1.4166×10^{-5}	3.1%	4.26×10^{-7}	34	4
SORM (Tvedt)	1.3654×10^{-5}	0.622%	8.6×10^{-8}	34	4
SOSPA	1.3701×10^{-5}	0.283%	3.9×10^{-8}	34	4
MCS	1.374×10^{-5}	N/A	N/A	10^8	N/A

Table 5. p_f of the parabolic quadratic function in Case 2

Method	p_f	ε%	Absolute Error	Function Calls	β
FORM	6.9146×10^{-1}	61.4%	2.6295×10^{-1}	115	0.5
SORM (Breitung)	N/A	N/A	N/A	N/A	0.5
SORM (Tvedt)	N/A	N/A	N/A	N/A	0.5
SOSPA	4.5262×10^{-1}	5.63%	2.411×10^{-2}	118	0.5
MCS	4.2851×10^{-1}	N/A	N/A	10^8	N/A

4.1.3. Example 3: Hyperbola. Two quadratic limit-state functions with hyperbolic contours are defined by

$$G_1(\mathbf{U}) = 1 - \left(\frac{U_2^2}{4^2} - \frac{U_1^2}{3^2} \right) \tag{45}$$

$$G_2(\mathbf{U}) = 1 - \left(\frac{(U_2 - 1.8)^2}{6^2} - \frac{U_1^2}{10^2} \right) \tag{46}$$

Their contours are plotted in Figures 8 and 9. The contour is symmetric with respect to the origin in Case 1 but asymmetric in Case 2.

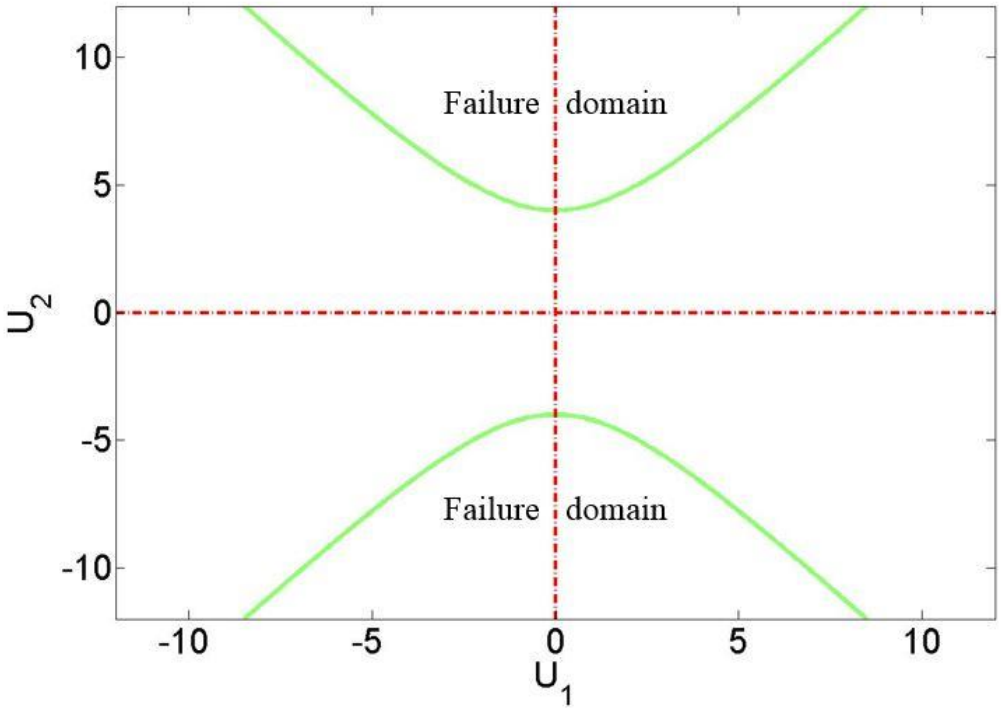

Figure 8. Hyperbolic contour of the limit-state function in Case 1

The results are given in Tables 6 and 7. They show that SOSPA is the most accurate method. In Case 1, the probability of failure calculated by Breitung's and

Tvedt's methods are $p_{f,\text{Breitung}} = 1.9003 \times 10^{-5}$ and $p_{f,\text{Tvedt}} = 1.8494 \times 10^{-5}$, respectively. They are almost one half of the one obtained by MCS, which is $p_{f,\text{MCS}} = 3.779 \times 10^{-5}$. The reason is that both of the SORM methods approximate the limit-state function containing two parabolic contours by only one parabolic contour. In Case 2, the two SORM methods are accurate because the failure domain associated with the upper contour ignored by SORM has small contribution to the failure.

The three mathematical examples show that SOSPA has the highest accuracy and that SOSPA can deal with quadratic functions in an elliptic, a parabolic, or a hyperbolic form. SOSPA has the same efficiency as the traditional SORM methods.

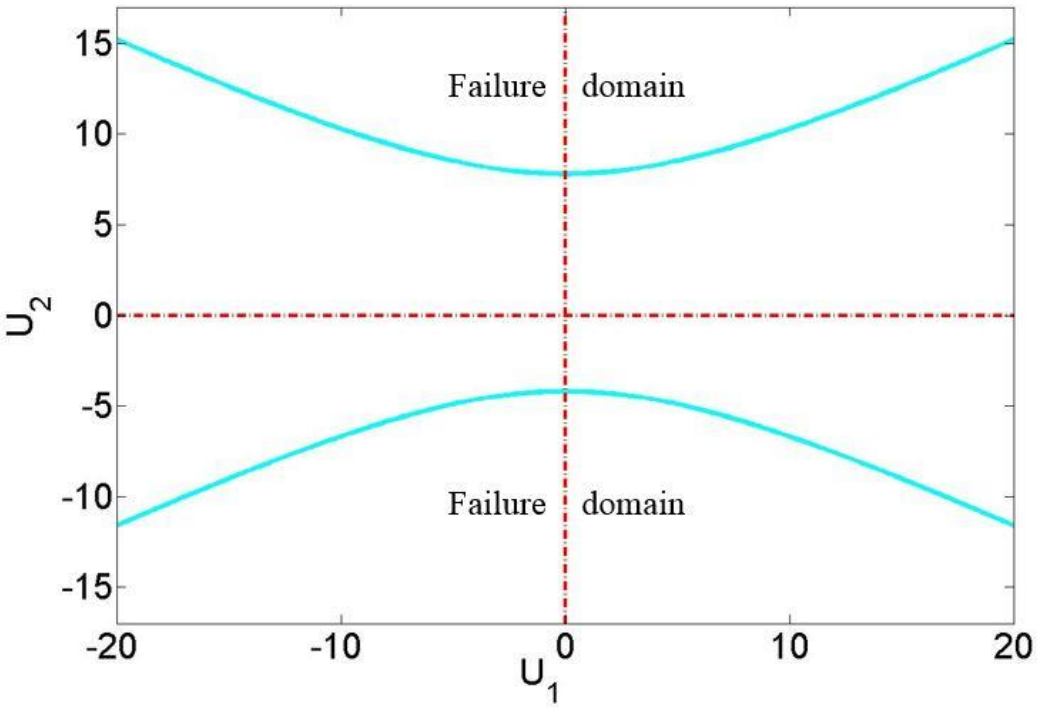

Figure 9. Hyperbolic contour of the limit-state function in Case 2

Table 6. p_f of the hyperbola quadratic function in Case 1

Method	p_f	ε%	Absolute Error	Function Calls	β
FORM	3.1671×10^{-5}	16.2%	6.119×10^{-6}	48	4
SORM (Breitung)	1.9003×10^{-5}	49.7%	1.8787×10^{-5}	51	4
SORM (Tvedt)	1.8494×10^{-5}	51.1%	1.9296×10^{-5}	51	4
SOSPA	3.9383×10^{-5}	4.21%	1.593×10^{-6}	51	4
MCS	3.779×10^{-5}	N/A	N/A	10^8	N/A

Table 7. p_f of the hyperbola quadratic function in Case 2

Method	p_f	ε%	Absolute Error	Function Calls	β
FORM	1.3346×10^{-5}	8.68%	1.066×10^{-6}	28	4.2
SORM (Breitung)	1.1927×10^{-5}	2.87%	3.53×10^{-7}	31	4.2
SORM (Tvedt)	1.1856×10^{-5}	3.45%	4.24×10^{-7}	31	4.2
SOSPA	1.1963×10^{-5}	2.58%	3.17×10^{-7}	31	4.2
MCS	1.228×10^{-5}	N/A	N/A	10^8	N/A

4.1.4. Example 4: High Dimensional Quadratic Function. We modify the example in Ref. [33] to test the effectiveness of SOSPA for solving the problem with a large number of input variables. The limit-state function is given by

$$g(\mathbf{U}) = -\left(U_n - \beta\right) + \frac{1}{2}\sum_{i=1}^{n-1} k_i U_i^2 \tag{47}$$

where $\mathbf{U} = [U_1, U_2, ..., U_n]$, n is the number of random variables, β is 3, and k_i is 0.1. The results with various dimensions are given in Table 8 and 9.

Table 8. p_f of quadratic function with n=10 and 20

Method	$n=10$			$n=20$		
	p_f	ε%	Absolute Error	p_f	ε%	Absolute Error
FORM	1.3499×10^{-3}	284%	9.9860×10^{-4}	1.3499×10^{-3}	1880%	1.2817×10^{-3}
SORM (Breitung)	4.1453×10^{-4}	18%	6.323×10^{-5}	1.1164×10^{-4}	63.7%	4.344×10^{-5}
SORM (Tvedt)	3.4769×10^{-4}	1.03%	3.61×10^{-6}	6.0905×10^{-5}	10.7%	7.295×10^{-6}
SOSPA	3.5308×10^{-4}	0.51%	1.78×10^{-6}	7.0806×10^{-5}	3.82%	2.606×10^{-6}
MCS	3.5130×10^{-4}	N/A	N/A	6.82×10^{-5}	N/A	N/A

Table 9. p_f of quadratic function with n=30 and 40

Method	$n=30$			$n=40$		
	p_f	ε%	Absolute Error	p_f	ε%	Absolute Error
FORM	1.3499×10^{-3}	10400%	1.3371×10^{-3}	1.3499×10^{-3}	67400%	1.3479×10^{-3}
SORM (Breitung)	3.0069×10^{-5}	135%	1.7269×10^{-5}	8.0987×10^{-6}	305%	6.0987×10^{-6}
SORM (Tvedt)	4.8265×10^{-6}	62.3%	7.9735×10^{-6}	-2.1865×10^{-6}	209%	4.1865×10^{-6}
SOSPA	1.2648×10^{-5}	1.19%	1.52×10^{-7}	2.0256×10^{-6}	1.28%	2.56×10^{-8}
MCS	1.28×10^{-5}	N/A	N/A	2.0×10^{-6}	N/A	N/A

As the results show, SOSPA constantly yields accurate results while other methods produce larger errors as the dimensions of random variables increase. When $n=40$, the Tvedt's formulas results in a negative probability of failure.

4.2. ENGINEERING EXAMPLES

After demonstrating the high accuracy of SOSPA for quadratic limit-state functions, we now use it for engineering problems with general limit-state functions, which are not quadratic.

4.2.1. Example 1: A Slider-Crank Mechanism. A slider-crank mechanism is shown in Figure 10. The position of the mechanism is required to be $s_r = 2.3\,\text{cm}$ when $\theta = 60^\circ$. If the difference between the actual position s and the required positon is outside the tolerance range $\varepsilon = \pm 0.16\,\text{cm}$, the mechanism fails.

Thus the limit-state function of the slider crank mechanism is given by

$$g(\mathbf{X}) = \varepsilon^2 - \left(a\cos\theta + \sqrt{b^2 - (a\sin\theta)^2} - s_r \right)^2 \tag{48}$$

where $\mathbf{X} = [a, b]$. All the random variables are assumed to be independently and normally distributed, and their parameters are listed in Table 10. The contour of the limit-state function is plotted in Figure 11.

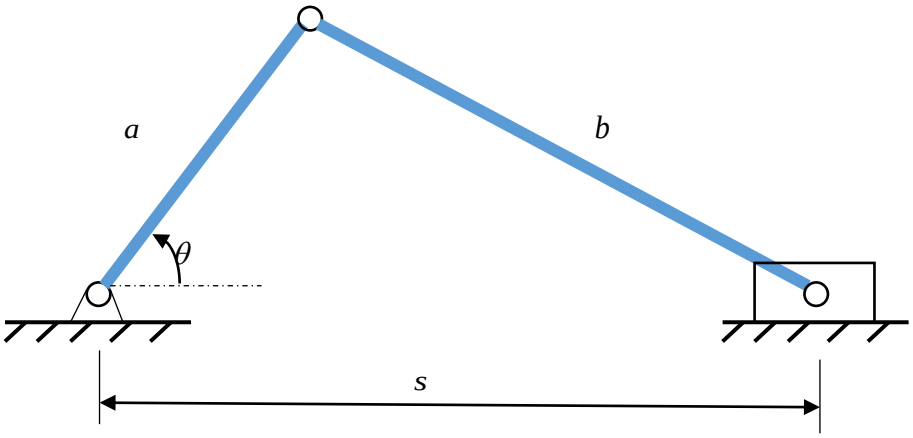

Figure 10. A slider crank system

Table 10. Distributions of the random variables in slider crank mechanism

Random Variable	Distribution	Mean	Standard Deviation
$a\,(\mathrm{cm})$	Normal	1	0.02
$b\,(\mathrm{cm})$	Normal	2	0.04

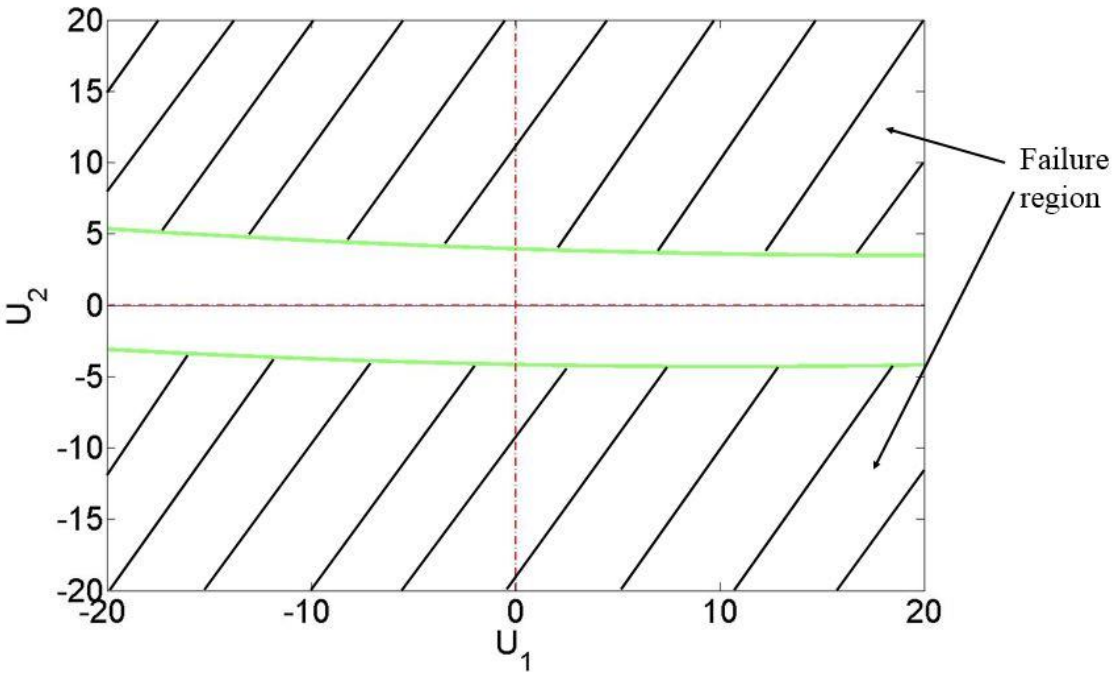

Figure 11. The contour of the slider crank system

Table 11 gives the results, which show that FORM and both of the SORM methods produce relatively large errors. The reason is that the above methods only consider half of the failure domain by approximating one of the two contours. SOSPA can take all the failure domains into account and estimate the probability of failure accurately while maintaining the same efficiency as the two SORM methods.

Table 11. The probability of failure of nonlinear oscillator system

Method	p_f	ε%	Absolute Error	Function Calls	β
FORM	1.8193×10^{-4}	43.4%	1.3949×10^{-4}	26	3.57
SORM (Breitung)	1.8140×10^{-4}	46.6%	1.4002×10^{-4}	29	3.57
SORM (Tvedt)	1.8136×10^{-4}	43.6%	1.4006×10^{-4}	29	3.57
SOSPA	3.1615×10^{-4}	1.64%	5.27×10^{-6}	29	3.57
MCS	3.2142×10^{-4}	N/A	N/A	10^8	N/A

4.2.2. Example 2: Cantilever Tube. In order to investigate the effectiveness of SOSPA for problems with non-normal random variables, we modify the example of a cantilever tube [34, 35] shown in Figure 12. The tube is subjected to three forces F_1, F_2 and P as well as a torque T. A failure occurs if the maximum von Mises stress $\sigma_{\max}$ is larger than the yield strength S_y. The limit-state function is defined by

$$g(\mathbf{X}) = S_y - \sigma_{\max} \tag{49}$$

where $\mathbf{X} = [F_1, F_2, P, T, \theta_1, \theta_2, t, d, S_y]$, and $\sigma_{\max}$ is given by

$$\sigma_{\max} = \sqrt{\sigma_x^2 + 3\tau_{zx}^2} \tag{50}$$

in which

$$\sigma_x = \frac{P}{A} + \frac{M}{I} \tag{51}$$

$$\tau_{xz} = \frac{[2T + F_1 d\sin(\theta_1) + F_2 d\sin(\theta_2)]d}{8I} \tag{52}$$

$$I = \frac{\pi}{64}[d^4 - (d-2t)^4] \tag{53}$$

$$A = \frac{\pi}{4}[d^2 - (d - 2t)^2] \tag{54}$$

and

$$M = F_1 L_1 \cos(\theta_1) + F_2 L_2 \cos(\theta_2) \tag{55}$$

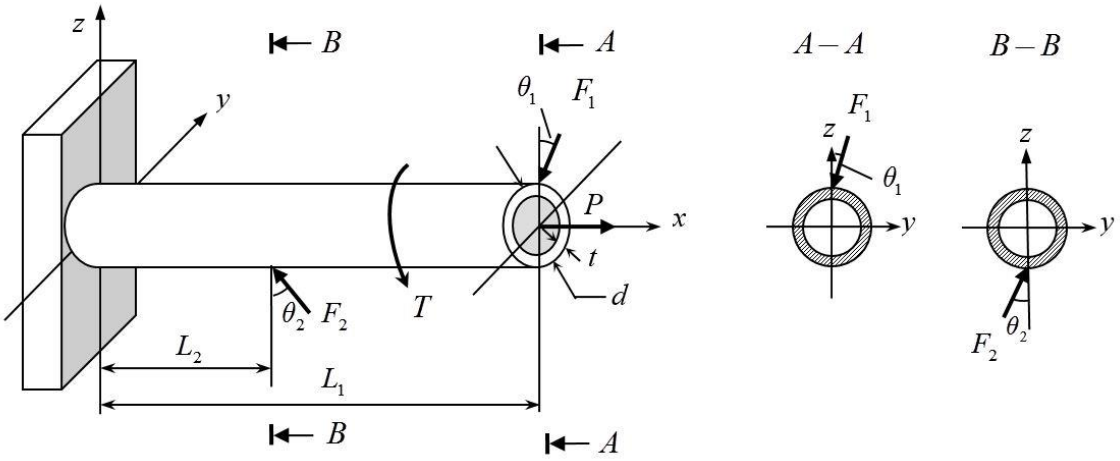

Figure 12. A cantilever tube

Table 12. Distributions of the random variables in cantilever tube

Random Variable	Distribution	Mean	Standard Deviation
F_1 (N)	Lognormal	2000	400
F_2 (N)	Lognormal	2500	875
P(N)	Normal	1000	100
T(N·m)	Normal	200	20
$\theta_1(^\circ)$	Normal	20	1
$\theta_2(^\circ)$	Normal	20	1
t(mm)	Normal	5	0.1
d(mm)	Normal	43	0.1
S_y(MPa)	Normal	170	25

Table 13. p_f of cantilever tube

Method	p_f	ε%	Absolute Error	Function Calls	β
FORM	9.5299×10^{-4}	34.1%	4.94×10^{-4}	180	3.10
SORM (Breitung)	1.3692×10^{-3}	5.38%	7.78×10^{-5}	225	3.10
SORM (Tvedt)	1.3997×10^{-3}	3.27%	4.73×10^{-5}	225	3.10
SOSPA	1.4068×10^{-3}	2.78%	4.02×10^{-5}	225	3.10
MCS	1.4470×10^{-3}	N/A	N/A	10^7	N/A

All the input variables are given in Table 12. This problem involves nine independent random variables, in which two of them follow lognormal distributions with large coefficients of variations, and others follow normal distributions.

The results are given in Table 13, showing that both the SORM methods and SOSPA have high accuracy. SOSPA is still more accurate than the SORM methods while maintaining the same efficiency.

5. CONCLUSIONS

This work improves the accuracy of the second order reliability methods (SORM) without sacrificing computational efficiency. This is achieved by combing SORM and the saddlepoint approximation. The proposed second order saddlepoint approximation (SOSPA) method first approximates a limit-state function with a second-order Taylor expansion at the most probable point (MPP) as the traditional SORM methods do. After transforming the approximated limit-state function into a linear combination of noncentral chi-square variables without accuracy loss, in a straightforward way, SOSPA employs the saddlepoint approximation to estimate the probability of failure.

SOSPA does not require any further approximations after the limit-state function is approximated as a quadratic function. It is therefore in general more accurate than the other SORM methods that require a further approximation.

Since SOSPA is essentially a SORM method based on the MPP, it shares the same limitations of SORM. For example, it may not be accurate when multiple MPPs exist. If a limit-state function is highly nonlinear, far away from a quadratic function, the accuracy will not be good either.

ACKNOWLEDGEMENTS

This material is based in part upon the work supported by the National Science Foundation under Grant Number CMMI 1562593. Any opinions, findings, and conclusions or recommendations expressed in this material are those of the authors and do not necessarily reflect the views of the National Science Foundation. The support from the Intelligent Systems Center at the Missouri University of Science and Technology is also acknowledged.

REFERENCES

[1] Choi SK, Grandhi R, Canfield RA. Reliability-based structural design. New York: Springer Science & Business Media; 2006.

[2] Elishakoff I, Van Manen S, Arbocz J. First-order second-moment analysis of the buckling of shells with random imperfections. AIAA journal. 1987;25:1113-7.

[3] Mahadevan S, Haldar A. Probability, reliability and statistical method in engineering design. New York: John Wiley & Sons; 2000.

[4] Hasofer AM, Lind NC. An exact and invariant first-order reliability format. Journal of Engineering Mechanics. 1974; 100:111-121.

[5] Hohenbichler M, Rackwitz R. First-order concepts in system reliability. Structural safety. 1983;1:177-88.

[6] Der Kiureghian A, Dakessian T. Multiple design points in first and second-order reliability. Structural Safety. 1998;20:37-49.

[7] Breitung K. Asymptotic approximations for multinormal integrals. Journal of Engineering Mechanics. 1984;110:357-66.

[8] Tvedt L. Two second-order approximations to the failure probability. Report No. RDIV/20-004-83. Det Norske Veritas, Hovik, Norway, 1983.

[9] Tvedt L. Distribution of quadratic forms in normal space-application to structural reliability. Journal of Engineering Mechanics. 1990;116:1183-97.

[10] Zhao Y-G, Ono T. New approximations for SORM: Part 1. Journal of Engineering Mechanics. 1999;125:79-85.

[11] Hohenbichler M, Gollwitzer S, Kruse W, Rackwitz R. New light on first-and second-order reliability methods. Structural safety. 1987;4:267-84.

[12] Köylüoğlu HU, Nielsen SR. New approximations for SORM integrals. Structural Safety. 1994;13:235-46.

[13] Madsen HO, Krenk S, Lind NC. Methods of structural safety. Chelmsford: Courier Corporation; 2006.

[14] Ditlevsen O, Madsen HO. Structural reliability methods. New York: Wiley; 1996.

[15] Mansour R, Olsson M. A closed-form second-order reliability method using noncentral chi-squared distributions. Journal of Mechanical Design. 2014;136:101402.

[16] Du X. Saddlepoint approximation for sequential optimization and reliability analysis. Journal of Mechanical Design. 2008;130:011011.

[17] Du X, Chen W. Sequential optimization and reliability assessment method for efficient probabilistic design. Journal of Mechanical Design. 2004;126:225-33.

[18] Du X, Guo J, Beeram H. Sequential optimization and reliability assessment for multidisciplinary systems design. Structural and Multidisciplinary Optimization. 2008;35:117-30.

[19] Lee I, Choi K, Gorsich D. System reliability-based design optimization using the MPP-based dimension reduction method. Structural and Multidisciplinary Optimization. 2010;41:823-39.

[20] McDonald M, Mahadevan S. Design optimization with system-level reliability constraints. Journal of Mechanical Design. 2008;130:021403.

[21] Zhao Y-G, Ono T. A general procedure for first/second-order reliabilitymethod (FORM/SORM). Structural safety. 1999;21:95-112.

[22] Rosenblatt M. Remarks on a multivariate transformation. The annals of mathematical statistics. 1952;23:470-2.

[23] Hohenbichler M, Rackwitz R. Non-normal dependent vectors in structural safety. Journal of the Engineering Mechanics Division. 1981;107:1227-38.

[24] Konishi S, Niki N, Gupta AK. Asymptotic expansions for the distribution of quadratic forms in normal variables. Annals of the Institute of Statistical Mathematics. 1988;40:279-96.

[25] Johnson NL, Kotz S, Balakrishnan N. Continuous univariate distributions , vol. 1. New York: John Wiley & Sons; 1994.

[26] Tanizaki H. Computational methods in statistics and econometrics. Boca Raton: CRC Press; 2004.

[27] Daniels HE. Saddlepoint approximations in statistics. The Annals of Mathematical Statistics. 1954;25:631-50.

[28] Lugannani R, Rice S. Saddle point approximation for the distribution of the sum of independent random variables. Advances in applied probability. 1980;12:475-90.

[29] Daniels HE. Tail probability approximations. International Statistical Review/Revue Internationale de Statistique. 1987;55:37-48.

[30] Goutis C, Casella G. Explaining the saddlepoint approximation. The American Statistician. 1999;53:216-24.

[31] Du X, Sudjianto A. A saddlepoint approximation method for uncertainty analysis. ASME 2004 International Design Engineering Technical Conferences and Computers and Information in Engineering Conference: American Society of Mechanical Engineers; 2004. p. 445-52.

[32] Zhang J, Du X. A second-order reliability method with first-order efficiency. Journal of Mechanical Design. 2010;132:101006.

[33] Der Kiureghian A, Lin H-Z, Hwang S-J. Second-order reliability approximations. Journal of Engineering Mechanics. 1987;113:1208-25.

[34] Du X, Sudjianto A, Huang B. Reliability-based design with the mixture of random and interval variables. Journal of mechanical design. 2005;127:1068-76.

[35] Hu Z, Du X. A random field approach to reliability analysis with random and interval variables. ASCE-ASME Journal of Risk and Uncertainty in Engineering Systems, Part B: Mechanical Engineering. 2015;1:041005.

III. EFFICIENT RELIABILITY-BASED DESIGN WITH SECOND ORDER APPROXIMATIONS

Zhangli Hu and Xiaoping Du

Department of Mechanical and Aerospace Engineering
Missouri University of Science and Technology

ABSTRACT

Sequential optimization and reliability analysis (SORA) is an efficient approach to reliability-based design (RBD). It decouples the double loop structure of RBD into a serial cycles of deterministic optimization and reliability analysis. The first order approximation is used in SORA for reliability analysis due to its good balance between accuracy and efficiency. However, it may result in a large error when a constraint function is highly nonlinear. This study proposes a new numerical method so that second order approximations for the reliability analysis can be used for higher accuracy. To minimize the increased computational cost due to second order approximations, this study also develops an efficient algorithm for searching for an equivalent reliability index with the help of the saddlepoint approximation. The efficiency and accuracy of the proposed method are verified through numerical examples.

1. INTRODUCTION

Reliability-based design (RBD) is a design methodology for accounting for uncertainties associated with material properties, geometry, manufacturing processes, and operational environments [1]. RBD aims to obtain an optimal design with high reliability by ensuring design constraints be satisfied at desired probability levels.

RBD formulates a probabilistic optimization problem by minimizing a cost-type object while maintaining reliability constraints [2-5]. During RBD, reliability is numerically evaluated repeatedly by reliability analysis. The most commonly used reliability analysis method is the First Order Reliability Method (FORM) [6, 7]. FORM provides a good balance between accuracy and efficiency [8, 9]. Since the direct use of FORM is computationally expensive due to the Most Probable Point (MPP) search, the inverse FORM has been developed to improve the efficiency by modifying the formulation of reliability constraints, and one of the methods is the performance measure approach (PMA) [10, 11]. Both the direct and inverse FORM need an iterative numerical process, and combining optimization with either FORM or inverse FORM becomes a double-loop process, resulting in a high computational cost.

The decoupled approaches have been therefore developed to reduce the computational cost. The sequential optimization and reliability assessment (SORA) [3, 12-14] is one of the decoupled approaches. In SORA, the reliability analysis loop is decoupled from the optimization loop. Both loops are performed sequentially. Then the double loop structure is transformed into decoupled sequential loops. Furthermore, inverse FORM is employed as an integral part to maintain the efficiency of the reliability analysis loop. SORA is more efficient than double loop RBD methods with the same

accuracy. Yin and Chen [15] developed an enhanced SORA to improve the efficiency for solving problems with varying variances of random variables. Saddlepoint approximation is integrated with SORA to improve the accuracy of RBD when FORM is not appropriate [16]. Chao and Lee [17] integrated the convex linearization with SORA to improve the efficiency of RBD. The MPP-based dimensional reduction method is combined with SORA to ensure high accuracy of RBD when the performance functions are highly nonlinear [18]. The approximate SORA [19] was proposed to further reduce the number of reliability analyses.

SORA was originally developed for the use of FORM, which approximates a constraint function by the first-order Taylor expansion at the MPP. SORA may result in a large error in reliability estimation when the constraint function is highly nonlinear. The Second Order Reliability Method (SORM) [20-24] is more accurate than FORM due to the second-order approximation. It makes the constraint function a complete quadratic function in standard normal variables. Then a further rotation transformation is performed after the second-order Taylor expansion and constraint function becomes a paraboloid. Finally the reliability is analytically evaluated by Breitung's formula or Tvedt's formula. The other second order approximation method is the saddlepoint approximation [16, 25]. It calculates the reliability without further transformation and approximation of the quadratic function. Its accuracy is in general higher than Breitung's and Tvedt's formulas.

The objective of this work is to introduce SORM into SORA in order to improve the accuracy of SORA. The new method is termed as SORA/SORM. It improves the

accuracy by replacing the inverse FORM with an inverse SORM and maintains the high efficiency by using the same structure of SORA.

The rest of this article is organized as follows: Section 2 reviews the theoretical background of this work. Then the proposed computational procedure and algorithms of inverse SORM are discussed in Section 3. Section 4 presents the proposed SORA/SORM, followed by illustrative examples in Section 5. Conclusions are given in Section 6.

2. REVIEW OF FUNDAMENTAL METHODOLOGIES

In this section, the basic formulation of RBD and the common methods for the reliability analysis are briefly reviewed, including the direct FORM, inverse FORM, and SORM. SORA is also reviewed herein.

2.1. RBD AND FORM

A typical RBD model is expressed as

$$\begin{cases} \underset{(\mathbf{d},\boldsymbol{\mu}_\mathbf{X})}{\text{Min}} & f(\mathbf{d},\boldsymbol{\mu}_\mathbf{X},\boldsymbol{\mu}_\mathbf{P}) \\ s.t. & \Pr\left\{g_i(\mathbf{d},\mathbf{X},\mathbf{P})\le 0\right\}\ge[R_i]=1-[p_{fi}], \quad i=1,2,...,n_g \\ & \mathbf{d}^L\le\mathbf{d}\le\mathbf{d}^U \\ & \boldsymbol{\mu}_\mathbf{X}^L\le\boldsymbol{\mu}_\mathbf{X}\le\boldsymbol{\mu}_\mathbf{X}^U \end{cases} \tag{1}$$

In the above model, $\mathbf{d}$ is the vector of deterministic design variables, $\mathbf{d}^L$ and $\mathbf{d}^U$ represent the lower and upper bounds of $\mathbf{d}$, respectively. $\mathbf{X}=[X_1,X_2,...,X_n]^T$ is the vector of independent random design variables whose mean values $\boldsymbol{\mu}_\mathbf{X}=[\mu_{X_1},\mu_{X_2},...,\mu_{X_n}]^T$ are to be determined, and its lower bound and upper bound are $\boldsymbol{\mu}_\mathbf{X}^L$ and $\boldsymbol{\mu}_\mathbf{X}^U$, respectively. $\mathbf{P}=[P_1,P_2,...,P_m]^T$ is the vector of independent random parameters, which cannot be controlled by designers. $f(\cdot)$ is the objective function, which is evaluated at $\mathbf{d}$, $\boldsymbol{\mu}_\mathbf{X}$, and $\boldsymbol{\mu}_\mathbf{P}$. $g_i(\mathbf{d},\mathbf{X},\mathbf{P})$ is a constraint function or performance function, and the probability of constraint satisfaction or reliability $\Pr\left\{g_i(\mathbf{d},\mathbf{X},\mathbf{P})\le 0\right\}$ should be greater than or equal to the desired reliability $[R_i]$ or $1-[p_{fi}]$, where $[p_{fi}]$ is the prescribed allowable probability of failure.

In the above model, the probability of constraint satisfaction or reliability is obtained by

$$\Pr\left\{g\left(\mathbf{d},\mathbf{X},\mathbf{P}\right)\le 0\right\}=\int_{g(\mathbf{d},\mathbf{X},\mathbf{P})\le 0} f_{\mathbf{X},\mathbf{P}}(\mathbf{x},\mathbf{p})d\mathbf{x}d\mathbf{p} \tag{2}$$

where $f_{\mathbf{X},\mathbf{P}}(\mathbf{x},\mathbf{p})$ is the joint probability density function of $\mathbf{X}$ and $\mathbf{P}$. Generally, it is difficult to compute the above multidimensional integration. FORM is usually used to approximate the reliability. FORM first transforms $\mathbf{X}$ and $\mathbf{P}$ into standard normal variables $\mathbf{U}_{\mathbf{X}}$ and $\mathbf{U}_{\mathbf{P}}$ [9, 26, 27]. The performance function then becomes

$$g\left(\mathbf{d},\mathbf{X},\mathbf{P}\right)=g\left(\mathbf{d},T(\mathbf{U})\right)=g\left(\mathbf{d},T(\mathbf{U}_{\mathbf{X}},\mathbf{U}_{\mathbf{P}};\boldsymbol{\mu}_{\mathbf{X}})\right)=G(\mathbf{d},\mathbf{U}) \tag{3}$$

where $\mathbf{U}=(\mathbf{U}_{\mathbf{X}},\mathbf{U}_{\mathbf{P}})$, and $T(\cdot)$ stands for the transformation from standard normal space (U-space) to original random space (X-space). Note that the transformation depends on $\boldsymbol{\mu}_{\mathbf{X}}$. FORM then linearizes $G(\mathbf{d},\mathbf{U})$ at the MPP, where the integrand $f_{\mathbf{X},\mathbf{P}}(\mathbf{x},\mathbf{p})$ in Eq. (2) is maximized, thereby minimizing the error of the linearization.

MPP $\mathbf{u}_{MPP}$ is obtained by solving

$$\begin{cases}\text{Min} \ \ \|\mathbf{u}\|=\sqrt{\mathbf{u}\mathbf{u}^{T}}\\ \text{s.t.} \quad g\left(\mathbf{d},T(\mathbf{u})\right)=0\end{cases} \tag{4}$$

where $\|\cdot\|$ stands for the magnitude of a vector.

Finally the reliability is calculated by

$$\Pr\left\{g\left(\mathbf{d},\mathbf{X},\mathbf{P}\right)\le 0\right\}=\Phi(\beta)=\Phi(\|\mathbf{u}_{MPP}\|) \tag{5}$$

where $\beta=\|\mathbf{u}_{MPP}\|$ is the reliability index, and $\Phi(\cdot)$ is the cumulative distribution function (CDF) of a standard normal random variable.

When FORM is directly used to solve the optimization model in Eq. (1), the efficiency is usually low due to the nested optimization loop [10, 28, 29]. Inside the outer optimization loop, FORM needs to call the performance function repeatedly for the reliability analysis.

2.2. RBD AND INVERSE FORM

As discussed above, directly using FORM in RBD is computationally expensive. So the inverse FORM has been proposed to improve the efficiency by modifying the formulations of reliability constraints. Using inverse FORM, the equivalent RBD model becomes [10, 30, 31]

$$\begin{cases} \underset{(\mathbf{d},\boldsymbol{\mu}_\mathbf{X})}{\text{Min}} & f(\mathbf{d},\boldsymbol{\mu}_\mathbf{X},\boldsymbol{\mu}_\mathbf{P}) \\ s.t. & g_i^{1-[p_{fi}]}(\mathbf{d},\mathbf{X},\mathbf{P}) \le 0, \quad i=1,2,...,n_g \\ & \mathbf{d}^L \le \mathbf{d} \le \mathbf{d}^U \\ & \boldsymbol{\mu}_\mathbf{X}^L \le \boldsymbol{\mu}_\mathbf{X} \le \boldsymbol{\mu}_\mathbf{X}^U \end{cases} \tag{6}$$

where $g_i^{1-[p_{fi}]}$ is the performance measure, which is defined by

$$\Pr\left\{ g_i(\mathbf{d},\mathbf{X},\mathbf{P}) \le g_i^{1-[p_{fi}]} \right\} = 1-[p_{fi}] \tag{7}$$

The performance measure is calculated by inverse FORM.

$$g^{1-[p_f]}(\mathbf{d},\mathbf{X},\mathbf{P}) = g(\mathbf{d},T(\mathbf{u}_{MPP})) = g\left(\mathbf{d},T(\mathbf{u}_{\mathbf{x}_{MPP}},\mathbf{u}_{\mathbf{p}_{MPP}})\right) = g(\mathbf{d},\mathbf{x}_{MPP},\mathbf{p}_{MPP}) \tag{8}$$

where $\mathbf{u}_{MPP} = \left(\mathbf{u}_{\mathbf{x}_{MPP}},\mathbf{u}_{\mathbf{p}_{MPP}}\right)$ is the inverse MPP in the U-space, and $\left(\mathbf{x}_{MPP},\mathbf{p}_{MPP}\right)$ is corresponding inverse MPP in the X-space. The inverse MPP is obtained through an optimization problem given by

$$\begin{cases} \underset{\mathbf{u}}{\text{Min}} & g(\mathbf{d},\mathbf{u}) \\ s.t. & \|\mathbf{u}\| = [\beta] \end{cases} \tag{9}$$

where $[\beta]$ is the target reliability index and is calculated by

$$[\beta] = \|\mathbf{u}_{MPP}\| = -\Phi^{-1}([p_f]) \tag{10}$$

in which $\Phi^{-1}(\cdot)$ represents the inverse CDF of a standard normal random variable.

With Eq. (8), the RBD model is then rewritten as

$$\begin{cases} \underset{(\mathbf{d},\boldsymbol{\mu}_\mathbf{X})}{\text{Min}} & f(\mathbf{d},\boldsymbol{\mu}_\mathbf{X},\boldsymbol{\mu}_\mathbf{P}) \\ s.t. & g_i\left(\mathbf{d}, T(\mathbf{u}_{i,\mathbf{x}_{MPP}};\boldsymbol{\mu}_\mathbf{X}), T(\mathbf{u}_{i,\mathbf{p}_{MPP}})\right) \le 0, \quad i = 1,2,...,n_g \\ & \mathbf{d}^L \le \mathbf{d} \le \mathbf{d}^U \\ & \boldsymbol{\mu}_\mathbf{X}^L \le \boldsymbol{\mu}_\mathbf{X} \le \boldsymbol{\mu}_\mathbf{X}^U \end{cases} \tag{11}$$

Inverse FORM can transform a probabilistic constraint to a deterministic constraint. However, finding the MPP needs a numerical iterative search process, and solving the RBD model in Eq. (11) still requires a double loop procedure.

2.3. SORA

SORA [3, 12] overcomes the drawback of the poor efficiency of the double loop structure. It decouples the optimization loop and reliability loop, and performs the two loops sequentially. In the first cycle, the deterministic optimization is performed at the means of random design variables and random parameters.

$$\begin{cases} \underset{(\mathbf{d},\boldsymbol{\mu}_\mathbf{X})}{\text{Min}} & f(\mathbf{d},\boldsymbol{\mu}_\mathbf{X},\boldsymbol{\mu}_\mathbf{P}) \\ s.t. & g_i\left(\mathbf{d},\boldsymbol{\mu}_\mathbf{X},\boldsymbol{\mu}_\mathbf{P}\right) \le 0, \quad i = 1,2,...,n_g \end{cases} \tag{12}$$

After the deterministic optimization, the reliability analysis is implemented at the deterministic optimal point $(\boldsymbol{\mu}_{\mathbf{X}}^{(1)}, \boldsymbol{\mu}_{\mathbf{P}}^{(1)})$ to locate the inverse MPP $\left(\mathbf{u}_{i,\mathbf{x}_{MPP}}^{(1)}, \mathbf{u}_{i,\mathbf{p}_{MPP}}^{(1)}\right)$. From the second cycle, the constraint function in deterministic optimization is modified using the inverse MPP.

$$\begin{cases} \underset{(\mathbf{d},\boldsymbol{\mu}_{\mathbf{X}})}{\text{Min}} & f(\mathbf{d}, \boldsymbol{\mu}_{\mathbf{X}}, \boldsymbol{\mu}_{\mathbf{P}}) \\ s.t. & g_i\left(\mathbf{d}, T(\mathbf{u}_{i,\mathbf{x}_{MPP}}^{(1)}; \boldsymbol{\mu}_{\mathbf{X}}), T(\mathbf{u}_{i,\mathbf{p}_{MPP}}^{(1)})\right) \le 0, \quad i = 1, 2, ..., n_g \end{cases} \tag{13}$$

Then the process is repeated until convergence. It is illustrated in Figure 1. Since SORA requires fewer reliability analyses, its efficiency is high.

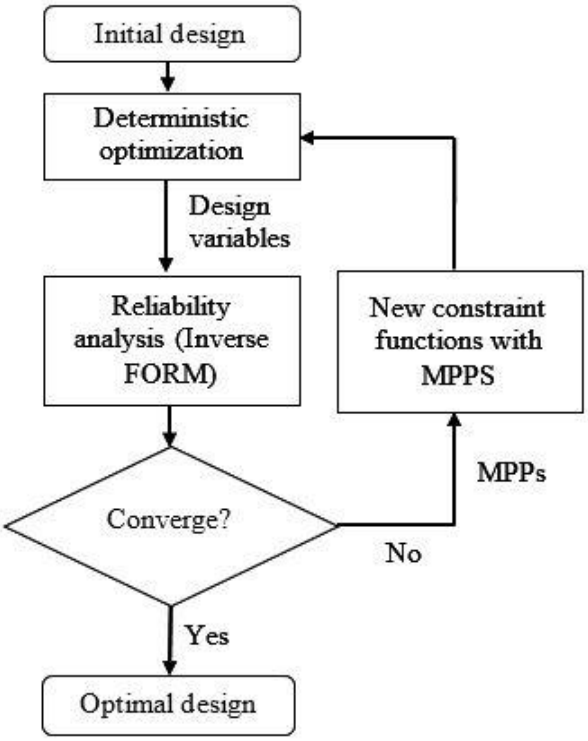

Figure 1. Flowchart of SORA

2.4. SORM

SORA uses inverse FORM to solve RBD problems. However, its accuracy may not be good when the performance functions are highly nonlinear. For this case, SORM can be employed since it is in general more accurate than FORM due to the second order approximation. The most common methods are Breitung's method [21] and Tvedt's method [32].

2.4.1. Traditional SORM Methods. The traditional methods such as Breitung's and Tvedt's methods first approximate the performance function by the second-order Taylor expansion at the MPP.

$$\begin{aligned} g\left(\mathbf{d},\mathbf{X},\mathbf{P}\right) = G\left(\mathbf{U}\right) \approx G(\mathbf{u}_{MPP}) + \nabla G(\mathbf{u}_{MPP})(\mathbf{U}-\mathbf{u}_{MPP})^T \\ + \frac{1}{2}(\mathbf{U}-\mathbf{u}_{MPP})\nabla^2 G(\mathbf{u}_{MPP})(\mathbf{U}-\mathbf{u}_{MPP})^T \end{aligned} \tag{14}$$

where $\nabla G(\mathbf{u}_{MPP}) = \left(\left.\frac{\partial G}{\partial U_1}\right|_{\mathbf{u}_{MPP}}, \cdots, \left.\frac{\partial G}{\partial U_n}\right|_{\mathbf{u}_{MPP}} \right)$ is the gradient vector, and $\nabla^2 G(\mathbf{u}_{MPP})$ is a Hessian matrix.

After a set of linear transformations, such as coordinate rotation and orthogonal diagonalization, the performance function is further simplified as a hyperparabola given by

$$G(\mathbf{V}) = V_n - \left(\beta + \frac{1}{2}\mathbf{V}\mathbf{W}\mathbf{V}^T \right) \tag{15}$$

where $\mathbf{W}$ is a $(n-1)\times(n-1)$ diagonal matrix whose elements are determined by Hessian matrix. $\mathbf{V} = \left(V_1, V_2, ..., V_n\right)^T$ is the vector of orthogonal standard normal random variables.

Finally, the reliability is analytically calculated by the asymptotic formulation [21].

$$\Pr\left\{g\left(\mathbf{d},\mathbf{X},\mathbf{P}\right)\le 0\right\}=\Phi(-\beta)\prod_{i=1}^{n-1}(1+k_i\beta)^{-1/2} \tag{16}$$

where k_i stands for the main curvatures of performance function $G\left(\mathbf{U}\right)$ at the MPP.

2.4.2. Second Order Saddlepoint Approximation. Besides the traditional SORM methods, the alternative method for reliability analysis is the second order saddlepoint approximation (SOSPA) [25] , which is considered more accurate than Breitung's and Tvedt's methods.

Once the performance function is approximated by the quadratic form in Eq. (15), the cumulant generating function (CGF) can be obtained.

$$K(t)=-\beta t+\frac{1}{2}t^2-\frac{1}{2}\sum_{i}^{n-1}\log(1-2tk_i) \tag{17}$$

The derivatives of CGF are

$$K'(t)=-\beta+t+\sum_{i=1}^{n-1}\frac{k_i}{1-2tk_i} \tag{18}$$

$$K''(t)=1+\sum_{i=1}^{n-1}\frac{k_i^2}{\left(1-2tk_i\right)^2} \tag{19}$$

The saddlepoint t_s is obtained by solving the following equation:

$$K'(t)=-\beta+t+\sum_{i=1}^{n-1}\frac{k_i}{1-2tk_i}=0 \tag{20}$$

Then the reliability is evaluated by

$$\Pr\left\{g\left(\mathbf{d},\mathbf{X},\mathbf{P}\right)\le 0\right\}=\Phi(w)+\phi(w)(\frac{1}{w}-\frac{1}{\upsilon}) \tag{21}$$

where $\phi(\cdot)$ is the probability density function (PDF) of a standard normal distribution,

$$w=\mathrm{sgn}(t_s)\left\{2\left[-K(t_s)\right]\right\}^{1/2} \tag{22}$$

$$\upsilon = t_s \left[K''(t_s) \right]^{1/2} \tag{23}$$

in which $\text{sgn}(t_s) = +1, -1$ or 0, depending on whether t_s is positive, negative, or zero.

Saddlepoint approximation has several excellent features. It yields an extremely accurate probability estimation, especially in the tail area of a distribution [16, 33, 34]. For this reason, SOSPA is employed in the proposed SORA/SORM method.

3. SORA WITH INVERSE SORM

In this section, the details of the proposed SORA/SORM method are discussed.

3.1. OVERVIEW OF SORA/SORM

The objective of this study is to improve the accuracy of SORA by replacing inverse FORM with inverse SORM. SORA is originally developed for FORM such that the MPPs from FORM are directly used to formulate constraint functions for the deterministic optimization, which can be then decoupled from the reliability analysis with FORM.

The major contributor to the high efficiency of SORA is the use of the MPPs that are directly related to required reliabilities. The MPPs are identified by inverse FORM. When the inverse SORM is used to replace the inverse FORM, an MPP is no longer directly related to the required reliability or probability of failure through the simple relationship $[p_f] = \Phi(-\|\mathbf{u}_{MPP}\|)$. To maintain the high efficiency, the same structure of SORA is used, which relies on the MPPs. To make this happen, the same relationship is maintained between the allowable probability of failure and the MPP in the inverse SORM, and the new MPP is called *the equivalent MPP*, namely,

$$[p_f] = \Phi(-\|\mathbf{u}_{MPP}^{Equ}\|) \tag{24}$$

where $\mathbf{u}_{MPP}^{Equ}$ is the equivalent MPP. The other advantage of using the equivalent MPP is that the exiting MPP search algorithms can still be used.

With the equivalent MPP, the same structure of the original SORA is able to be used. Then the flowchart for SORA/SORM can be obtained with slight modifications based on original SORA. The modified flowchart is given below.

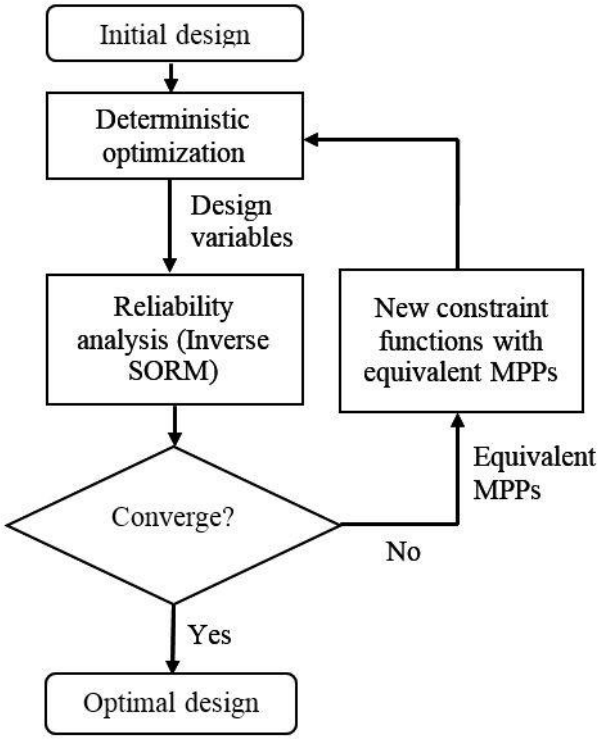

Figure 2. Flowchart of SORA/SORM

As shown in the flowchart, the key to SORA/SORM is to search for the equivalent MPPs through inverse SORM, which is discussed in the Section 3.2.

3.2. ALGORITHM FOR INVERSE SORM

Recall that the MPP of inverse FORM is located on the condition that the magnitude of the MPP or the required reliability index [β] is given, as indicated by the

MPP search model in Eq. (9). In the original SORA or SORA/FORM, $[\beta]$ is directly related with allowable probability of failure $[p_f]$ by $[\beta] = \|\mathbf{u}_{MPP}\| = -\Phi^{-1}([p_f])$. But now such a relationship is not available when using the second order approximation. The required reliability index is no longer the magnitude of the MPP, or $\|\mathbf{u}_{MPP}\|$. Let the magnitude of $\mathbf{u}$ be γ, namely,

$$\gamma = \|\mathbf{u}\| \tag{25}$$

Then the model for searching for the equivalent MPP is

$$\begin{cases} \underset{\mathbf{u},\gamma}{\text{Min}} & g(\mathbf{d},\mathbf{u}) \\ s.t. & \|\mathbf{u}\| = \gamma \\ & p_f = \Pr\{g(\mathbf{d},T(\mathbf{u})) > 0\} = [p_f] \end{cases} \tag{26}$$

The solution is the equivalent MPP $\mathbf{u}_{MPP}^{Equ}$, and $\gamma = \|\mathbf{u}_{MPP}^{Equ}\|$ is called the equivalent reliability index. There are some drawbacks if the above model is solved directly. The model has two equality constraints, which make the solution process inefficient. Existing inverse MPP search algorithms cannot be used because of the second constraint function. In addition, p_f has to be computed by SORM, which requires the second derivatives of the performance function. Then a new numerical procedure is proposed so that existing inverse MPP search algorithms can be used. The central idea is to vary γ, and then search for the MPP until $p_f = [p_f]$ is satisfied. For a given value of γ, the inverse MPP search is performed.

$$\begin{cases} \underset{\mathbf{u}}{\text{Min}} & g(\mathbf{d},\mathbf{u}) \\ s.t. & \|\mathbf{u}\| = \gamma \end{cases} \tag{27}$$

Note that the search is the same as that in Eq. (9) for the original SORA.

After the MPP $\mathbf{u}_{MPP}$ is found, SORM is performed to calculate the probability of failure p_f . If p_f is not equal to $[p_f]$, γ is updated and the inverse MPP search is performed in Eq. (27) again. This process is repeated until the difference between p_f and $[p_f]$ is small enough. The SORM method used in this work is the second order saddlepoint approximation. The flowchart and steps of the inverse SORM are given as follows.

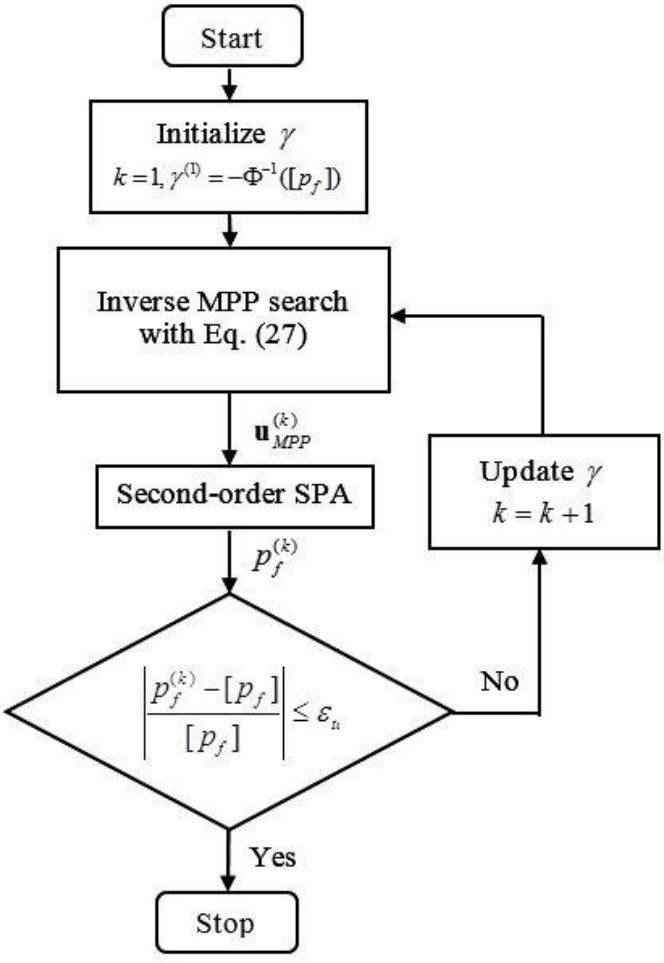

Figure 3. Flowchart of the inverse SORM

The details shown in Figure 3 are discussed below.

Step 1: Set $k=1$, and initialize $\gamma^{(1)}$ based on allowable probability of failure $[p_f]$, $\gamma^{(1)} = -\Phi^{-1}([p_f])$

Step 2: Perform the inverse MPP search using Eq. (27), and find the MPP $\mathbf{u}_{MPP}^{(k)}$.

Step 3: Calculate the probability of failure $p_f^{(k)}$ using the second-order SPA method.

Step 4: Update $\gamma^{(k+1)}$.

Step 5: Check the convergence criteria, which is chosen as the

$$\varepsilon = \left| \frac{p_f^{(k)} - [p_f]}{[p_f]} \right| \le \varepsilon_{tol} \tag{28}$$

where ε is the absolute value of the relative error, and ε_{tol} is a user-defined threshold for the convergence check.

If $\varepsilon \le \varepsilon_{tol}$, terminate the iteration, and $\gamma^{(k+1)}$ is the equivalent reliability index. Otherwise, set $k = k+1$ and return to step 2.

The key to searching for the equivalent MPP is to update γ. The algorithms of updating γ are developed in Section 3.3.

3.3. ALGORITHMS FOR UPDATING γ

To make the inverse SORM efficient, the number of inverse MPP searches is minimized. Efficient algorithms to update γ are critical. Recall that the purpose of updating γ is to satisfy $p_f^{SORM} = [p_f]$. The p_f^{SORM} is assumed to be a function of γ,

expressed by $p_f^{SORM}(\gamma)$. Since the probability of failure from FORM is $p_f^{FORM} = \Phi^{-1}(-\gamma)$, the relationship between $p_f^{SORM}(\gamma)$ and p_f^{FORM} can be used to derive equations for γ. Next, two possible relationships are assumed between $p_f^{SORM}(\gamma)$ and p_f^{FORM}, based on which algorithms are designed to update γ.

3.3.1. Additive Relationship. The difference between p_f^{SORM} and p_f^{FORM} is assumed to be constant.

$$p_f^{SORM}(\gamma) = p_f^{FORM}(\gamma) + c = \Phi(-\gamma) + c \tag{29}$$

where c is a constant.

At current iteration k and next iteration $k+1$, the probabilities of failure are given by

$$\begin{cases} p_f^{(k+1)} = \Phi(-\gamma^{(k+1)}) + c \\ p_f^{(k)} = \Phi(-\gamma^{(k)}) + c \end{cases} \tag{30}$$

In the above equations, p_f is the probability of failure from SORM, or p_f^{SORM} (For brevity, the superscript SORM is dropped). Then

$$p_f^{(k+1)} - p_f^{(k)} = \Phi(-\gamma^{(k+1)}) - \Phi(-\gamma^{(k)}) \tag{31}$$

Replacing $p_f^{(k+1)}$ by the allowable probability of failure $[p_f]$ yields the first updating algorithm as follows:

$$\gamma^{(k+1)} = -\Phi^{-1}\left([p_f] - p_f^{(k)} + \Phi(-\gamma^{(k)})\right) \tag{32}$$

Alternatively, the derivative of Eq. (29) may be taken, and this gives

$$\frac{dp_f}{d\gamma} = -\phi(-\gamma) \tag{33}$$

The derivative can be approximated with the finite difference method (FDM) with the forward scheme. Then

$$\frac{p_f^{(k+1)} - p_f^{(k)}}{\gamma^{(k+1)} - \gamma^{(k)}} = -\phi(-\gamma^{(k)}) \tag{34}$$

Thus the second updating algorithm is thus given by

$$\gamma^{(k+1)} = \gamma^{(k)} - \frac{[p_f] - p_f^{(k)}}{\phi(-\gamma^{(k)})} \tag{35}$$

3.3.2. Multiplicative Relationship. The alternative relationship between p_f^{SORM} and p_f^{FORM} is assumed to be

$$p_f^{SORM}(\gamma) = c p_f^{FORM} = c\Phi(-\gamma) \tag{36}$$

where c is not constant.

Using the FDM in Section 3.3.1, the first-order derivative of the above equation is given by

$$\frac{p_f^{(k+1)} - p_f^{(k)}}{\gamma^{(k+1)} - \gamma^{(k)}} = c^{(k)}\phi(-\gamma^{(k)}) \tag{37}$$

where

$$c^{(k)} = \frac{p_f^{(k)}}{\Phi(-\gamma^{(k)})} \tag{38}$$

Thus the third updating algorithm is obtained as

$$\gamma^{(k+1)} = \gamma^{(k)} - \frac{[p_f] - p_f^{(k)}}{c^{(k)}\phi(-\gamma^{(k)})} \tag{39}$$

Besides updating γ to satisfy $p_f^{SORM} = [p_f]$, directly solving the following nonlinear equation may be considered:

$$h(\lambda) = [p_f] - p_f^{SORM} = [p_f] - c\Phi(-\gamma) = 0 \tag{40}$$

A convex acceleration of Newton's method [35] can be used to solve the above equation due to its cubic and fast convergence [36, 37]. Then the forth updating algorithm is yielded.

$$\gamma^{(k+1)} = \gamma^{(k)} - \frac{h(\gamma^{(k)})}{h'(\gamma^{(k)})}\left(1 + \frac{L_h(\gamma^{(k)})}{2\left(1 - L_h(\gamma^{(k)})\right)}\right) \tag{41}$$

where

$$h'(\gamma^{(k)}) = c^{(k)}\phi(-\gamma^{(k)}) \tag{42}$$

$$h''(\gamma^{(k)}) = -c^{(k)}(\gamma^{(k)})\phi(-\gamma^{(k)}) \tag{43}$$

$$L_h(\gamma^{(k)}) = h(\gamma^{(k)})\left(h''(\gamma^{(k)})\right)\Big/\left(h'(\gamma^{(k)})\right)^2 \tag{44}$$

and $c^{(k)}$ is calculated with Eq. (38).

The four algorithms for updating γ are summarized in Table 1.

Table 1. Algorithms to update the reliability index

Algorithms	Equations
1	$\gamma^{(k+1)} = -\Phi^{-1}\left([p_f] - p_f^{(k)} + \Phi(-\gamma^{(k)})\right)$
2	$\gamma^{(k+1)} = \gamma^{(k)} - \dfrac{[p_f] - p_f^{(k)}}{\phi(-\gamma^{(k)})}$
3	$\gamma^{(k+1)} = \gamma^{(k)} - \dfrac{[p_f] - p_f^{(k)}}{c^{(k)}\phi(-\gamma^{(k)})}$
4	$\gamma^{(k+1)} = \gamma^{(k)} - \dfrac{h(\gamma^{(k)})}{h'(\gamma^{(k)})}\left(1 + \dfrac{L_h(\gamma^{(k)})}{2\left(1 - L_h(\gamma^{(k)})\right)}\right)$

Next a numerical example is used to demonstrate the performance of the algorithms. The example contains four standard normal variables, and the performance function is given by

$$g(\mathbf{X}) = 90 - (X_1 - 5)^2 - (X_2 - 6)^2 - (X_3 - 6)^2 - (X_4 - 6)^2 \tag{45}$$

where $\mathbf{X} = [X_1, X_2, X_3, X_4]^T$.

The allowable probability of failure is set to be $[p_f] = 10^{-5}$, and the tolerance for convergence criterion is chosen as $\varepsilon_{tol} = 0.1\%$. The proposed four updating algorithms are compared in terms of accuracy and efficiency. The accuracy is evaluated by comparing with the result from Monte Carlo Simulation (MCS). And the efficiency is measured by the number of performance function calls.

The results are presented in Table 2, which show that all the four algorithms achieve the same target reliability. p_f^{MCS} in the table is the probability of failure of $\Pr\{g(\mathbf{X}) > g(\mathbf{u}_{MPP})\}$ calculated by MCS with a sample size of 10^7. The results are the same for four algorithms and are close to the allowable probability of failure $[p_f] = 10^{-5}$. So the four algorithms have the same accuracy. But algorithm 4 achieves the highest efficiency. Considering efficiency and accuracy, algorithm 4 is chosen as the method of updating reliability index when inverse SORM is used.

Figure 4 shows the iteration history of the probability of failure calculated by inverse SORM with algorithm 4. It indicates that the probability of failure coverages to the allowable probability of failure quickly.

Table 2. Results of inverse SORM

Algorithm	$\mathbf{u}_{MPP}$	γ	$g(\mathbf{u}_{MPP})$	p_f^{MCS}	Function Calls	Number of MPP searches
1	(1.7792, 2.1351, 2.1351, 2.1351)	4.1037	34.8134	1.02×10^{-5}	242	11
2	(1.7792, 2.1351, 2.1351, 2.1351)	4.1037	34.8134	1.02×10^{-5}	242	11
3	(1.7791, 2.1350, 2.1350, 2.1350)	4.1037	34.8115	1.02×10^{-5}	122	6
4	(1.7791, 2.1350, 2.1350, 2.1350)	4.1037	34.8110	1.02×10^{-5}	98	5

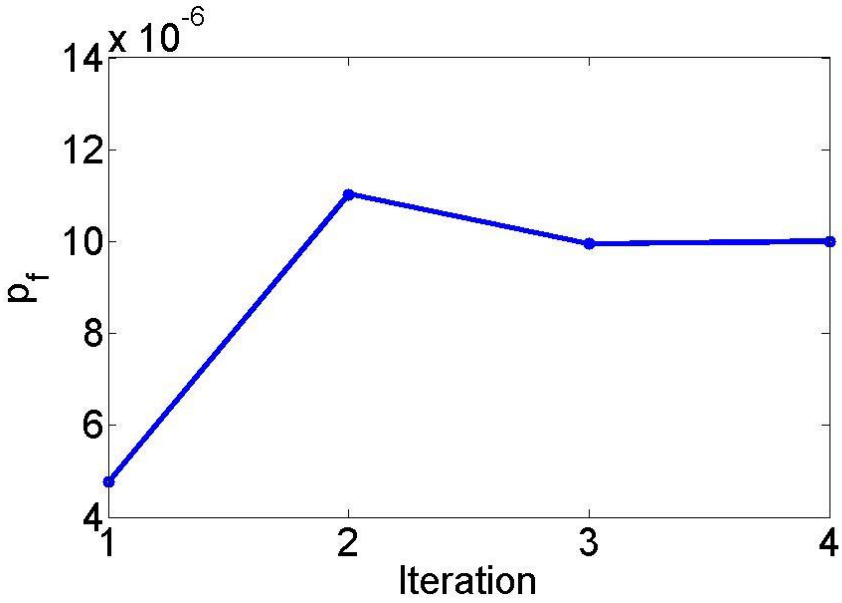

Figure 4. Convergence history

4. SORA/SORM

The purpose of SORA/SORM is to improve the accuracy. At the same time, high efficiency is also required. For high efficiency, the complete inverse SORM is not performed after the deterministic optimization in each cycle of SORA. Instead, only one iteration of inverse SORM is performed, and γ is updated only once. With the progress of cycles, γ will gradually converge to the equivalent reliability index for an active constraint. The detailed steps of SORA/SORM are summarized below.

Step 1: Set the initial design point $\mathbf{d}^{(1)}$ and $\boldsymbol{\mu}_{\mathbf{X}}^{(1)}$.

Step 2: Set $k=1$. Use the means of random variables as the initial MPP for each performance function. Calculate the initial $\gamma_i^{(1)} = -\Phi^{-1}([p_{fi}])$.

Step 3: Perform the following deterministic optimization and obtain $\mathbf{d}^{(k+1)}$ and $\boldsymbol{\mu}_{\mathbf{X}}^{(k+1)}$.

$$\begin{cases} \underset{(\mathbf{d},\boldsymbol{\mu}_{\mathbf{X}})}{\text{Min}} & f(\mathbf{d},\boldsymbol{\mu}_{\mathbf{X}},\boldsymbol{\mu}_{\mathbf{P}}) \\ s.t. & g_i\left(\mathbf{d}, T(\mathbf{u}_{i,\mathbf{x}_{MPP}}^{(1)},\boldsymbol{\mu}_{\mathbf{X}}), T(\mathbf{u}_{i,\mathbf{p}_{MPP}}^{(1)})\right) \le 0, \quad i=1,2,...,n_g \\ & \mathbf{d}^L \le \mathbf{d} \le \mathbf{d}^U \\ & \boldsymbol{\mu}_{\mathbf{X}}^L \le \boldsymbol{\mu}_{\mathbf{X}} \le \boldsymbol{\mu}_{\mathbf{X}}^U \end{cases} \tag{46}$$

Step 4: Implement reliability analysis using inverse SORM for each constraint function.

(1) Perform MPP search given $\gamma^{(k)}$. Obtain the MPP $\mathbf{u}_{MPP}^{(k)}$,and the gradient of the performance function $\nabla g(\mathbf{u}_{MPP}^{(k)})$, and evaluate it at MPP.

(2) Calculate the probability of failure $p_f^{(k)}$ using second-order SPA.

(3) Update the reliability index $\gamma^{(k+1)}$ using Eq. (41).

(4) Update the MPP using the advanced mean-value method [38, 39].

$$\mathbf{u}_{MPP}^{(k+1)} = \gamma^{(k+1)} \frac{\nabla g(\mathbf{u}_{MPP}^{(k)})}{\left\| \nabla g(\mathbf{u}_{MPP}^{(k)}) \right\|} \tag{47}$$

Step 5: Check convergence. The convergence criterion is defined as

$$\varepsilon = \left| \frac{p_f^{(k)} - [p_f]}{[p_f]} \right| \le \varepsilon_{tol} \tag{48}$$

If $\varepsilon \le \varepsilon_{tol}$, terminate the iteration, and $\left(\mathbf{d}^{(k+1)}, \boldsymbol{\mu}_{\mathbf{X}}^{(k+1)}\right)$ is the optimal point. Otherwise, set $k = k+1$ and return to step 3.

The flowchart of overall procedure of SORA/SORM is shown in Figure 5.

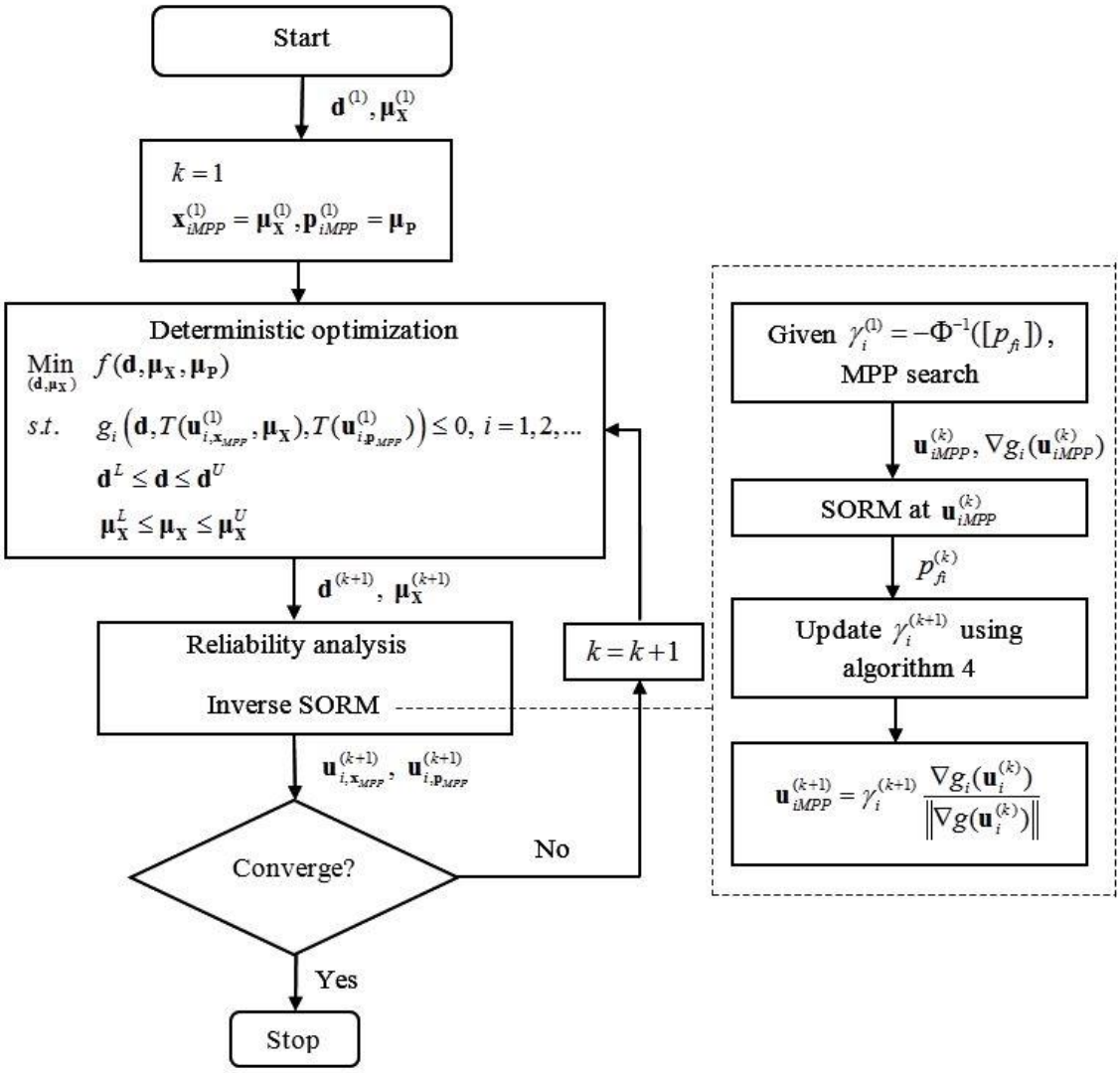

Figure 5. Flowchart of SORA/SORM method

5. EXAMPLES

In this section, three problems are given to test the effectiveness of SORA/SORM. To show the effectiveness, SORA/SORM is compared with double-loop method using direct SORM, denoted as DL-SORM, and SORA/FORM. The accuracy is evaluated by the relative error between the probability of failure at the optimal point calculated by MCS with a large number of sample size and the allowable probability of failure for active constraint functions. The number of function calls is provided as the measure of efficiency, including those for both optimization and reliability analysis. The sequential quadratic programming (SQP) algorithm is used for optimization and the MPP search.

5.1. EXAMPLE 1: MATHEMATICAL PROBLEM

In this problem, there are two independent random variables and one reliability constraint. No deterministic variables and random parameters are involved. The RBD model [40] is modified as

$$\begin{cases} \underset{\boldsymbol{\mu}_{\mathbf{X}}}{\text{Min}} & f(\boldsymbol{\mu}_{\mathbf{X}}) = -\left(\mu_{X_1} + \mu_{X_2}\right) \\ s.t. & \Pr\left\{g(\mathbf{X}) = 1 - 80 \Big/ \left(X_1^2 + 8X_2 + 5\right) \le 0\right\} \ge 1 - [p_f] \\ & -10 \le \mu_{X_1} \le 5 \\ & -10 \le \mu_{X_2} \le 5 \end{cases} \tag{49}$$

Each of the random design variables follows a normal distribution with a standard deviation 0.6. The allowable probability of failure is $[p_f] = 1.35 \times 10^{-3}$.

Table 3 displays the convergence history of design variables $\boldsymbol{\mu}_{\mathbf{X}}$, equivalent reliability index γ, and the number of performance function calls in each cycle, denoted

by N. The optimal design is found with only three cycles of deterministic optimization and reliability analysis.

Table 3. Convergence history of SORA/SORM

Cycle k	$\boldsymbol{\mu}_{\mathbf{X}}$	γ	N
1	(5, 5)	3	60
2	(3.6991, 5)	3.0108	78
3	(3.6800, 5)	3.0181	60

Table 4. Results of example 1

Method	Objective	$\boldsymbol{\mu}_{\mathbf{X}}$	p_f^{MCS}	ε_{p_f} (Absolute Error)	N
SORA/FORM	-8.6938	(3.6937, 5)	1.442×10^{-3}	$6.81\%\left(9.20\times10^{-5}\right)$	171
DL-SORM	-8.6799	(3.6799, 5)	1.361×10^{-3}	$0.82\%\left(1.10\times10^{-5}\right)$	705
SORA/SORM	-8.68	(3.68, 5)	1.361×10^{-3}	$0.82\%\left(1.10\times10^{-5}\right)$	198

The problem is solved by DL-SORM, SORA/FORM and SORA/SORM. All the solutions are shown in Table 4. p_f^{MCS} is the probability of failure from MCS at optimal point from DL-SORM, SORA/FORM, or SORA/SORM, and MCS uses 10^7 samples. N stands for the number of performance function calls, including those for both optimization and reliability analysis. SORA/FORM produces a large relative error of $\varepsilon_{p_f} = 6.81\%$ due to the nonlinearity of the performance function. But it is the most efficient method with $N = 171$. SORA/SORM achieves a more accurate result with an error of $\varepsilon_{p_f} = 0.82\%$, and it requires additional computations due to the second-order approximation with $N = 198$. DL-SORM shows the same accuracy as SORA/SORM

since it also uses SORM for reliability analysis. However, its computational cost ($N = 705$) is much higher because of the double loop structure. Considering both efficiency and accuracy, the proposed SORA/SORM gives the best result.

5.2. EXAMPLE 2: CANTILEVER BEAM DESIGN

In the previous mathematical example, there is only one constraint. In this engineering example, two constraints are considered.

A cantilever beam design problem [30, 41, 42] is adopted in this example as shown in Figure 6. The objective is to minimize the weight

$$f = \mu_b \mu_h L \tag{50}$$

where b and h represents the width and height of the cross section, respectively, and their means, μ_b and μ_h, are to be determined. $L = 100$ in is the length of the beam.

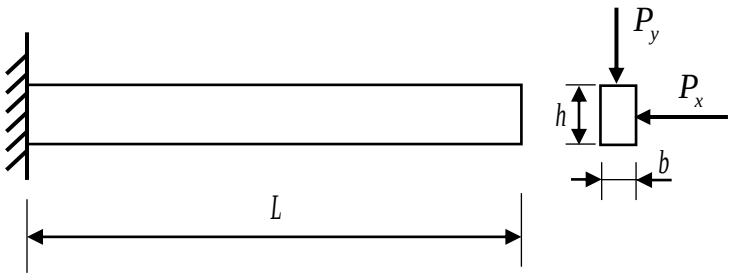

Figure 6. A cantilever beam

The first constraint is that the maximum stress at the fixed end of the cantilever should be less than the yield strength S_y ; the second constraint is that the tip

displacement should not exceed an allowable value D_0. The two performance functions are given by

$$g_1(\mathbf{X},\mathbf{P}) = \frac{6L}{bh}\left(\frac{P_x}{b}+\frac{P_y}{h}\right) - S_y \tag{51}$$

$$g_2(\mathbf{X},\mathbf{P}) = \frac{4L^3}{E}\sqrt{\left(\frac{P_x}{b^3h}\right)^2+\left(\frac{P_y}{bh^3}\right)^2} - D_0 \tag{52}$$

where $\mathbf{X}=(b,h)$, and $\mathbf{P}=(P_x,P_y,E,S_y)$, which include the horizontal load P_x, vertical load P_y, Young's modulus E, and yield strength S_y. The distributions of the random design variables and random parameters are shown in Table 5.

The RBD model is given by

$$\begin{cases} \underset{\mu_b,\mu_h}{\text{Min}} & f = \mu_b\mu_h L \\ s.t. & \Pr\left\{g_1(\mathbf{X},\mathbf{P}) = \frac{6L}{bh}\left(\frac{P_x}{b}+\frac{P_y}{h}\right) - S_y \le 0\right\} \ge 1-[p_{f1}] \\ & \Pr\left\{g_2(\mathbf{X},\mathbf{P}) = \frac{4L^3}{E}\sqrt{\left(\frac{P_x}{b^3h}\right)^2+\left(\frac{P_y}{bh^3}\right)^2} - D_0 \le 0\right\} \ge 1-[p_{f2}] \\ & 1 \le \mu_b \le 4 \\ & 1 \le \mu_h \le 4 \end{cases} \tag{53}$$

where the allowable probability of failure of each constraint is $[p_{f1}]=[p_{f2}]=1.35\times10^{-3}$, and the allowable displacement is $D_0 = 2.25$ in.

The results are given in Table 6. Compared with the results from MCS, all the three methods are accurate for the first constraint. SORA/SORM and DL-SORM are much more accurate than SORA/FORM for the second constraint. Theoretically,

SORA/SORM and DL-SORM should produce the same accuracy, and the slight difference of the results between the two methods is due to the numerical errors. In terms of efficiency, SORA/FORM is the most efficient method with $N = 489$, and SORA/SORM has a moderately increased value of N , which is 753, compared with $N = 9292$ from DL-SORM. Overall, SORA/SORM is the best method with respect to the accuracy and efficiency.

Table 5. Distributions of variables in example 2

Variable	Mean	Standard deviation	Distribution
b	μ_b in	0.01 in	Normal
h	μ_h in	0.01 in	Normal
P_x	500 lb	50 lb	Normal
P_y	1000 lb	100 lb	Normal
E	2.9×10^7 psi	1×10^5 psi	Normal
S_y	3.9×10^4 psi	500 psi	Normal

Table 6. Results of example 2

Method	Objective	$\boldsymbol{\mu}_{\mathbf{X}}$	p_{f1}^{MCS}	$\varepsilon_{p_{f1}}$ (Absolute Error)	p_{f2}^{MCS}	$\varepsilon_{p_{f2}}$ (Absolute Error)	N
SORA/ FORM	890.77	(2.2507, 3.9577)	1.355×10^{-3}	0.40% (5×10^{-6})	1.429×10^{-3}	5.85% (7.9×10^{-5})	489
DL-SORM	890.81	(2.2531, 3.9538)	1.355×10^{-3}	0.40% (5×10^{-6})	1.354×10^{-3}	0.33% (4×10^{-6})	9292
SORA/ SORM	890.81	(2.2530, 3.9539)	1.355×10^{-3}	0.40% (5×10^{-6})	1.357×10^{-3}	0.54% (7×10^{-6})	753

5.3. EXAMPLE 3: DESIGN OF A WELDED BEAM

A welded beam design problem [43-45] is modified and used as the third example. The objective is to minimize the cost of the beam subject to constraints on shear stress τ, bending stress σ in the beam and buckling load P_c. There are four random design variables, including the height of the weld h, the length of the weld l, the height of the beam t, and the width of the beam b as shown in Figure 7.

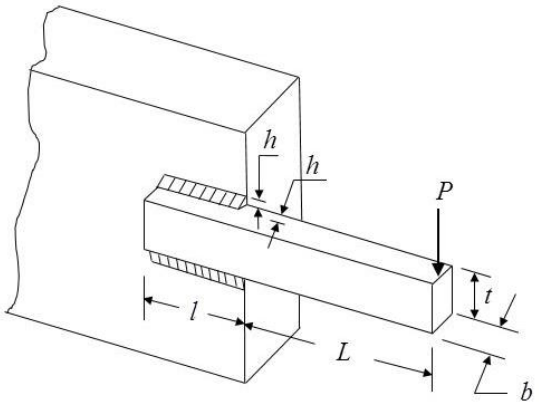

Figure 7. The welded beam problem

The RBD model is given below.

$$\begin{cases} \underset{\boldsymbol{\mu}_{\mathbf{X}}}{\text{Min}} & f = 1.10471\mu_h^2\mu_l + 0.04811\mu_t\mu_b(14.0+\mu_l) \\ s.t. & \Pr\{g_1(\mathbf{X},\mathbf{P}) = \tau - \tau_{\max} \le 0\} \ge 1-[p_{f1}] \\ & \Pr\{g_2(\mathbf{X},\mathbf{P}) = \sigma - \sigma_{\max} \le 0\} \ge 1-[p_{f2}] \\ & \Pr\{g_3(\mathbf{X},\mathbf{P}) = P - P_c \le 0\} \ge 1-[p_{f3}] \\ & 0.1 \le \mu_h \le 2.0 \\ & 0.1 \le \mu_l \le 10 \\ & 0.1 \le \mu_t \le 10 \\ & 0.1 \le \mu_b \le 2.0 \end{cases} \tag{54}$$

where

$$\tau = \sqrt{(\tau')^2 + 2\tau'\tau''l + (\tau'')^2}$$

$$\tau' = \frac{P}{\sqrt{2}hl},\ \tau'' = \frac{MR}{J},\ M = P\left(L + \frac{l}{2}\right),\ R = \sqrt{\frac{l^2}{4} + \left(\frac{h+t}{2}\right)^2}$$

$$J = 2\left\{\frac{hl}{\sqrt{2}}\left[\frac{l^2}{12} + \left(\frac{h+l}{2}\right)^2\right]\right\},\ \sigma = \frac{6PL}{bt^2} \tag{55}$$

$$P_c = \frac{4.013E\sqrt{\frac{t^2b^6}{36}}}{L^2}\left(1 - \frac{t}{2L}\sqrt{\frac{E}{4G}}\right)$$

$\mathbf{X} = (h, l, t, b)$ are random design variables, and $\mathbf{P} = (P, L, E, G)$ are random parameters, which include the load P, length L, modulus of elasticity E, and modulus of rigidity G. $\tau_{\max}$ is the design shear stress of the weld, and $\sigma_{\max}$ is the design normal stress of the beam material. The distributions and parameters of all the variables are shown in Table 7.

Table 7. Distributions of variables in example 3

Variable	Mean	Standard deviation	Distribution
h	μ_h in	0.01 in	Normal
l	μ_l in	0.01 in	Normal
t	μ_t in	0.01 in	Normal
b	μ_b in	0.01 in	Normal
P	8000 lb	600 lb	Lognormal
L	14 in	0.01 in	Normal
E	3×10^7 psi	3×10^6 psi	Normal
G	1.2×10^7 psi	1×10^6 psi	Normal
$\tau_{\max}$	1.4×10^4 psi	-	Deterministic
$\sigma_{\max}$	3.5×10^4 psi	-	Deterministic

The allowable probability of failure of each constraint is $[p_{f1}]=[p_{f2}]=[p_{f3}]=1.35\times10^{-3}$. The results of the welded beam design are presented in Tables 8 and 9. All three reliability constraints are active at optimal points. Even though SORA/FORM is more efficient than SORA/SORM, it produces a very large error for the third constraint. SORA/SORM accurately satisfies the reliability requirement and is more accurate than SORA/FORM. DL-SORM has the same accuracy as SORA/SORM, but its efficiency is the worst.

Table 8. The optimization results of welded beam design problem

Method	Objective	$\boldsymbol{\mu}_{\mathbf{X}}$	N
SORA/FORM	3.1936	(0.4759, 3.9592, 9.6746. 0.2636)	2338
DL-SORM	3.1996	(0.4888, 3.8258, 9.6648, 0.2642)	27230
SORA/SORM	3.1987	(0.4763, 3.9598, 9.6653, 0.2642)	2814

Table 9. Reliability constraints of welded beam design problem

Method	p_{f1}^{MCS}	$\varepsilon_{p_{f1}}$ (Absolute Error)	p_{f2}^{MCS}	$\varepsilon_{p_{f2}}$ (Absolute Error)	p_{f3}^{MCS}	$\varepsilon_{p_{f3}}$ (Absolute Error)
SORA/ FORM	1.365×10^{-3}	1.13% (1.5×10^{-5})	1.397×10^{-3}	3.51% (4.7×10^{-5})	1.555×10^{-3}	15.16% (2.05×10^{-4})
DL-SORM	1.353×10^{-3}	0.26% (3×10^{-6})	1.362×10^{-3}	0.90% (1.2×10^{-5})	1.351×10^{-3}	0.06% (1×10^{-6})
SORA/ SORM	1.355×10^{-3}	0.38% (5×10^{-6})	1.367×10^{-3}	1.23% (1.7×10^{-5})	1.364×10^{-3}	1.02% (1.4×10^{-5})

6. CONCLUSIONS

This study demonstrates that the second order reliability method (SORM) can be introduced to sequential optimization and reliability analysis (SORA), which is an efficient method for reliability-based design and was originally proposed for the use of the first order reliability method (FORM). The new SORA/SORM method developed in this work improves the accuracy of reliability-based design with an increased computational cost. The increase of the computational cost, however, is minimized by new algorithms for the reliability analysis that employs the inverse SORM with the saddlepoint approximation.

SORA/SORM is in general more accurate than the original SORA with FORM because of the second order approximation. This is demonstrated by the numerical examples. SORA/SORM can therefore be used for problems where performance functions are not close to linear with respect to transformed standard normal variables.

SORA/SORM is less efficient than the original SORA because the second order approximation requires second derivatives of a performance function. Nevertheless, much higher efficiency than the direct use of SORM is achieved through the following means: first, decoupling deterministic optimization and inverse SORM; second, performing each iteration of inverse SORM after each deterministic optimization, instead of the complete process of inverse SORM; and third, developing and using an efficient algorithm for updating the equivalent reliability index.

ACKNOWLEDGEMENTS

The authors would like to acknowledge the support provided by the National Science Foundation under Grant Number CMMI 1727329 and the Intelligent Systems Center at the Missouri University of Science and Technology.

REFERENCES

[1] Choi, S.-K., Grandhi, R., and Canfield, R. A., 2006, Reliability-based structural design, Springer Science & Business Media.

[2] Agarwal, H., and Renaud, J., 2004, "Reliability based design optimization using response surfaces in application to multidisciplinary systems," Engineering Optimization, 36(3), pp. 291-311.

[3] Du, X., and Chen, W., 2004, "Sequential optimization and reliability assessment method for efficient probabilistic design," Journal of Mechanical Design, 126(2), pp. 225-233.

[4] Hyeon Ju, B., and Chai Lee, B., 2008, "Reliability-based design optimization using a moment method and a kriging metamodel," Engineering Optimization, 40(5), pp. 421-438.

[5] Shin, J., and Lee, I., 2015, "Reliability analysis and reliability-based design optimization of roadway horizontal curves using a first-order reliability method," Engineering Optimization, 47(5), pp. 622-641.

[6] Hu, Z., and Du, X., 2016, "Reliability-based design optimization under stationary stochastic process loads," Engineering Optimization, 48(8), pp. 1296-1312.

[7] Xie, S., Pan, B., and Du, X., 2016, "An efficient hybrid reliability analysis method with random and interval variables," Engineering Optimization, 48(9), pp. 1459-1473.

[8] Hasofer, A., Lind, N., and Division, U. o. W. S. M., 1973, An exact and invariant first-order reliability format, University of Waterloo, Solid Mechanics Division.

[9] Hohenbichler, M., and Rackwitz, R., 1983, "First-order concepts in system reliability," Structural safety, 1(3), pp. 177-188.

[10] Tu, J., Choi, K. K., and Park, Y. H., 1999, "A new study on reliability-based design optimization," Journal of mechanical design, 121(4), pp. 557-564.

[11] Yi, P., and Cheng, G., 2008, "Further study on efficiency of sequential approximate programming for probabilistic structural design optimization," Structural and Multidisciplinary Optimization, 35(6), pp. 509-522.

[12] Aoues, Y., and Chateauneuf, A., 2010, "Benchmark study of numerical methods for reliability-based design optimization," Structural and multidisciplinary optimization, 41(2), pp. 277-294.

[13] Chen, Z., Qiu, H., Gao, L., and Li, P., 2013, "An optimal shifting vector approach for efficient probabilistic design," Structural and Multidisciplinary Optimization, 47(6), pp. 905-920.

[14] Chen, Z., Qiu, H., Gao, L., Su, L., and Li, P., 2013, "An adaptive decoupling approach for reliability-based design optimization," Computers & Structures, 117, pp. 58-66.

[15] Yin, X., and Chen, W., 2006, "Enhanced sequential optimization and reliability assessment method for probabilistic optimization with varying design variance," Structures and Infrastructure Engineering, 2(3-4), pp. 261-275.

[16] Du, X., 2008, "Saddlepoint approximation for sequential optimization and reliability analysis," Journal of Mechanical Design, 130(1), p. 011011.

[17] Cho, T. M., and Lee, B. C., 2011, "Reliability-based design optimization using convex linearization and sequential optimization and reliability assessment method," Structural Safety, 33(1), pp. 42-50.

[18] Lim, J., Lee, B., and Lee, I., 2015, "Sequential optimization and reliability assessment based on dimension reduction method for accurate and efficient reliability-based design optimization," Journal of Mechanical Science and Technology, 29(4), p. 1349.

[19] Yi, P., Zhu, Z., and Gong, J., 2016, "An approximate sequential optimization and reliability assessment method for reliability-based design optimization," Structural and Multidisciplinary Optimization, 54(6), pp. 1367-1378.

[20] Tvedt, L., 1983, "Two second-order approximations to the failure probability," Section on structural reliability.

[21] Breitung, K., 1984, "Asymptotic approximations for multinormal integrals," Journal of Engineering Mechanics, 110(3), pp. 357-366.

[22] Der Kiureghian, A., Lin, H.-Z., and Hwang, S.-J., 1987, "Second-order reliability approximations," Journal of Engineering Mechanics, 113(8), pp. 1208-1225.

[23] Zhao, Y.-G., and Ono, T., 1999, "New approximations for SORM: Part 1," Journal of Engineering Mechanics, 125(1), pp. 79-85.

[24] Lim, J., Lee, B., and Lee, I., 2014, "Second‐order reliability method‐based inverse reliability analysis using Hessian update for accurate and efficient reliability‐based design optimization," International Journal for Numerical Methods in Engineering, 100(10), pp. 773-792.

[25] Du, X., and Sudjianto, A., "A saddlepoint approximation method for uncertainty analysis," Proc. Proceedings of DETC'04: ASME 2004 Design Engineering Technical Conferences and Computers and Information in Engineering Conference.

[26] Du, X., Guo, J., and Beeram, H., 2008, "Sequential optimization and reliability assessment for multidisciplinary systems design," Structural and Multidisciplinary Optimization, 35(2), pp. 117-130.

[27] Hu, Z., and Du, X., "A Random Field Method for Time-Dependent Reliability Analysis With Random and Interval Variables," Proc. ASME 2016 International Design Engineering Technical Conferences and Computers and Information in Engineering Conference, American Society of Mechanical Engineers, pp. V02BT03A044-V002BT003A044.

[28] Reddy, M. V., Grandhi, R. V., and Hopkins, D. A., 1994, "Reliability based structural optimization: a simplified safety index approach," Computers & structures, 53(6), pp. 1407-1418.

[29] Wang, L., Grandhi, R. V., and Hopkins, D. A., 1995, "Structural reliability optimization using an efficient safety index calculation procedure," International Journal for Numerical Methods in Engineering, 38(10), pp. 1721-1738.

[30] Wu, Y.-T., Shin, Y., Sues, R., and Cesare, M., "Safety-factor based approach for probability-based design optimization," Proc. 19th AIAA Applied Aerodynamics Conference, p. 1522.

[31] Park, Y. H., 2003, "Hybrid analysis method for reliability-based design optimization."

[32] Tvedt, L., 1990, "Distribution of quadratic forms in normal space-application to structural reliability," Journal of Engineering Mechanics, 116(6), pp. 1183-1197.

[33] Daniels, H. E., 1987, "Tail probability approximations," International Statistical Review/Revue Internationale de Statistique, pp. 37-48.

[34] Goutis, C., and Casella, G., 1999, "Explaining the saddlepoint approximation," The American Statistician, 53(3), pp. 216-224.

[35] Ezquerro, J., and Hernández, M., 1999, "On a convex acceleration of Newton's method," Journal of Optimization Theory and Applications, 100(2), pp. 311-326.

[36] Varona, J. L., 2002, "Graphic and numerical comparison between iterative methods," The Mathematical Intelligencer, 24(1), pp. 37-46.

[37] Babajee, D., and Dauhoo, M., 2006, "An analysis of the properties of the variants of Newton's method with third order convergence," Applied Mathematics and Computation, 183(1), pp. 659-684.

[38] Wu, Y.-T., Millwater, H., and Cruse, T., 1990, "Advanced probabilistic structural analysis method for implicit performance functions," AIAA journal, 28(9), pp. 1663-1669.

[39] Wu, Y.-T., 1994, "Computational methods for efficient structural reliability and reliability sensitivity analysis," AIAA journal, 32(8), pp. 1717-1723.

[40] Yang, R., and Gu, L., 2004, "Experience with approximate reliability-based optimization methods," Structural and Multidisciplinary Optimization, 26(1-2), pp. 152-159.

[41] Qu, X., and Haftka, R., 2004, "Reliability-based design optimization using probabilistic sufficiency factor," Structural and Multidisciplinary Optimization, 27(5), pp. 314-325.

[42] Liao, K.-W., and Ha, C., 2008, "Application of reliability-based optimization to earth-moving machine: hydraulic cylinder components design process," Structural and Multidisciplinary Optimization, 36(5), pp. 523-536.

[43] Ragsdell, K., and Phillips, D., 1976, "Optimal design of a class of welded structures using geometric programming," Journal of Engineering for Industry, 98(3), pp. 1021-1025.

[44] Huang, F.-z., Wang, L., and He, Q., 2007, "An effective co-evolutionary differential evolution for constrained optimization," Applied Mathematics and computation, 186(1), pp. 340-356.

[45] Rao, R. V., and Savsani, V. J., 2012, Mechanical design optimization using advanced optimization techniques, Springer Science & Business Media.

IV. SECOND ORDER RELIABILITY METHOD FOR TIME-DEPENDENT RELIABILITY ANALYSIS USING SEQUENTIAL EFFICIENT GLOBAL OPTIMIZATION

Zhangli Hu

Department of Mechanical and Aerospace Engineering
Missouri University of Science and Technology

Xiaoping Du

Department of Mechanical and Energy Engineering
Indiana University - Purdue University Indianapolis

ABSTRACT

Reliability depends on time if the associated limit-state function includes time. A time-dependent reliability problem can be converted into a time-independent reliability problem by using the extreme value of the limit-state function. Then the first order reliability method can be used but it may produce a large error since the extreme limit-state function is usually highly nonlinear. This study proposes a new reliability method so that the second order reliability method can be applied to time-dependent reliability analysis for higher accuracy while maintaining high efficiency. The method employs sequential efficient global optimization to transform the time-dependent reliability analysis into the time-independent problem. The Hessian approximation and envelope theorem are used to obtain the second order information of the extreme limit-state function. Then the second order saddlepoint approximation is utilized to evaluate the reliability. The accuracy and efficiency of the proposed method are verified through numerical examples.

1. INTRODUCTION

Reliability is the probability that a product performs its intended function under specified conditions over a period of time [1]. Higher reliability means a lower chance of failure. It is especially critical to maintain high reliability because failures may be costly and catastrophic. Predicting reliability during a design stage is therefore imperative for many products.

For many engineering applications, reliability depends on time if the associated limit-state function involves time-dependent parameters, such as time-variant loads and the deterioration of material properties. For example, the wave loads on offshore structures are time-dependent since the typical wave heights and periods change randomly over time [2]; the material and dimensional properties of concrete structures vary with respect to time due to the time-dependent chloride corrosion damage [3, 4]; For kinematic mechanism, the motion error involves time-dependent input motion [5, 6].

Extensive research has been conducted on time-dependent reliability analysis. Existing time-dependent reliability methodologies can be roughly classified into three group. The first group is Rice's formula based methods, whose key step is the computation of the upcrossing rate. For instance, a PHI2 method was developed to compute the time-variant reliability [7]. Hu and Du proposed a time-dependent reliability method for hydrokinetic turbine blades [8]. Besides, many other empirical modifications [5, 9-14] have also been made. This group has advantages over other groups for its efficiency. But it may produce large errors when upcrossings are strongly dependent.

The second group includes simulation-based methods using surrogate models. Most of these methods build a surrogate model to replace the original limit-state function

by evaluating the response variable at a number of points predefined through Design of Experiment (DoE) [15-17]. Then Monte Carlo simulation (MCS) is performed based on the surrogate model. The methods include artificial neural networks (ANN) [18, 19], polynomial chaos expansions (PCE) [20, 21], and Gaussian process based method, also known as Kriging model based methods [22-26]. This group can evaluate the time-dependent reliability accurately if the surrogate model is well trained. Nevertheless, this may result in a high computational cost.

The third group contains the methods that convert time-dependent reliability analysis into the time-independent reliability analysis using the extreme value of the time-dependent limit-state function. If the distribution of the extreme value can be estimated accurately, the accuracy of this group is higher than the first group. The typical methods in this group are extreme value response method [22, 27], extreme value distribution method [28], composite limit-state function method [29], and the envelope function method [6]. However, it is often a challenging task to obtain the distribution of the extreme value accurately and efficiently.

Motivated by the above challenges, we propose a new time-dependent method using sequential efficient global optimization (SEGO). The new method first converts the time-dependent problem into a time-independent counterpart by using the extreme value. Then the Hessian approximation and envelope theorem are employed to obtain the second order approximation to the extreme value. Finally the second order saddlepoint approximation (SOSPA) [30, 31] is utilized to estimate the distribution of the extreme value. The new method is termed as SEGO/SOSPA. It improves the accuracy by using

second order approximation to the extreme value of the limit-state function and maintains high efficiency by using SEGO.

The reminder of this paper is organized as follows: Section 2 reviews the theoretical background of this work. Then the new SEGO/SOSPA method is discussed in Section 3 followed by three examples in Section 4. Conclusions are given in Section 5.

2. REVIEW OF FUNDAMENTAL METHODOLOGIES

In this section, we briefly review the basic definition of time dependent reliability. We also discuss the commonly used first order reliability method (FORM).

2.1. TIME-DEPENDENT RELIABILITY

In this work, we consider a limit-state function given by

$$Y = g(\mathbf{X}, t) \tag{1}$$

where $g(\mathbf{X}, t)$ is explicit with respect to time t, $\mathbf{X} = [X_1, ..., X_N]$ is a N-dimensional vector of random variables.

For a given period of time $[0, T]$, the reliability is defined by

$$R[0, T] = \Pr\left\{ g(\mathbf{X}, t) \geq 0, \ \forall t \in [0, T] \right\} \tag{2}$$

where $\forall$ means "for all".

And the associated probability of failure is given by

$$p_f = \Pr\left\{ g(\mathbf{X}, t) < 0, \ \exists t \in [0, T] \right\} \tag{3}$$

where $\exists$ means "there exists at least one".

2.2. FIRST ORDER RELIABILITY METHOD (FORM)

FORM is the most commonly used method in time-dependent reliability analysis since it can convert the general non-Gaussian process into equivalent Gaussian process [32].

$\mathbf{X}$ is transformed into standard normal variables $\mathbf{U}$. Then the most probable point (MPP) $\mathbf{u}_{MPP}$ identified by the following model:

$$\begin{cases} \min \ \sqrt{\mathbf{U}\mathbf{U}^T} \\ \text{s.t.} \quad g(\mathbf{X},t) = g(T(\mathbf{U}),t) = 0 \end{cases} \tag{4}$$

in which $T(\cdot)$ is an operator of the transformation from $\mathbf{U}$ to $\mathbf{X}$.

The limit-state function is linearized at $\mathbf{u}_{MPP}$ by

$$g(T(\mathbf{U}),t) = g(\mathbf{u}_{MPP},t) + \sum_{i=1}^{N} \left.\frac{\partial g}{\partial U_i}\right|_{\mathbf{U}=\mathbf{u}_{MPP}} (U_i - u_{iMPP}) = \nabla g(\mathbf{u}_{MPP},t)(\mathbf{U} - \mathbf{u}_{MPP}) \tag{5}$$

where $\nabla g(\mathbf{u}_{MPP},t) = \left[\left.\frac{\partial g}{\partial U_1}\right|_{\mathbf{U}=\mathbf{u}_{MPP}}, ..., \left.\frac{\partial g}{\partial U_N}\right|_{\mathbf{U}=\mathbf{u}_{MPP}} \right]^T$ is the gradient vector.

Finally, the probability of failure can be estimated by

$$\begin{aligned} p_f &= \Pr\left\{ g(\mathbf{X},t) < 0, \ \exists t \in [0,T] \right\} \\ &= \Pr\left\{ g(\mathbf{u}_{MPP},t) + \sum_{i=1}^{N} \left.\frac{\partial g}{\partial U_i}\right|_{\mathbf{U}=\mathbf{u}_{MPP}} (U_i - u_{iMPP}) < 0, \ \exists t \in [0,T] \right\} \\ &= \Pr\{ \beta(t) + \boldsymbol{\alpha}(t)\mathbf{U} < 0, \ \exists t \in [0,T] \} \end{aligned} \tag{6}$$

in which $\beta(t)$ is the time-dependent reliability index

$$\beta(t) = \left\| \mathbf{u}_{MPP} \right\| \tag{7}$$

and $\boldsymbol{\alpha}(t)$ is the time-dependent unit gradient vector

$$\boldsymbol{\alpha}(t) = \frac{\nabla g(\mathbf{u}_{MPP},t)}{\left\| \nabla g(\mathbf{u}_{MPP},t) \right\|} = \left[\alpha_1(t), \alpha_2(t), ..., \alpha_N(t) \right] \tag{8}$$

As Eq. (6) shows, the non-Gaussian process $g(\mathbf{X},t)$ has been transformed into an equivalent Gaussian process represented as a sum of standard normal random variables. A common method is to build the surrogate models of $\beta(t)$ and $\boldsymbol{\alpha}(t)$ with respect to t, and then use MCS to estimate the probability of failure. However, it might be computational expensive to build accurate surrogate models.

3. SEGO/SOSPA

The objective of this study is to improve the accuracy of the time-dependent reliability analysis by employing the second-order approximation. The central idea is to convert the time-dependent problem into a time-independent problem using sequential efficient global optimization (SEGO). The second order approximation is obtained by using the Hessian approximation and envelope theorem. Then the time-independent problem is solved with the second-order saddlepoint approximation (SOSPA) [30].

3.1. OVERVIEW

The time-dependent probability of failure can be evaluated through the extreme value of the limit-state function, expressed by [27]

$$\begin{aligned} p_f(0,T) &= \Pr\left\{ g(\mathbf{X},t) < 0, \exists t \in [0,T] \right\} \\ &= \Pr\left\{ \min_{t\in[0,T]} g(\mathbf{X},t) < 0 \right\} \end{aligned} \tag{9}$$

The extreme limit-state function, also known as the envelope function [6], or the composite limit-state function [29], $\min_{t\in[0,T]} g(\mathbf{X},t)$ is obtained by

$$G(\mathbf{X}) = \min_{t\in[0,T]} g(\mathbf{X},t) = g(\mathbf{X},\tilde{t}(\mathbf{X})) \tag{10}$$

where $G(\mathbf{X})$ is global minimal value of $g(\mathbf{X},t)$ with respect to time t. $G(\mathbf{X})$ is time independent and only depends on $\mathbf{X}$. Let $\tilde{t}$ be the time instant when the global minimal value occurs. $\tilde{t}$ is a function of $\mathbf{X}$.

$$\tilde{t} = \left\{ t \middle| \min_{t\in[0,T]} g(\mathbf{X},t) \right\} \tag{11}$$

Now the Eq. (9) can be converted into time-independent problem

$$\begin{aligned} p_f(0,T) &= \Pr\left\{ g(\mathbf{X},t) < 0, \exists t \in [0,T] \right\} \\ &= \Pr\left\{ G(\mathbf{X}) < 0 \right\} \end{aligned} \tag{12}$$

Then a time-independent reliability method can be applied after the conversion. In this work, we assume that $G(\mathbf{X})$ exists and is continuously differentiable.

3.2. SEGO

3.2.1. Sequential Optimization. It is very difficult to analytically obtain the extreme limit-state function $G(\mathbf{X})$. So FORM is generally used to approximate $G(\mathbf{X})$, and the MPP of $G(\mathbf{X})$ is found using the following formulas

$$\begin{cases} \min \ \sqrt{\mathbf{U}\mathbf{U}^T} \\ \text{s.t.} \quad G(T(\mathbf{U})) = \min\limits_{t\in[0,T]} g(T(\mathbf{U}),t) = 0 \end{cases} \tag{13}$$

Eq. (13) is formulated as a double loop structure. The inner loop is the global optimization with respect to time t, while the outer loop is the MPP search with respect to $\mathbf{U}$. The computational cost of the double loop optimization is very high.

Inspired by sequential optimization and reliability assessment (SORA) [33], we use sequential strategy to decouple the global optimization from the MPP search and performs the two loops sequentially. In the first cycle, FORM is used to locate the MPP $\mathbf{u}_{MPP}^{(1)}$ at the initial time t_0.

$$\begin{cases} \min \ \sqrt{\mathbf{U}\mathbf{U}^T} \\ \text{s.t.} \quad g(T(\mathbf{U}),t_0) = 0 \end{cases} \tag{14}$$

After the MPP search, the global optimization is performed by fixing $\mathbf{U}$ at the $\mathbf{u}_{MPP}^{(1)}$, and optimal time is obtained as $\tilde{t}^{(1)}$.

$$\tilde{t}^{(1)} = \arg\min_{t\in[0,T]} g(T(\mathbf{u}_{MPP}^{(1)}), t) \tag{15}$$

In the second cycle, the new MPP $\mathbf{u}_{MPP}^{(2)}$ is located at the time instant $\tilde{t}^{(1)}$ using Eq. (14). And then the optimal time is updated to $\tilde{t}^{(2)}$ by performing global optimization at $\mathbf{u}_{MPP}^{(2)}$.

$$\tilde{t}^{(2)} = \arg\min_{t\in[0,T]} g(T(\mathbf{u}_{MPP}^{(2)}), t) \tag{16}$$

Finally, the process is repeated cycle by cycle until convergence. The global optimization is discussed in Section 3.2.2.

The flowchart of the above procedure is illustrated in Figure 1.

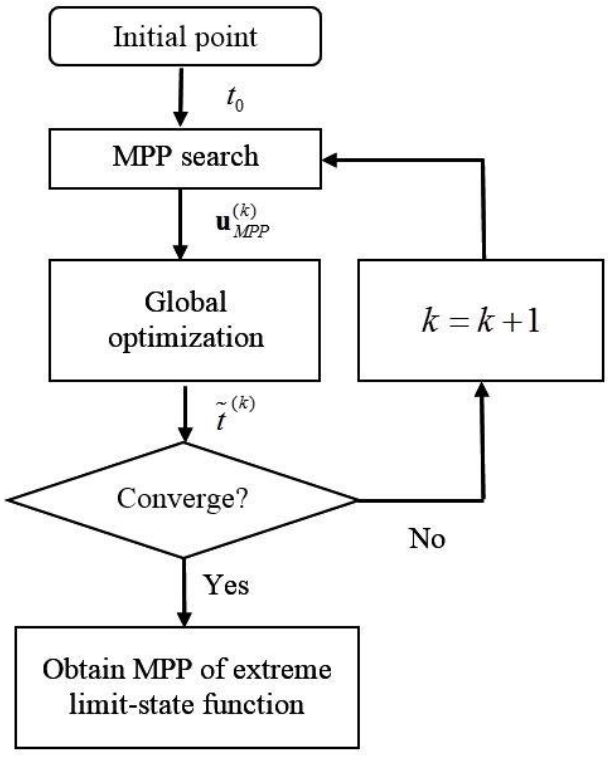

Figure 1. Flowchart of sequential optimization

3.2.2. Efficient Global Optimization (EGO). The global optimization method used in this study is the efficient global optimization (EGO) [22, 27, 34]. EGO has been widely used in various areas [35, 36] because it can search for the global optimum with high computational efficiency. In this work, we search for a time instant where $Y = g(T(\mathbf{u}_{MPP}), t)$ is minimized. Recall that $\mathbf{u}_{MPP}$ is fixed during the optimization process, and then $g(T(\mathbf{u}_{MPP}), t)$ is one-dimensional function. We denote this function as $g(t)$; namely, $g(t) = g(T(\mathbf{u}_{MPP}), t)$.

$$y = g(t) = g(T(\mathbf{u}_{MPP}), t) = \mathbf{F}(t)^T \boldsymbol{\gamma} + Z(t) \tag{17}$$

where $\mathbf{F}(t)^T \boldsymbol{\gamma}$ is a deterministic term, $\mathbf{F}(t)$ is a vector of regression functions, $\boldsymbol{\gamma}$ is a vector of regression coefficients, and $Z(t)$ is a stationary Gaussian process with zero mean and a covariance given by

$$\mathrm{Cov}[Z(t_1), Z(t_2)] = \sigma_Z^2 R(t_1, t_2) \tag{18}$$

in which σ_Z^2 is process variance, and $R(\cdot,\cdot)$ is the correlation function.

The output of the surrogate model is a Gaussian random variable following

$$y = g(t) \sim N\left(\mu(t), \sigma^2(t)\right) \tag{19}$$

where $\mu(t)$ and $\sigma(t)$ are the mean and standard deviation of y. If t is a training point, $\mu(t) = g(t)$ and $\sigma(t) = 0$. This means that the surrogate model is exact at a point where the model is trained.

After building the initial model, the expected improvement (EI) metric is used to identify the new training point with the highest probability to produce a better extreme value of the response. The improvement is defined by

$$I = \max(y - y^*, 0) \tag{20}$$

where $y^* = \min_{i=1,2,...,k} g(t_i)$ is the current minimum response obtained from the sampled training points.

Thus its expectation or EI is computed by [34]

$$\begin{aligned} \mathrm{EI}(t) &= E[\max(y^* - y, 0)] \\ &= \left(y^* - \mu(t)\right)\Phi\left(\frac{y^* - \mu(t)}{\sigma(t)}\right) + \sigma(t)\phi\left(\frac{y^* - \mu(t)}{\sigma(t)}\right) \end{aligned} \tag{21}$$

in which $\Phi(\cdot)$ and $\phi(\cdot)$ are the cumulative distribution function (CDF) and probability density function (PDF) of a standard normal variable, respectively.

The new training point t_{k+1} is identified as the time maximizes the expected improvement.

$$t_{k+1} = \arg\max_t \mathrm{EI}(t) \tag{22}$$

The procedure of EGO is described in Table 1. More details can be found in Ref. [34].

Table 1. Algorithms of EGO

Steps	Procedure
1	Generate initial training point $\mathbf{t}^s = [t_1, t_2, ..., t_k]$ and compute the response of limit-state function $\mathbf{y}^s = [g(t_1), g(t_2), \ldots, g(t_k)]$
2	Construct a Kriging model $y = g(t)$ using $\left\{\mathbf{t}^s, \mathbf{y}^s\right\}$
3	Find the global minimum $y^* = \min_{i=1,2,...,k} g(t_i)$
4	Search for $t_{k+1} = \arg\max_t \mathrm{EI}(t)$, where $\mathrm{EI}(t)$ is computed by Eq. (21)
5	Compare $\max_t \mathrm{EI}(t)$ with $\varepsilon_{\mathrm{EI}}$: if $\max_t \mathrm{EI}(t) < \varepsilon_{\mathrm{EI}}$, stop and give the final optimum y^* and t^*; Otherwise, go to next step
6	Update $\mathbf{y}^s = [\mathbf{y}^s, g(t_{k+1})]$ and $\mathbf{t}^s = [\mathbf{t}^s, t_{k+1}]$, and repeat steps 2-5

In this work, the convergence criterion of EGO $\varepsilon_{\mathrm{EI}}$ is choses as $\varepsilon_{\mathrm{EI}} = \left|y^*\right| \times 2\%$.

By combining sequential strategy with EGO, the MPP $\mathbf{u}^*$ of extreme limit-state function $G(\mathbf{X})$ can be obtained efficiently by solving Eq. (13). If FORM is used, the probability of failure can be estimated by

$$\begin{aligned} p_f(0,T) &= \Pr\left\{g(\mathbf{X},t) < 0, \exists t \in [0,T]\right\} \\ &= \Pr\left\{G(\mathbf{X}) < 0\right\} \\ &= \Phi(-\beta_F^*) \end{aligned} \tag{23}$$

where $\beta_F^* = \left\|\mathbf{u}^*\right\|$ is the first order reliability index of extreme limit-state function.

Since the above method uses FORM and SEGO, we denote this method as SEGO/FORM. In general, the extreme limit-state function can be highly nonlinear and SEGO/FORM may not be accurate enough. In Section 3.3, we discuss how to develop a second-order approximation method. This method uses the Hessian approximation and envelope theorem to obtain the second order information of the extreme limit-state function. Then SOSPA is used to estimate the probability of failure.

3.3. HESSIAN APPROXIMATION AND ENVELOP THEOREM

The second-order approximation requires the Hessian matrix. But it is challenging to calculate the Hessian because it consists of second derivatives of the extreme limit-state function with respect to random input variables $\mathbf{X}$. Hence a quasi-Newton approach [37, 38] is introduced in this work to approximate the Hessian matrix. This Hessian approximation method can take advantage of the MPP search information in SEGO, leading to high efficiency.

The Hessian matrix is updated using the following formulas [38]

$$\mathbf{H}^{(k+1)} = \mathbf{H}^{(k)} + \frac{(\mathbf{r}^{(k)} - \mathbf{H}^{(k)}\mathbf{s}^{(k)})(\mathbf{r}^{(k)} - \mathbf{H}^{(k)}\mathbf{s}^{(k)})^T}{(\mathbf{r}^{(k)} - \mathbf{H}^{(k)}\mathbf{s}^{(k)})^T \mathbf{s}^{(k)}} \tag{24}$$

where

$$\begin{cases} \mathbf{s}^{(k)} = \mathbf{u}_{MPP}^{(k+1)} - \mathbf{u}_{MPP}^{(k)} \\ \mathbf{r}^{(k)} = \nabla G^{(k+1)} - \nabla G^{(k)} \end{cases} \tag{25}$$

in which $\mathbf{u}_{MPP}^{(k)}$ represents the MPP at current step k used in the SEGO, $\nabla G^{(k)} = \left[\partial G^{(k)}/\partial U_1, ..., \partial G^{(k)}/\partial U_n\right]^T$ is the gradient vector of the extreme limit-state function, and $\mathbf{s}^{(k)}$ and $\mathbf{r}^{(k)}$ are the variation of the MPP and the gradient between two successive iterations, respectively.

The approximated Hessian is expected to converge to the true Hessian as the MPP reaches the true MPP. However, SEGO does not provide the gradient information of the extreme limit-state function, and the extra computational effort is needed. In this case, the finite difference method is used.

$$\frac{\partial G}{\partial U_i} = \frac{G(u_i + \Delta u_i) - G(u_i)}{\Delta u_i} = \frac{\min\limits_t g(u_i + \Delta u_i, t) - \min\limits_t g(u_i, t)}{\Delta u_i} \tag{26}$$

As Eq. (26) shows, $\min\limits_t g(u_i + \Delta u_i, t)$ needs additional global optimization at $u_i + \Delta u_i$. Directly using finite difference method will increase N times of global optimization at each iteration in order to obtain the gradient. This is very computationally expensive.

To reduce to computational cost, we use the envelope theorem, which is a widely used method in economic optimization field [39, 40]. The envelope theorem can connect

the derivative of extreme limit-state function with the derivative of original limit-state function.

$$\frac{\partial}{\partial U_i} G(\mathbf{U}) = \frac{\partial}{\partial U_i} g\left(\mathbf{U}, \tilde{t}(\mathbf{U})\right) = \frac{\partial}{\partial U_i} g(\mathbf{U}, t)\Big|_{t=\tilde{t}(\mathbf{U})} \tag{27}$$

Eq. (27) indicates that the gradient of the extreme limit-state function at $\mathbf{U}$ equals to the gradient of original limit-state function at time instant $t = \tilde{t}(\mathbf{U})$.

And Eq. (26) becomes

$$\frac{\partial G}{\partial U_i} = \frac{G(u_i + \Delta u_i) - G(u_i)}{\Delta u_i} = \frac{g(u_i + \Delta u_i, t) - g(u_i, t)}{\Delta u_i}\Big|_{t=\tilde{t}(\mathbf{u})} \tag{28}$$

Then only N function calls are required in each iteration by using the envelope theorem. This makes the method more efficient.

Combining Eqs. (24) and (28) yields the gradient ∇G and Hessian matrix $\mathbf{H}$ of the extreme limit-state function. Then the second order reliability method can be used.

3.4. SOSPA

Once the MPP $\mathbf{u}^*$, gradient ∇G, and Hessian matrix $\mathbf{H}$ of the extreme limit-state function are available, the second approximation to the extreme limit-stat function is formulated as

$$G(\mathbf{U}) = a + \mathbf{b}^T\mathbf{U} + \mathbf{U}^T\mathbf{C}\mathbf{U} \tag{29}$$

where

$$\begin{cases} a = \frac{1}{2}\left(\mathbf{u}^*\right)^T \mathbf{H}\mathbf{u}^* - \nabla G(\mathbf{u}^*)^T \mathbf{u}^* \\ \mathbf{b} = \nabla G(\mathbf{u}^*) - \mathbf{H}\mathbf{u}^* \\ \mathbf{C} = \frac{1}{2}\mathbf{H} \end{cases} \tag{30}$$

Then SOSPA [32, 44] is employed to estimate the probability of failure, and it is considered in general to be more accurate than the traditional SORM methods such as Breitung's [45] and Tvedt's methods [46].

After the extreme limit-state function is approximated in Eq. (29), we can obtain the cumulant generating function (CGF).

$$K(t) = -\beta_F^* t + \frac{1}{2}t^2 - \frac{1}{2}\sum_i^{n-1} \log(1 - 2tk_i) \tag{31}$$

The derivatives of CGF are

$$K'(t) = -\beta_F^* + t + \sum_{i=1}^{n-1} \frac{k_i}{1 - 2tk_i} \tag{32}$$

$$K''(t) = 1 + \sum_{i=1}^{n-1} \frac{k_i^2}{\left(1 - 2tk_i\right)^2} \tag{33}$$

The saddlepoint t_s is obtained by solving the following equation:

$$K'(t) = -\beta_F^* + t + \sum_{i=1}^{n-1} \frac{k_i}{1 - 2tk_i} = 0 \tag{34}$$

Then the probability of failure is evaluated by

$$\begin{aligned} p_f(0,T) &= \Pr\left\{g(\mathbf{X},t) < 0, \exists t \in [0,T]\right\} \\ &= \Pr\left\{G(\mathbf{X}) < 0\right\} \\ &= \Phi(w) + \phi(w)\left(\frac{1}{w} - \frac{1}{\upsilon}\right) \end{aligned} \tag{35}$$

where

$$w = \text{sgn}(t_s)\left\{2\left[-K(t_s)\right]\right\}^{1/2} \tag{36}$$

$$\upsilon = t_s\left[K''(t_s)\right]^{1/2} \tag{37}$$

in which $\text{sgn}(t_s) = +1, -1$ or 0, depending on whether t_s is positive, negative, or zero.

Saddlepoint approximation has several excellent features. It yields an extremely accurate probability estimation, especially in the tail area of a distribution [43-46]. More details can be found in Ref. [30].

3.5. SEGO/SOSPA PROCEDURE

The detailed steps of SEGO/SOSPA are summarized below.

Step 1: Set $k = 1$. Use the initial time instant as the initial critical time $\tilde{t}^{(0)} = t_0$ and use unit vector as the initial MPP $\mathbf{u}_{MPP}^{(1)} = \mathbf{u}_0$

Step 2: Perform MPP search at time instant $\tilde{t}^{(k-1)}$ and obtain MPP $\mathbf{u}_{MPP}^{(k)}$ by solving the following formulas

$$\begin{cases} \min \ \sqrt{\mathbf{U}\mathbf{U}^T} \\ \text{s.t.} \quad g(T(\mathbf{U}), \tilde{t}^{(k-1)}) = 0 \end{cases} \tag{38}$$

Step 3: Implement efficient global optimization by fixing $\mathbf{U}$ at $\mathbf{u}_{MPP}^{(k)}$. The critical time $\tilde{t}^{(k)}$ that minimizes the limit-state function is found and the corresponding minimum value $g_{\min}^{(k)}$ is also obtained.

Step 4: Perform Hessian approximation by using quasi-Newton approach with Eq. (24) and envelope theorem with Eq. (28)

Step 5: Check convergence. The convergence criterion is defined as

$$\varepsilon = \left| g_{\min}^{(k)} \right| \le \varepsilon_{tol} \tag{39}$$

If $\varepsilon \le \varepsilon_{tol}$, terminate the iteration, and $\left(\mathbf{u}_{MPP}^{(k)}, \nabla G^{(k)}, \mathbf{H}^{(k)}\right)$ is the output. Otherwise, set $k = k+1$ and return to step 2.

Step 6: Calculate the p_f using SOSPA based on the information $\left(\mathbf{u}_{MPP}^{(k)}, \nabla G^{(k)}, \mathbf{H}^{(k)}\right)$.

The flowchart of overall procedure of SEGO/SOSPA is shown in Figure 2.

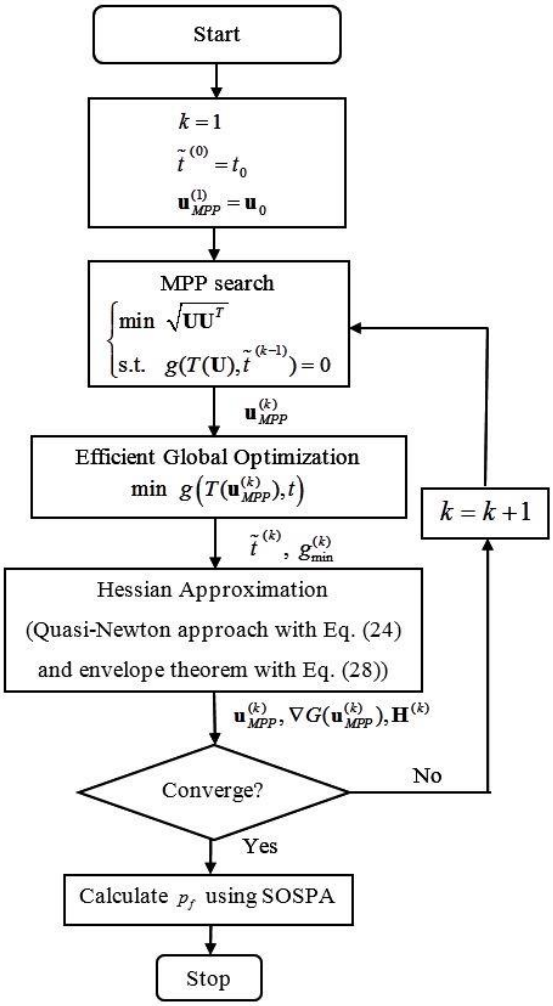

Figure 2. Flowchart of SEGO/SOSPA

4. EXAMPLES

In this section, three examples are used to test SEGO/SOSPA. To show its benefits, we compare it with SEGO using FORM, denoted as SEGO/FORM. The accuracy is evaluated by the relative error with respect to the result from MCS with a large sample size. The relative error is defined as

$$\varepsilon\% = \left| \frac{p_f - p_{f,\mathrm{MCS}}}{p_{f,\mathrm{MCS}}} \right| \times 100\% \tag{40}$$

where p_f is the result from SEGO/FORM or SEGO/SOSPA. We also use the number of function calls as a measure of efficiency.

4.1. EXAMPLE 1: MATHEMATICAL PROBLEM

A mathematical example modified from [27] is used as the first example, which has two independent normal random variables. The limit-state function is given by

$$g(\mathbf{X},t) = X_1^2 X_2 - 5X_1 t + (X_2 + 1)t^2 - 9 \tag{41}$$

where t varies within $[0,5]$, $\mathbf{X} = [X_1, X_2]$ with $X_1 \sim N(3.5, 0.3^2)$ and $X_2 \sim N(3.5, 0.3^2)$.

Figure 3 shows the extreme failure surface formed by the instantaneous limit-state surfaces at different discretized instants within the interval $[0,5]$. The extreme limit-state function has a parabolic curve.

The extreme failure surface is confirmed by the one from an analytical equation obtained by solving $\frac{\partial g}{\partial t} = 0$, leading to

$$G(\mathbf{X}) = X_1^2 X_2 - \frac{25X_1^2}{4(X_2 - 1)} - 9 \tag{42}$$

The contour of the analytical extreme limit-state function is plotted in Figure 4, where the grey region represents the failure domain.

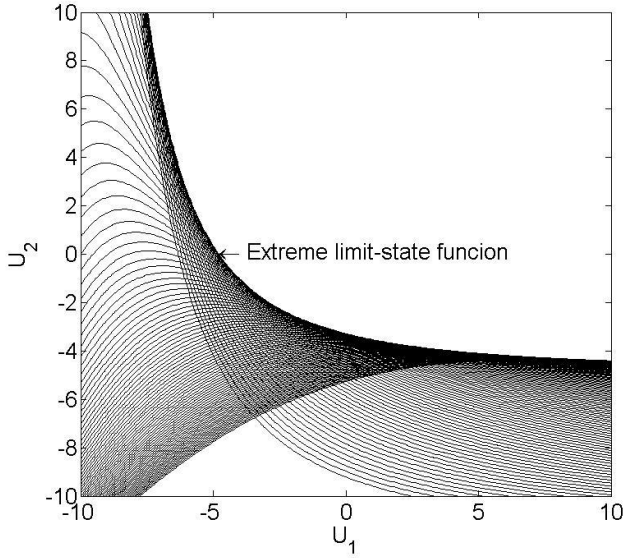

Figure 3. Extreme limit-state surface formed by instantaneous limit-state surfaces

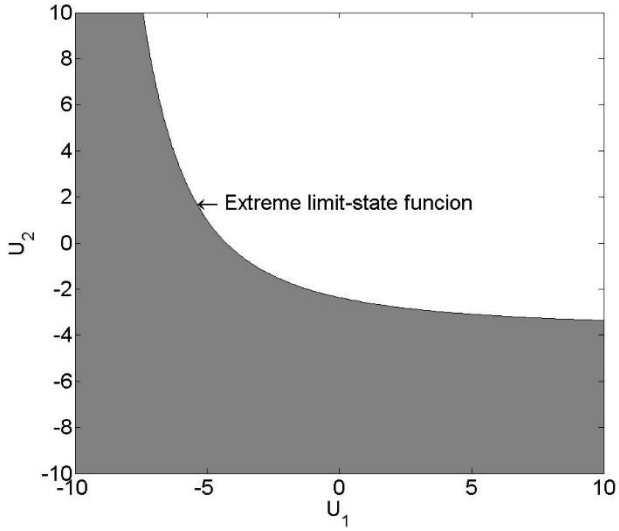

Figure 4. Extreme limit-state surface

Table 2. Iteration history of MPP search for Example 1

Iterations	$\mathbf{u}_{MPP}$	$g_{\min}$	$\tilde{t}$
1	(-5.8805, -1.7106)	-4.1627	1.4636
2	(-2.1135, -2.7084)	-0.8475	1.9414
3	(-1.4111, -2.8275)	-0.0997	2.1070
4	(-1.2110, -2.8875)	-0.0095	2.1594
5	(-1.1504, -1.1314)	-8.1489×10^{-4}	2.1760
6	(-1.1314, -2.9165)	-3.3407×10^{-4}	2.1824

SEGO is used to find the MPP of the extreme limit-sate function. The iteration history of the MPP search is shown in Table 2. Figure 5 displays the convergence history of first order reliability index β_F. The MPP obtained from SEGO algorithm quickly converges to (-1.1314, -2.9165). It is close to the true MPP at (-1.1290, -2.9174), which is directly obtained from the extreme limit-state function Eq. (42).

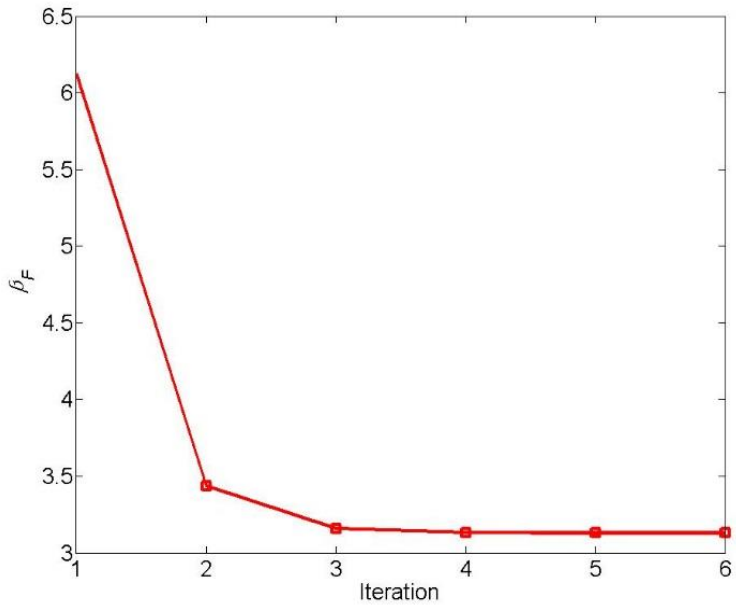

Figure 5. Convergence history of Example 1

After SEGO, FORM and SOSPA are used. For MCS, 10^6 samples are drawn for input random variables $\mathbf{X}$, and the time variable t is discretized evenly into 100 time instants within interval $[0,5]$. The results are shown in Table 3. And they indicate that SEGO/FORM produces a large error of $\varepsilon = 18.5\%$ due to the nonlinearity of the extreme limit-state function. SEGO/SOSPA achieves a more accurate result with an error of $\varepsilon = 2.47\%$. With respect to SEGO/FROM, SEGO/SOSPA requires additional computations which equal to the multiplication of number of iteration k and number of input random variables N, i.e. $kN = 6 \times 2 = 12$. SEGO/SOSPA has much higher accuracy with slightly decreased efficiency.

Table 3. Results of Example 1

Methods	p_f	ε%	Absolute Error	Number of Function Calls
SEGO/SOSPA	1.0524×10^{-3}	2.47%	2.66×10^{-5}	124
SEGO/FORM	8.7918×10^{-4}	18.5%	1.998×10^{-4}	112
MCS	1.0790×10^{-3}	-	-	10^8

4.2. EXAMPLE 2: AUTOMOBILE FRONT AXLE

An automobile front axle beam [47] is subjected to a torque T and a bending moment $M = M_0(0.1\sin(0.25t) + 0.9)$ N·mm in which $t \in [0,12]$. The limit-state function is given by

$$g(\mathbf{X},t) = S_y - \sqrt{\sigma^2 + 3\tau^2} = S_y - \sqrt{\left(\frac{M}{W_x}\right)^2 + 3\left(\frac{T}{W_\rho}\right)^2} \tag{43}$$

in which S_y is the yield strength, σ and τ are the maximum normal stress and shear stress respectively, and W_x and W_ρ are section factor and polar section factor given by

$$W_x = \frac{a(h-2c)^3}{6h} + \frac{b}{6h}\left[h^3 - (h-2c)^3\right] \tag{44}$$

$$W_\rho = 0.8bc^2 + \frac{0.4a^3(h-2c)}{c} \tag{45}$$

where a, b, c and h are dimension variables of the I-beam. All the parameters are independent and are listed in Table 4.

Table 4. Distribution of parameters for axle beam example

Variable (Unit)	Distribution	Mean	Standard Deviation
a (mm)	Normal	12	0.6
b (mm)	Normal	65	3.25
c (mm)	Normal	14	0.7
h (mm)	Normal	85	4.25
M_0 (N·mm)	Normal	7×10^6	7×10^5
T_0 (N·mm)	Normal	3.1×10^6	3×10^5
S_y (MPa)	Deterministic	610	-

10^6 samples are used for MCS and t is discretized into 100 time instants within interval $[0,12]$. Results are given in Table 5. Even though SEGO/FORM is more efficient than SEGO /SOSPA, it produces a relatively large error. SEGO/SOSPA is more accurate with only 18 additional function calls compared to SEGO/FORM.

Table 5. Results of Example 2

Methods	p_f	ε%	Absolute Error	Number of Function Calls
SEGO/SOSPA	4.3800×10^{-3}	0.37%	1.60×10^{-5}	176
SEGO/FORM	4.1899×10^{-3}	4.69%	2.061×10^{-4}	158
MCS	4.3960×10^{-3}	-	-	10^8

4.3. EXAMPLE 3: A VIBRATION PROBLEM

This example involves a forced vibration system modified from [22, 48]. There are five random variables, including the stiffness of spring k_1, the mass m_1, the stiffness of the spring k_2, the mass m_2, and the damping coefficient c_2. All the random variables are independent and are listed in the Table 6.

Table 6. Distribution of parameters for vibration example

Variable (Unit)	Distribution	Mean	Standard Deviation
k_1 (N/ m)	Normal	3×10^6	1×10^5
m_1 (kg)	Normal	2×10^4	2×10^2
k_2 (N/ m)	Normal	8.5×10^4	2×10^3
m_2 (kg)	Normal	480	5
c_2 (Ns/ m)	Normal	3.5×10^6	7.5×10^5

The mass m_1 in the main system is subjected to a sinusoidal force $f_0\sin(\Omega t)$ and the amplitude is given by

$$q_{1,\max} = f_0\left(\frac{c_2^2\Omega^2+\left(k_2-m_2\Omega^2\right)^2}{c_2^2\Omega^2\left(k_1-m_1\Omega^2-m_2\Omega^2\right)^2+\left(k_2m_2\Omega^2-\left(k_1-m_1\Omega^2\right)\left(k_2-m_2\Omega^2\right)\right)^2}\right)^{1/2} \quad (46)$$

Eq. (46) may be non-dimensionalised using a "static" deflection of main system, and the non-dimensional displacement of mass m_1 is obtained as

$$\delta = \frac{q_{1,\max}}{f_0 / k_1} = k_1 \left(\frac{c_2^2\Omega^2 + \left(k_2 - m_2\Omega^2\right)^2}{c_2^2\Omega^2\left(k_1 - m_1\Omega^2 - m_2\Omega^2\right)^2 + \left(k_2 m_2\Omega^2 - \left(k_1 - m_1\Omega^2\right)\left(k_2 - m_2\Omega^2\right)\right)^2} \right)^{1/2} \quad (47)$$

where δ is the displacement and is considered over a wide excitation frequency band $12 \le \Omega \le 30$ (rad/s). Ω is the excitation frequency and is treated as the time variable t within interval $[12, 30]$ rad/s. A failure occurs when the displacement δ is larger than 30. The probability of failure is given by

$$p_f = \Pr\left\{ g\left(\mathbf{X}, \Omega\right) = 30 - \delta < 0,\ \exists \Omega \in [12, 30] \right\} \quad (48)$$

where $\mathbf{X} = \left[k_1, m_1, k_2, m_2, c_2\right]$.

SEGO/FORM and SEGO/SOSPA are used to calculate the probability of failure. For MCS, 10^6 samples are used and the time variable Ω is discretized evenly into 500 instants within the interval $[12, 30]$. Table 7 shows the results from different methods. The results indicate that SEGO/SOSPA achieves a higher accuracy than SEGO/FORM while it needs 20 additional function calls.

Table 7. Results of Example 3

Methods	p_f	ε%	Absolute Error	Number of Function Calls
SEGO/SOSPA	7.8284×10^{-2}	2.48%	1.988×10^{-3}	465
SEGO/FORM	8.8295×10^{-2}	9.99%	8.023×10^{-3}	445
MCS	8.0272×10^{-2}	-	-	5×10^{8}

5. CONCLUSIONS

A new time-dependent reliability method, sequential efficient global optimization/second order saddlepoint approximation, is proposed for limit-state functions which are explicit with respect to time. This new method employs sequential efficient global optimization (SEGO) to convert a time-dependent problem into a time-independent counterpart where the most probable point (MPP) of the extreme limit-state function is obtained. Then a quasi-Newton approach and the envelope theorem are introduced to approximate the Hessian matrix of the extreme limit-state function. Finally the second order saddplepoint approximation (SOSPA) is used to evaluate the probability of failure.

The new method improves the accuracy of time-dependent reliability analysis with a reasonably increased computational effort. It is generally more accurate than the SEGO with first order reliability method (FORM) due to the second-order approximation to the extreme limit-state function. Therefore the new method can be applied to the problems in which extreme limit-state functions are not close to linear. The new method, however, is less efficient than first order approximation method because it requires second derivatives of extreme limit-state function. But the increase in the computational cost is minimized by the Hessian approximation method and envelope theorem, which make the new method more efficient than the direct second-order approximation.

Our future work includes applying the proposed method into time-dependent reliability-based design and extending the idea to more general limit-state functions.

ACKNOWLEDGEMENTS

The authors wound like to gratefully acknowledge the support from the National Science Foundation under Grant Number CMMI 1727329.

REFERENCES

[1] Choi, S.-K., Grandhi, R. V., and Canfield, R. A., 2006, Reliability-based structural design, Springer Science & Business Media.

[2] Ditlevsen, O., 2002, "Stochastic model for joint wave and wind loads on offshore structures," Structural Safety, 24(2), pp. 139-163.

[3] Hime, W., Backus, L., and Li, C., 1999, "Modeling time-to-corrosion cracking in chloride contaminated reinforced concrete structures. discussions and closure," ACI Materials Journal, 96(5).

[4] Suo, Q., and Stewart, M. G., 2009, "Corrosion cracking prediction updating of deteriorating RC structures using inspection information," Reliability engineering & system safety, 94(8), pp. 1340-1348.

[5] Zhang, J., and Du, X., 2011, "Time-dependent reliability analysis for function generator mechanisms," Journal of Mechanical Design, 133(3), p. 031005.

[6] Du, X., 2014, "Time-dependent mechanism reliability analysis with envelope functions and first-order approximation," Journal of Mechanical Design, 136(8), p. 081010.

[7] Andrieu-Renaud, C., Sudret, B., and Lemaire, M., 2004, "The PHI2 method: a way to compute time-variant reliability," Reliability Engineering & System Safety, 84(1), pp. 75-86.

[8] Hu, Z., and Du, X., 2012, "Reliability analysis for hydrokinetic turbine blades," Renewable Energy, 48, pp. 251-262.

[9] Hagen, Ø., and Tvedt, L., 1991, "Vector process out-crossing as parallel system sensitivity measure," Journal of engineering mechanics, 117(10), pp. 2201-2220.

[10] Engelund, S., Rackwitz, R., and Lange, C., 1995, "Approximations of first-passage times for differentiable processes based on higher-order threshold crossings," Probabilistic Engineering Mechanics, 10(1), pp. 53-60.

[11] Streicher, H., and Rackwitz, R., 2004, "Time-variant reliability-oriented structural optimization and a renewal model for life-cycle costing," Probabilistic Engineering Mechanics, 19(1), pp. 171-183.

[12] Lutes, L. D., and Sarkani, S., 2009, "Reliability analysis of systems subject to first-passage failure."

[13] Singh, A., Mourelatos, Z. P., and Li, J., 2010, "Design for lifecycle cost using time-dependent reliability," Journal of Mechanical Design, 132(9), p. 091008.

[14] Zhang, J., Wang, J., and Du, X., 2011, "Time-dependent probabilistic synthesis for function generator mechanisms," Mechanism and Machine Theory, 46(9), pp. 1236-1250.

[15] Condra, L., 2001, Reliability improvement with design of experiment, CRC Press.

[16] Holman, J. P., and Gajda, W. J., 2001, Experimental methods for engineers, McGraw-Hill New York.

[17] Lundstedt, T., Seifert, E., Abramo, L., Thelin, B., Nyström, Å., Pettersen, J., and Bergman, R., 1998, "Experimental design and optimization," Chemometrics and intelligent laboratory systems, 42(1), pp. 3-40.

[18] Papadrakakis, M., and Lagaros, N. D., 2002, "Reliability-based structural optimization using neural networks and Monte Carlo simulation," Computer methods in applied mechanics and engineering, 191(32), pp. 3491-3507.

[19] Deng, J., Gu, D., Li, X., and Yue, Z. Q., 2005, "Structural reliability analysis for implicit performance functions using artificial neural network," Structural Safety, 27(1), pp. 25-48.

[20] Hu, Z., Li, H., Du, X., and Chandrashekhara, K., 2013, "Simulation-based time-dependent reliability analysis for composite hydrokinetic turbine blades," Structural and Multidisciplinary Optimization, 47(5), pp. 765-781.

[21] Li, R., and Ghanem, R., 1998, "Adaptive polynomial chaos expansions applied to statistics of extremes in nonlinear random vibration," Probabilistic engineering mechanics, 13(2), pp. 125-136.

[22] Hu, Z., and Du, X., 2015, "Mixed efficient global optimization for time-dependent reliability analysis," Journal of Mechanical Design, 137(5), p. 051401.

[23] Hu, Z., and Mahadevan, S., 2016, "A Single-Loop Kriging Surrogate Modeling for Time-Dependent Reliability Analysis," Journal of Mechanical Design, 138(6), p. 061406.

[24] Martin, J. D., and Simpson, T. W., 2005, "Use of kriging models to approximate deterministic computer models," AIAA J, 43(4), pp. 853-863.

[25] Zhang, J., and Du, X., 2015, "Time-dependent reliability analysis for function generation mechanisms with random joint clearances," Mechanism and Machine Theory, 92, pp. 184-199.

[26] Zhu, Z., and Du, X., 2016, "Reliability analysis with monte carlo simulation and dependent kriging predictions," Journal of Mechanical Design, 138(12), p. 121403.

[27] Wang, Z., and Wang, P., 2012, "A nested extreme response surface approach for time-dependent reliability-based design optimization," Journal of Mechanical Design, 134(12), p. 121007.

[28] Li, J., Chen, J.-b., and Fan, W.-l., 2007, "The equivalent extreme-value event and evaluation of the structural system reliability," Structural Safety, 29(2), pp. 112-131.

[29] Singh, A., and Mourelatos, Z. P., 2010, "On the Time-Dependent Reliability of Non-Monotonic, Non-Repairable Systems," SAE International Journal of Materials and Manufacturing, 3(2010-01-0696), pp. 425-444.

[30] Hu, Z., and Du, X., 2018, "Saddlepoint approximation reliability method for quadratic functions in normal variables," Structural Safety, 71, pp. 24-32.

[31] Hu, Z., and Du, X., 2018, "Efficient reliability-based design with second order approximations," Engineering Optimization, pp. 1-19.

[32] Hu, Z., and Du, X., "A Random Field Method for Time-Dependent Reliability Analysis With Random and Interval Variables," Proc. ASME 2016 International Design Engineering Technical Conferences and Computers and Information in Engineering Conference, American Society of Mechanical Engineers, pp. V02BT03A044-V002BT003A044.

[33] Du, X., and Chen, W., 2004, "Sequential optimization and reliability assessment method for efficient probabilistic design," Journal of Mechanical Design, 126(2), pp. 225-233.

[34] Jones, D. R., Schonlau, M., and Welch, W. J., 1998, "Efficient global optimization of expensive black-box functions," Journal of Global optimization, 13(4), pp. 455-492.

[35] Lockwood, B., and Mavriplis, D., 2013, "Gradient-based methods for uncertainty quantification in hypersonic flows," Computers & Fluids, 85, pp. 27-38.

[36] Raghavan, B., and Breitkopf, P., 2013, "Asynchronous evolutionary shape optimization based on high-quality surrogates: application to an air-conditioning duct," Engineering with Computers, 29(4), pp. 467-476.

[37] Arora, J. S., 2004, Introduction to optimum design, Elsevier.

[38] Lim, J., Lee, B., and Lee, I., 2014, "Second-order reliability method-based inverse reliability analysis using Hessian update for accurate and efficient reliability-based design optimization," International Journal for Numerical Methods in Engineering, 100(10), pp. 773-792.

[39] Chambers, R. G., Chung, Y., and Färe, R., 1996, "Benefit and distance functions," Journal of economic theory, 70(2), pp. 407-419.

[40] Carter, M., 2001, Foundations of mathematical economics, MIT Press.

[41] Breitung, K., 1984, "Asymptotic approximations for multinormal integrals," Journal of Engineering Mechanics, 110(3), pp. 357-366.

[42] Tvedt, L., 1990, "Distribution of quadratic forms in normal space—application to structural reliability," Journal of Engineering Mechanics, 116(6), pp. 1183-1197.

[43] Daniels, H. E., 1987, "Tail probability approximations," International Statistical Review/Revue Internationale de Statistique, pp. 37-48.

[44] Goutis, C., and Casella, G., 1999, "Explaining the saddlepoint approximation," The American Statistician, 53(3), pp. 216-224.

[45] Du, X., and Sudjianto, A., "A saddlepoint approximation method for uncertainty analysis," Proc. ASME 2004 International Design Engineering Technical Conferences and Computers and Information in Engineering Conference, American Society of Mechanical Engineers, pp. 445-452.

[46] Hu, Z., and Du, X., 2019, "Reliability Methods for Bimodal Distribution With First-Order Approximation," ASCE-ASME Journal of Risk and Uncertainty in Engineering Systems, Part B: Mechanical Engineering, 5(1), p. 011005.

[47] Shi, Y., Lu, Z., Cheng, K., and Zhou, Y., 2017, "Temporal and spatial multi-parameter dynamic reliability and global reliability sensitivity analysis based on the extreme value moments," Structural and Multidisciplinary Optimization, 56(1), pp. 117-129.

[48] Zang, C., Friswell, M., and Mottershead, J., 2005, "A review of robust optimal design and its application in dynamics," Computers & structures, 83(4-5), pp. 315-326.

SECTION

2. CONCLUSIONS

The objective of this research is to develop accurate and efficient reliability methodologies under time-independent uncertainty and then extend them into time-dependent reliability analysis. To achieve this objective, four saddlepoint approximation (SPA) based methods have been developed.

The first method investigates the applicability of mean value saddlepoint approximation (MVSPA) and first order saddlepoint approximation (FOSPA) for the reliability problems where the bimodal distributions are involved. The second method approximates a limit-state function with the second-order Taylor expansion and obtains its cumulant generating function (CGF). Then SPA is used to predict the probability of failure with high accuracy. The third method introduces the second method into reliability-based design (RBD). The new method improves the accuracy of reliability estimation by replacing FORM with the second order SPA and maintains high efficiency by developing an algorithm to search for the equivalent reliability index. The fourth method is an extension of second method to time-dependent reliability analysis. The time-dependent problem is converted into a time-independent counterpart by using the extreme value of the limit-state function. A sequential efficient global optimization is developed for the first order approximation to the extreme value of the time-dependent limit-state function. Then Hessian approximation and envelope theorem are employed to obtain the second order approximation. Finally the second order SPA is used to estimate the reliability. Based on the above studies, the following conclusions are drawn.

(1) The widely used first order second moment method (FOSM) and first order reliability method (FORM) may produce large errors for reliability problems with bimodal distributions.

(2) The SPA based methods can estimate the reliability accurately when bimodal distributions are involved.

(3) The second order saddlepoint approximation (SOSPA) is in general more accurate than the traditional second order reliability method (SORM).

(4) Using SOSPA for RBD can produce better optimal designs because of higher reliability accuracy.

(5) Sequential efficient global optimization with SOSPA is able to convert a time-dependent reliability problem into a time-independent problem and achieves higher accuracy over FORM.

Our future work includes the improvement of developed methodologies and their applications into the most general space- and time-dependent problems. Another work is to incorporate the methods into product design and lifecycle management of engineering systems.

BIBLIOGRAPHY

[1] Choi, S.-K., Grandhi, R., and Canfield, R. A., 2006, Reliability-based structural design, Springer Science & Business Media.

[2] Binder, K., Heermann, D., Roelofs, L., Mallinckrodt, A. J., and McKay, S., 1993, "Monte Carlo simulation in statistical physics," Computers in Physics, 7(2), pp. 156-157.

[3] Ditlevsen, O., and Madsen, H. O., 1996, Structural reliability methods, Wiley New York.

[4] Mooney, C. Z., 1997, Monte carlo simulation, Sage Publications.

[5] Elishakoff, I., Van Manen, S., and Arbocz, J., 1987, "First-order second-moment analysis of the buckling of shells with random imperfections," AIAA journal, 25(8), pp. 1113-1117.

[6] Haldar, A., and Mahadevan, S., 2000, Probability, reliability, and statistical methods in engineering design, John Wiley.

[7] Der Kiureghian, A., and Dakessian, T., 1998, "Multiple design points in first and second-order reliability," Structural Safety, 20(1), pp. 37-49.

[8] Du, X., and Hu, Z., 2012, "First order reliability method with truncated random variables," Journal of Mechanical Design, 134(9), p. 091005.

[9] Hasofer, A., and Lind, N., 1974, "An exact and invariant first order reliability format," J Eng Mech Div, ASCE, 100(EM1), pp. 111-121.

[10] Hohenbichler, M., and Rackwitz, R., 1982, "First-order concepts in system reliability," Structural safety, 1(3), pp. 177-188.

[11] Breitung, K., 1984, "Asymptotic approximations for multinormal integrals," Journal of Engineering Mechanics, 110(3), pp. 357-366.

[12] Tvedt, L., 1983, "Two second-order approximations to the failure probability," Section on structural reliability.

[13] Tvedt, L., 1990, "Distribution of quadratic forms in normal space-application to structural reliability," Journal of Engineering Mechanics, 116(6), pp. 1183-1197.

[14] Zhao, Y.-G., and Ono, T., 1999, "New approximations for SORM: Part 1," Journal of Engineering Mechanics, 125(1), pp. 79-85.

[15] Hohenbichler, M., Gollwitzer, S., Kruse, W., and Rackwitz, R., 1987, "New light on first-and second-order reliability methods," Structural safety, 4(4), pp. 267-284.

[16] Köylüoğlu, H. U., and Nielsen, S. R., 1994, "New approximations for SORM integrals," Structural Safety, 13(4), pp. 235-246.

[17] Daniels, H. E., 1954, "Saddlepoint approximations in statistics," The Annals of Mathematical Statistics, pp. 631-650.

[18] Lugannani, R., and Rice, S., 1980, "Saddle point approximation for the distribution of the sum of independent random variables," Advances in applied probability, pp. 475-490.

[19] Daniels, H. E., 1987, "Tail probability approximations," International Statistical Review/Revue Internationale de Statistique, pp. 37-48

[20] Goutis, C., and Casella, G., 1999, "Explaining the saddlepoint approximation," The American Statistician, 53(3), pp. 216-224.

[21] Du, X., and Sudjianto, A., 2004, "First-order saddlepoint approximation for reliability analysis," AIAA journal, 42(6).

[22] Huang, B., and Du, X., 2008, "Probabilistic uncertainty analysis by mean-value first order saddlepoint approximation," Reliability Engineering & System Safety, 93(2), pp. 325-336.

[23] Huang, B., Du, X., and Lakshminarayana, R. E., 2006, "A saddlepoint approximation based simulation method for uncertainty analysis," International Journal of Reliability and Safety, 1(1), pp. 206-224.

[24] Du, X., 2008, "Saddlepoint approximation for sequential optimization and reliability analysis," Journal of Mechanical Design, 130(1), p. 011011.

[25] Du, X., 2010, "System reliability analysis with saddlepoint approximation," Structural and Multidisciplinary Optimization, 42(2), pp. 193-208.

[26] Rice, S. O., 1944, "Mathematical analysis of random noise," Bell Labs Technical Journal, 23(3), pp. 282-332.

[27] Andrieu-Renaud, C., Sudret, B., and Lemaire, M., 2004, "The PHI2 method: a way to compute time-variant reliability," Reliability Engineering & System Safety, 84(1), pp. 75-86.

[28] Hu, Z., and Du, X., 2012, "Reliability analysis for hydrokinetic turbine blades," Renewable Energy, 48, pp. 251-262.

[29] Hu, Z., and Du, X., 2013, "Time-dependent reliability analysis with joint upcrossing rates," Structural and Multidisciplinary Optimization, 48(5), pp. 893-907.

[30] Zhang, J., and Du, X., 2011, "Time-dependent reliability analysis for function generator mechanisms," Journal of Mechanical Design, 133(3), p. 031005.

[31] Li, R., and Ghanem, R., 1998, "Adaptive polynomial chaos expansions applied to statistics of extremes in nonlinear random vibration," Probabilistic engineering mechanics, 13(2), pp. 125-136.

[32] Xiong, F., Liu, Y., Xiong, Y., and Yang, S., 2012, "A double weighted stochastic response surface method for reliability analysis," Journal of mechanical science and technology, 26(8), pp. 2573-2580.

[33] Cheng, J., and Li, Q., 2008, "Reliability analysis of structures using artificial neural network based genetic algorithms," Computer Methods in Applied Mechanics and Engineering, 197(45), pp. 3742-3750.

[34] Deng, J., Gu, D., Li, X., and Yue, Z. Q., 2005, "Structural reliability analysis for implicit performance functions using artificial neural network," Structural Safety, 27(1), pp. 25-48

[35] Elhewy, A. H., Mesbahi, E., and Pu, Y., 2006, "Reliability analysis of structures using neural network method," Probabilistic Engineering Mechanics, 21(1), pp. 44-53.

[36] Chen, K.-Y., 2007, "Forecasting systems reliability based on support vector regression with genetic algorithms," Reliability Engineering & System Safety, 92(4), pp. 423-432.

[37] Hurtado, J. E., 2007, "Filtered importance sampling with support vector margin: a powerful method for structural reliability analysis," Structural Safety, 29(1), pp. 2-15.

[38] Hu, Z., and Mahadevan, S., 2016, "A Single-Loop Kriging Surrogate Modeling for Time-Dependent Reliability Analysis," Journal of Mechanical Design, 138(6), p. 061406.

[39] Martin, J. D., and Simpson, T. W., 2005, "Use of kriging models to approximate deterministic computer models," AIAA J, 43(4), pp. 853-863.

[40] Zhang, J., and Du, X., 2015, "Time-dependent reliability analysis for function generation mechanisms with random joint clearances," Mechanism and Machine Theory, 92, pp. 184-199

[41] Zhu, Z., and Du, X., 2016, "Reliability analysis with monte carlo simulation and dependent kriging predictions," Journal of Mechanical Design, 138(12), p. 121403.

[42] Wang, Z., and Wang, P., 2012, "A nested extreme response surface approach for time-dependent reliability-based design optimization," Journal of Mechanical Design, 134(12), p. 121007.

[43] Hu, Z., and Du, X., 2015, "Mixed efficient global optimization for time-dependent reliability analysis," Journal of Mechanical Design, 137(5), p. 051401.

[44] Li, J., Chen, J.-b., and Fan, W.-l., 2007, "The equivalent extreme-value event and evaluation of the structural system reliability," Structural Safety, 29(2), pp. 112-131.

[45] Singh, A., and Mourelatos, Z. P., 2010, "On the Time-Dependent Reliability of Non-Monotonic, Non-Repairable Systems," SAE International Journal of Materials and Manufacturing, 3(2010-01-0696), pp. 425-444.

[46] Du, X., 2014, "Time-dependent mechanism reliability analysis with envelope functions and first-order approximation," Journal of Mechanical Design, 136(8), p. 081010

[47] Laman, J. A., and Nowak, A. S., 1996, "Fatigue-load models for girder bridges," Journal of Structural Engineering, 122(7), pp. 726-733.

[48] Haider, S. W., Harichandran, R. S., and Dwaikat, M. B., 2009, "Closed-form solutions for bimodal axle load spectra and relative pavement damage estimation," Journal of transportation engineering, 135(12), pp. 974-983.

[49] Hu, Z., and Du, X., 2019, "Reliability Methods for Bimodal Distribution With First-Order Approximation," ASCE-ASME Journal of Risk and Uncertainty in Engineering Systems, Part B: Mechanical Engineering, 5(1), p. 011005.

[50] Hu, Z., and Du, X., 2018, "Saddlepoint approximation reliability method for quadratic functions in normal variables," Structural Safety, 71, pp. 24-32.

[51] Hu, Z., and Du, X., 2019, "Efficient reliability-based design with second order approximations," Engineering Optimization, 51(1), pp. 101-119.

[52] Hu, Z., and Du, X., 2019, "Second Order Reliability Method for Time-Dependent Reliability Analysis using Sequential Efficient Global Optimization," accepted by the ASME 2019 International Design Engineering Technical Conferences and Computers and Information in Engineering Conference, American Society of Mechanical Engineers.

VITA

Zhangli Hu was born in Zigong, Sichuan, the People's Republic of China. He received his Bachelor of Science degree in Aerospace Engineering in June 2012 from Beijing Institute of Technology, Beijing, China. He continued his education in Beijing Institute of Technology until May 2015. Then he transferred to the Department of Mechanical and Aerospace Engineering at Missouri University of Science and Technology and started pursuing the degree of direct Doctor of Philosophy. He worked with Dr. Xiaoping Du and Dr. Daoru Han in the areas of uncertainty quantification, reliability analysis, reliability-based optimization design and statistical modeling. In May 2019, he received his Doctor of Philosophy in Mechanical Engineering from Missouri University of Science and Technology, Rolla, Missouri.